Simulation of the heat and coolant flow for a PMR200 reactor using a network approach in Flownex.

GJ Nel

orcid.org / 0000-0002-1050-2659

Thesis accepted in fulfilment of the requirements for the degree Doctor of Philosophy in Engineering with Nuclear Engineering at the North-West University

Supervisor: Prof CG du Toit

Graduation: May 2022

Student number: 24118699

ACKNOWLEDGMENTS

Sincere thanks to the following persons for their support during this study:

- Prof. Jat du Toit, Study Leader
- South African Research Chairs Initiative of the Department of Science and Technology and National Research Foundation of South Africa, Funding
- Ockert Koekemoer, Simulation and Research assistance
- A sincere thanks to Dr JS Jun and Dr NI Tak for providing the necessary data of the PMR200.

ABSTRACT

The VHTR (Very High-Temperature Reactor) Prismatic block reactor is one of the reactor designs considered in the range of 4th Generation Reactors which are under development today. The heat generated by the gas-cooled reactor can be used to produce electricity or as process heat to produce amongst others hydrogen. For the reactor's operation under normal and upset conditions, the conduction heat transfer through the prismatic block, convection heat transfer to the coolant, and radiative heat transfer to other critical components are of critical importance.

Most of the research that has been done on different aspects of the PMR200 prismatic block reactor and the associated RCCS (Reactor Cavity Cooling System) was performed using 1D (One-dimensional) and 3D (Three-dimensional) numerical simulation packages. There was also some physical experimental testing done on certain parts of the RCCS and selected aspects of the PMR200 (Prismatic Modular Reactor). 3D simulation packages are employed to model specific components of a nuclear reactor which can range from a partial core simulation to a small single channel fuel module (SCFM) model simulation. The 3D simulation models are computationally intensive and require large computational resources and the simulation takes a long time to complete. Although the 3D simulation packages can provide detailed results, the long completion times and the large computational resources make it impractical for the analysis of full systems.

1D simulation packages have also been used to simulate specific components that can range from a full core to an SCFM model. But with 1D simulation packages, the network models are constructed to be representative models of these specific components. The representative models that are constructed using 1D simulation packages are much less computationally intensive compared to 3D models. Although the 1D packages do not give the same detailed results as the 3D packages, they can provide results of sufficient detail and accuracy that can be used for the evaluation and design of full systems.

In the current study, the purpose is, to create a one-dimensional integrated full PMR200 reactor and RCCS thermal-hydraulic model that will give the required results of sufficient accuracy for the evaluation of the integrated system employing a 1D network approach. The 1D simulation package Flownex will be used to construct and test the network models for the PMR200 reactor, RCCS only and the combined PMR200 and RCCS. The integrated model will be used to evaluate the performance related to the heat transfer and coolant flow of the PMR200 reactor and the RCCS system for normal and selected off-normal conditions.

Selected thermal-hydraulic results obtained from steady-state simulations performed with the PMR200, RCCS and the integrated PMR200-RCCS models were compared with corresponding results obtained from literature and found to be in good agreement. It was therefore concluded that PMR200, RCCS only and integrated PMR200-RCCS model are valid representative models that can be used to evaluate the thermal-hydraulic performance of the reactor and associated RCCS. The capability of the models is shown to be helpful to evaluate the thermal-hydraulic performance of the reactor systems as demonstrated by the selected simulated scenarios.

Keywords: Very High Temperature Reactor, PMR 200, Prismatic fuel block, Conduction heat transfer, Convective heat transfer, Radiative heat transfer, One-dimensional Modelling

PREFACE

- This is to state that I, Gert Johannes Nel, have chosen the article format for submitting my thesis.
- The thesis is written in South African English.
- Articles are written by:

  GJ Nel, CG du Toit, OC Koekemoer

  South African Research Chairs Initiative of the Department of Science and Technology and National Research Foundation of South Africa (Grant No 61059).

  Area, North-West University, Potchefstroom 2520, South Africa

  Email: Gertt.nel@gmail.com, jat.dutoit@nwu.ac.za, ockie.koekemoer@gmail.com
- I, CG du Toit, hereby give permission that Gert J Nel may submit the article(s)/manuscript(s) for degree purposes.
- The peer-review article (Ch 2): 1D AND 3D CFD MODELS OF HEAT TRANSFER IN A PRISMATIC BLOCK OF A VHTR was published in the Proceedings of the 14th International Conference on Heat Transfer, Fluid Mechanics and Thermodynamics (HEFAT 2019)
- The Journal article (Ch 3): Numerical simulation of a representative PMR200 Reactor model in Flownex (Part 1) to be submitted for review and possible publication in Nuclear Engineering and Design.
- The Journal article (Ch 4): Numerical simulation of an integrated RCCS with a full representative PMR200 Reactor in Flownex (Part 2) to be submitted for review and possible publication in Nuclear Engineering and Design.
- The peer-review article (Co-Authored) (Appendix B): Coupled 3D and 1D Models of the heat transfer in a prismatic block of a VHTR was published in the Proceedings of the 14th International Conference on Heat Transfer, Fluid Mechanics and Thermodynamics (HEFAT 2019).
- Acknowledgements for all articles:

  This work is based upon research supported by the South African Research Chairs Initiative of the Department of Science and Technology and National Research Foundation (Grant No. 61059). Any opinion, finding and conclusion or recommendation expressed in this material is that of the author(s) and the NRF does not accept any liability in this regard.

  We thank all contributions made directly and indirectly by any involved party towards the studies presented below.

TABLE OF CONTENTS

CHAPTER 1: INTRODUCTION

1.1 Background

Very High Temperature Gas-Cooled Reactors are included in the generation IV design category for nuclear reactors/plants (World Nuclear Association, 2020). These reactors can reach up to 600 MW_{th} and can produce an outlet helium temperature of between 900-1000°C. Operating pressures can also vary between 4 MPa to 9 MPa. There are two types of VHTR reactor designs considered, namely the PBMR (Pebble Bed Modular Reactor) and the PMR (Prismatic Modular Reactor) designs (IAEA 2010). The reactor model considered for the current study is the PMR200 model (Jo et al., 2008) with a multi-hole prismatic block core configuration (Ribeiro et al., 2013). The core of the reactor is made up of prismatic fuel blocks stacked on top of each other with the height per layer/block being 0.793 m. On top of the active core assembly, a Top Reflector and Top Head Plenum is placed whilst at the bottom of the assembly a Bottom Reflector, Bottom Plenum and Bottom Support is used. TRISO particles are embedded in the fuel compacts that make up the fuel rods that are used in the reactor.

In normal or accident conditions heat needs to be removed to protect the nuclear system. In these accident or normal operating conditions, the RCCS (Reactive Cavity Cooling System) is imperative for the heat removal process from the reactor system. The RCCS is designed to operate naturally driven by buoyancy forces and is constructed to work as a water cooled, air-cooled or water-air-cooled system (Hassan, 2013; Du Toit et al., 2016).

Different thermal-fluid phenomena will occur within the different components of a prismatic reactor and RCCS, with such components including the fuel compacts, coolant channels, graphite blocks and the bypass and cross flow gaps between the different graphite blocks as well as the risers and downcomers of the RCCS. Computational Fluid Dynamics (CFD) has been used in the industry to simulate different phenomena in the different sections of a nuclear reactor to a very accurate level. Due to the amount of associated detail that is considered (geometric features, fluid flow, temperature distributions, heat transfer, etc), 3-dimensional simulations of the full reactor require extensive computational resources that are not generally available. Therefore, much research has been done by employing 3D explicit models (Ribeiro et al., 2013; Tak et al., 2008), which account for only parts of a reactor and generate detailed results but only for the partial reactor, fuel block or fuel assembly models simulated. A 1D system simulation approximation of a full or partial reactor, core, fuel block or fuel assembly generates results that are representative of the thermal hydraulic characteristics of the reactor or core (Sambureni, 2015; Khoza, 2019). Although the results are not as detailed as in the case of 3D simulations, the results that are obtained are very informative,

and the computational resources needed for the full 1D representative reactor are much less than that required for the full and partial 3D simulations.

Tak et al. (2011) developed a practical method for the analysis of a core of a prismatic gas cooled reactor. This method entails using a combination of CFD and a system approach that uses far less computational resources than a full 3D CFD approach. The CFD part accounts for the conduction heat transfer in the solids of the system and the one-dimensional approach accounts for the fluid flow in the system. The complex geometries are represented by a collection of purposed designed unit cells. The approach that is followed provided accurate results. Calculation time and computational resources were also reduced significantly using this approach.

A steady state and transient state analysis were performed by Jun et al. (2009) on the PMR200 reactor system. The steady state and transient analyses were done at LPCC (Low Pressure Conduction Cooling) and HPCC (High Pressure Conduction Cooling) conditions. A prismatic core is used with 6 layers of fuel blocks and with an air cooled RCCS system and VCS (Vessel Cooling System) system. The thermal-fluid analysis of the 200 MW^{th} reactor was performed using the systems GAMMA+ (Lim et al., 2006). Maximum temperature results are extracted from the fuel elements and the RPV (reactor pressure vessel), as well as other flow characteristics in the coolant flow components.

KAERI (Korea Atomic Energy Research Institute) and the NWU (North West University of South Africa) had an established program of "Joint Research Collaboration in the System Analysis of the Passive Safe Small Modular High Temperature Gas-Cooled Reactor" where the two organizations compared benchmark calculations of the natural circulation in an air-cooled RCCS. KAERI performed calculations using GAMMA+ and the NWU used the code Flownex for their calculations. Common input data such as the geometry and the material properties was given by KAERI for the $200MW_{th}$ PMR (Prismatic Modular Reactor) design that has been used by both KAERI and the NWU for the benchmarking of the RCCS.

1.2 Problem Statement

There have been many studies done on parts of the PMR200 reactor and the RCCS employing 3D and 1D simulation packages. No study has, however, been performed where a Full Core model of a PMR200 prismatic block reactor has been constructed in Flownex, as well as a Full integrated model of the PMR200 reactor and the associated RCCS.

The purpose of this study is to construct a full core numerical model of the PMR200 and the associated RCCS. The study aims to generate a network model of the PMR200 and the RCCS using Flownex, which uses less computational resources than other conventional CFD simulation models. The study uses the

necessary input data to perform a full-scale simulation of the PMR200 and the associated RCCS and to generate results of sufficient accuracy without the need for a full 3D simulation to evaluate the performance of the integrated system. The results are compared with available results obtained from various sources to determine the validity of the Flownex model and associated results.

The construction of the full reactor Flownex model is based on the information provided by KAERI (Ju, 2012, 2020) and simulations done by KAERI on the PMR200 in GAMMA+ and the RCCS simulations performed by Du Toit et al. (2014) and Rousseau et al. (2015) in Flownex. The RCCS models of Du Toit et al. (2014) and Rousseau et al. (2015) are adapted as required and integrated with the model of the full reactor of the PMR200 using all the relevant geometrical data provided by KAERI. Previous research and information that was gathered (Nel & Du Toit, 2018) during the modeling of a single channel fuel module (SCFM) are used in the construction of the Flownex model to model the convection heat transfer in the coolant channels.

1.3 Methodology

A single 1D system network model is constructed in Flownex of $1/6^{th}$ of an SCFM (Single Channel Fuel Module) and compared to a 3D model constructed in Star CCM+. The SCFM model is the elementary unit on which the construction of a representative model of a full PMR200 reactor is based. A 1D system network model of an RCCS is also constructed in Flownex and integrated with the PMR200 Flownex model. All the simulations of the different models account for conduction-, convection and radiative heat transfer as well as fluid flow in the different sections of the reactor and RCCS. The results of the different studies/investigations that are compared to literature or other extracted results are to be within 5%, as preferred by the general academic community. The results of the associated simulation model are extracted evaluated and compared to relevant data obtained from published sources to confirm the validity of the constructed models and their extracted results.

1.4 Contribution of the Study

By the completion of the study, the following contributions were made:

- A 1D system network model of an SCFM is modelled and evaluated to establish the validity of the SCFM model in Flownex and demonstrate that Flownex can be used for the modelling of the SCFM.

- A full representative model of the PMR200 reactor is constructed, simulated and evaluated in Flownex. From the results, it is shown that Flownex is capable of calculating various characteristics

with good accuracy. Thus, the constructed model can also be used and adapted in Flownex for the simulation of other types of VHTR's.

- A representative adapted model of RCCS is modelled in Flownex and is integrated with the full representative PMR200 reactor model. With the results gathered it is shown that Flownex is capable to predict the different thermal and fluid characteristics of the reactor and the attached RCCS to a good accuracy level. Thus the RCCS can also be adapted to accommodate different dimensions associated with other various reactors systems.

1.5 Chapter Outline

The thesis is consists of 3 articles. In chapter 2 the development and evaluation between a 1D constructed SCFM simulation and a 3D constructed SCFM simulation is discussed. This paper was presented at the 14th International Conference on Heat Transfer, Fluid Mechanics and thermodynamics (HEFAT 2019) and was included in the proceedings of HEFAT 2019. Chapter 3 deals with the development and evaluation of a 1D system network full representative PMR200 reactor constructed in Flownex. The article is ready to be submitted to NED (Nuclear Engineering and Design) for review and for possible publication in the Nuclear Engineering and Design journal. In chapter 4 the construction and integrations of a 1D RCCS (Reactor Cavity Cooling System) simulation model to a 1D full representative PMR200 simulation model are evaluated and discussed. The article is ready to be submitted to NED (Nuclear Engineering and Design) for review and for possible publication in the Nuclear Engineering and Design journal. A brief overview of the main outcomes of chapter 2, chapter 3 and chapter 4 and recommendations is given in chapter 5. Appendix A displays the layout of the Flownex model of the PMR200 reactor. Appendix B is an additional co-authored article that was also presented and accepted for inclusion in the proceedings of HEFAT 2019. The article discusses and evaluates the coupled 3D and 1D simulation models of an SCFM.

References

Du Toit, C.G.; Rousseau, P.G.; Jun, J.S.; Noh, J.M. (2014) '1D AND 3D NUMERICAL SIMULATION OF THE REACTOR CAVITY COOLING SYSTEM OF A VERY HIGH TEMPERATURE REACTOR', IHTC 15, Japan, August 2014.

Du Toit, C.G.; Rousseau, P.G.; Jun,J.S.; Kim, M-H (2016) 'NUMERICAL SIMULATION OF BREAK FLOWS OCCURING IN THE REACTOR CAVITY COOLING SYSTEM OF A VERY HIGH TEMPERATURE REACTOR USING A SYSTEM CFD APPROACH', HTR 2016, Las Vegas NV, November 2016.

Hassan, Y (2013) 'CFD Model Development and Validation for High Temperature Gas Cooled Reactor Cavity Cooling System (RCCS) Applications' Texas A&M University, Project No. 09-817

IAEA (2010) 'HIGH TEMPERATURE GAS COOLED REACTOR FUELS AND MATERIALS', IAEA, Vienna, ISBN 978-92-0-153110-2

Jo, C.K; Lim, H.S.; Noh, J.M., (2008) 'Pre conceptual Designs of the 200MW_{th} Prism and Pebble-type VHTR Cores', PHYSOR 2008, Switzerland, Interlaken.

Jun, J.S.; Lim, H.S.; Jo, C.K.; Noh, J.M., (2009) 'Thermal-Fluid Analysis of the PMR 200MW_{th} Reactor System at the Steady State and Transient Conditions', Transactions of the Korean Nuclear Society Spring Meeting,

Khoza, S.N. (2019) 'An integrated thermal hydraulic system CFD model of a prismatic block HTR core using Flownex', North-West University, South Africa

Lim, H.S.; No, H.C. (2006) ' GAMMA Multidimensional Multicomponent Mixture Analysis to Predict Air Ingress Phenomena in an HTGR', Nuclear Science and Engineering, 152, 1-11.

Nel, G.J. and du Toit, C .G. (2018) 'A System CFD Model of a Single-Channel Fuel Module in a Prismatic Block VHTR', South African Conference on Computational and Applied Mechanics 2018, South Africa.

Ribeiro, F.L.; Santos, A.A.C.; Pinto, J.P.C.A.; Mesquita, A.Z.; de Mattos, J.R.L., 'Numerical simulations of helium flow through prismatic fuel elements of very high temperature reactors', International Nuclear Atlantic Conference 2013, Brazil.

Rousseau, P.G., Du Toit, C.G., Jun, J.S., Noh, J.M. (2015) 'Code-to-code comparison for analysing the steady-state heat transfer and natural circulation in an air-cooled RCCS using GAMMA+ and Flownex', Nuclear Engineering and Design, 291, pp 72 – 89.

Sambureni, P (2015) 'Thermal fluid network model for a prismatic block in a gas-cooled reactor using FLOWNEX', North-West University, South Africa.

Tak, N; Kim, M; Lee, W.J. (2008) 'Numerical investigation of a heat transfer within the prismatic fuel assembly of a very high temperature reactor', Annals of Nuclear Energy, 35, pp. 1892-1899.

Tak, N.; Kim, M; Lim, H.S.; Noh, J.M., (2011) 'A Practical Method for Whole-Core Thermal Analysis of a Prismatic Gas Cooled Reactor', Nuclear Technology, 177, pp. 352-365.

World Nuclear Association (2020) 'Generation IV Nuclear Reactors', https://world-nuclear.org/information-library/nuclear-fuel-cycle/nuclear-power-reactors/generation-iv-nuclear-reactors.aspx

CHAPTER 2: 1D AND 3D CFD MODELS OF THE HEAT TRANSFER IN A PRISMATIC BLOCK OF A VHTR

1D AND 3D CFD MODELS OF THE HEAT TRANSFER IN A PRISMATIC BLOCK OF A VHTR

Nel GJ*, Koekemoer OC and du Toit CG.
*Author for correspondence
Unit for Energy and Technology Systems,
North West University,
Potchefstroom, 2531,
South Africa,
E-mail: Gertt.nel@gmail.com

ABSTRACT

The VHTR (Very High Temperature Reactor) Prismatic block reactor is one of the reactor designs considered in the range of 4th Generation Reactors which are under development today. The heat generated by the gas-cooled reactor can be used to produce electricity or as process heat to produce amongst others hydrogen. For the operation of the reactor under normal and upset conditions the conduction heat transfer through the prismatic block and the convection heat transfer to the coolant is of critical importance. This paper discusses 3D and 1D computational fluid dynamic (CFD) models to simulate the heat transfer and fluid flow in a single-channel fuel module of a prismatic block. These models account for conduction heat transfer in the solids, convection heat transfer between the solids and fluid and fluid flow in the coolant channel in the single-channel fuel module. The current models represent one sixth of a single-channel fuel module. Detailed results are obtained for uniform and cosine power profiles by employing a 3D CFD code whilst representative results are obtained by a 1D system CFD code. The models are evaluated by comparing the temperature distribution results of the fuel compacts, coolant channel wall and the coolant, obtained by the different models with each other. The analyses of the study are performed employing the 3D CFD code STAR CCM+ and the 1D system CFD code Flownex. The 1D model requires much less computational resources than the detailed 3D CFD and can form the basis of an integrated model for the entire core.

INTRODUCTION

Generation IV nuclear reactor designs include the design for the Very High Temperature Reactor which has a thermal power output of 200–600 MWth. The reactors operate at outlet temperatures of 700 ˚C to 1000 ˚C and a pressure of 4 MPa to 9 MPa (Travis & El-Genk, 2013b). Graphite is used for the moderator material and helium is used as the reactor coolant. The fuel compacts consist of Tristructural-isotropic (TRISO) particles dispersed in a graphite matrix. In the gas turbine- modular helium reactor (GT-MHR) prismatic fuel blocks are stacked to make 8000 mm fuel assemblies. A top graphite reflector of 1200 mm and a bottom graphite reflector of 800 mm are added to make the total fuel core height 10000 mm (Travis & El-Genk, 2013b).

The heat transfer and flow through the prismatic fuel blocks are very important for the safe operation of the VHTR core. Computational Fluid Dynamics (CFD) has been used in the industry to simulate different phenomena in the fuel blocks to a very accurate level. Johnson & Sato (2012), Tak et al. (2008), and Tung et al. (2013 & 2016) modelled 1/12th of a fuel assembly with explicit detail of the fuel compacts, graphite, coolant channels and bypass gaps. They studied the effect of prescribed power profiles and bypass gap size on the thermal-flow behaviour of the fuel assemblies. Tung et al. (2013 & 2016) also studied the natural circulation that occurs after a loss of flow accident (LOFA). Johnson & Sato(2012) used the CFD code ANSYS Fluent, Tak et al. (2008) the CFD code CFX, whilst Tung et al. (2013 & 2016) used the CFD code STAR CCM+ (2018).

A convection heat transfer correlation was developed by Travis & El-Genk (2013b) to calculate the convection heat transfer coefficient for the helium in the coolant channels. In this study, the heat transfer and fluid flow were simulated in a representative manner using different CFD codes. The simulations used full 1D and full 3D CFD models to model a 1/6th Single Channel Fuel Module (SCFM). The 1D simulations are performed using Flownex and the full 3D simulations are executed by employing STAR CCM+. The simulations account for the conduction heat transfer through the fuel compact and moderator graphite, the convection heat transfer from the coolant channel wall to the coolant channel fluid and the flow of the coolant in the coolant channel. The heat transfer through the SCFM accounted for the temperature distribution at the center and the wall of the fuel compact will be examined.

SINGLE-CHANNEL FUEL MODULE

Within a fuel block a single channel fuel module consists of one coolant channel and six partial fuel compacts. **Figure 1(a)** and **(b)** show a SCFM of a prismatic core block where the red elements in **Figure 1(b)** represent the fuel compacts and the blue circle elements represent the coolant channels. Ten fuel blocks

each with a height of 800 mm are stacked to form a fuel block assembly which has a total height of 8000 mm. The SCFM is represented by the hexagonal cross-sectional area contained around the coolant channel in **Figure 1(a)** and the area outlined by the dashed hexagon in **Figure 1(b).** The diameters of the fuel compacts and the coolant channels are respectively 12.7 mm and 15.875 mm and the distance from a fuel compact center to the adjacent fuel compact centre is 37.6 mm.

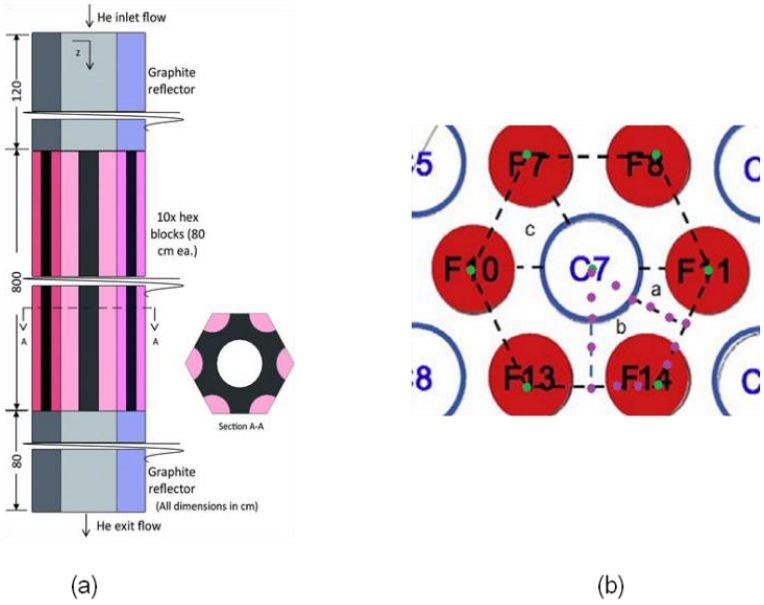

Figure 1 (a) Side and top view of the SCFM (Travis & El-Genk, 2013b); and (b) dashed hexagon outlining SCFM cross sectional area (Sambureni, P 2015).

The temperature distribution, heat flux and flow through the coolant channel of the SCFM were studied by Travis & El-Genk (2013b) using a 3D CFD approach.

In **Figure 1(b)** the different unit cells, namely a, b and c, that can be selected are shown. In this study unit cell b has been chosen as the most suitable and also because Sambureni (2015) has characterised the conduction shape factors required for a 1D analysis. This leads to representing $1/6^{th}$ of an SCFM. The mass flow rate, inlet pressure and inlet temperature were used as boundary conditions. The mass flow rate was assumed to be 0.0306 kg/s and the inlet pressure to be 7.07 MPa, whilst the inlet temperature was assumed to be 914 K. The required material properties that are used are stated in **Table 1**. The total power applied to the SCFM was 55.4 kW which corresponds to a 600 MWth HTGR. Two power profiles were assumed namely a uniform distribution and a (chopped) cosine distribution. In the case of the uniform distribution, a power density of 27.4026 $MWth/m^3$ (Travis & El-Genk, 2013b) was prescribed. In the case of the cosine power profile the power density PD(z) at the distance z from the entrance of the coolant channel is given as:

$$PD(z)=PD\_max*\cos(0.2566*z-0.8831) \quad (1)$$

Where the maximum power density is given as PDmax =33.135 MWth/m^3.

Table 1. Properties of materials used in SCFM of a VHTR (Travis & El-Genk, 2013b)

Property	Material	Correlation
Density, ρ (kg/m^3)	IG-110 graphite	1740
Specific heat, C_p (J/kg.K)		$6.05*10^{-7}T^3 -0.00269T^2 +4.19T -294$
Thermal conductivity, k (W/m.K)		$-13.2 +2.50*10^4/(T+268)^{0.78}$
Density, ρ (kg/m^3)	Composite Fuel	1650
Specific heat, C_p (J/kg.K)		$3.11*10^{-7} T^3 -0.00155 T^2 +2.73 T -82.4$
Thermal conductivity, k (W/m.K)		$8.5 +7.68*10^4/(T+268)^{0.995}$
Density, ρ (kg/m^3)	Helium	P/R_gT
Specific heat, C_p (J/kg.K)		5197.6
Thermal conductivity, k (W/m.K)		0.000258 T +0.103388
Dynamic viscosity, μ (Pa-s)		0.03319 T +13.0744

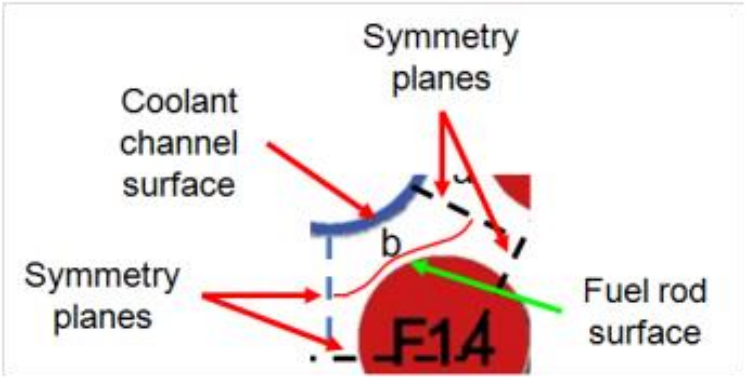

Figure 2 Unit cell for conduction between fuel compact and coolant channel.

1D FLOWNEX

Flownex is a system level simulation tool for the modelling of thermal-fluid systems and is used in many industries in the design and optimization of thermal-fluid systems. Flownex calculates amongst others the flow rates, temperatures, pressures and heat transfer rates using both steady state and transient models (M-Tech Industrial, 2017).

In **Figure,** only a $1/6^{tan}$ of an SCFM is shown and will be modelled in Flownex due to the symmetry in the geometry as stated previously. With the symmetry model used in Flownex, the model will consist of $1/6^{th}$ of a coolant channel, the accompanying graphite matrix and $1/3^{rd}$ of a fuel compact. The basic setup of the Flownex model of the SCFM is described in **Figure 3**. The conduction through the fuel compact is represented by a single conduction element and the conduction through the graphite moderator is represented by two conduction elements. For the conduction through the moderator, represented by the two conduction elements, the conduction lengths and areas needed were calculated by Sambureni (2015). The coolant channel section is characterized by the use of a convection element and a pipe element to represent heat transfer from the coolant channel wall to the coolant fluid, as well as the advective heat transport in the coolant channel. The heat transfer coefficients used in the convection elements were obtained by employing the Nusselt number correlation derived by Travis & El-Genk (2013b).

With the work performed by Nel & du Toit, (2018) the SCFM was discretized into 10 primary increments with each having a length of $\Delta z = 0.8$ m. As the inlet effects need to be accounted for the first increment is divided into ten 0.04 m and one 0.4 m increments respectively which leads to 20 increment layers in total.

As it can be seen in **Figure 4** a model is shown that represents the ten primary increments used to model the SCFM. With the current study, two additional models were constructed where the increment count was increased to 30 and 49. The increased increment count accounts for the increments between 0.4 m and 8 m. Thus, the coarse grid consists of 20 increments, the medium grid of 30 increments and the fine grid of 49 increments. In all three models, the effect of the uniform and cosine power profiles were considered.

3D STAR CCM+

With the 1D model of the SCFM constructed and simulated in Flownex a full 3D model of the SCFM was simulated in STAR CCM+ (2018) to evaluate the results obtained by the 1D simulations. The geometry of the SCFM was constructed in Solidworks 2016 and imported into STAR CCM+ where the necessary

regions and material continua were assigned. As three different materials were used, each material's continua properties were assigned as stated in **Table 1**.

A single mesh continua was constructed for all the components in the model to ensure that the cells faces on the interface between adjacent parts matched to form a conformal mesh. This ensured that no interpolation was necessary for the transfer of information across interfaces. It was found to play an important role in the stability of the solution. A basic base size of 6 mm, based on the radius of the fuel compact, was chosen for the mesh. A number of five prism layers was selected and the layer thickness of all the layers was chosen such that each layer stretched by a factor of 1.2 and the total thickness of the five prism layers together was 0.4 mm. This ensured that the temperature gradients at the interfaces were resolved sufficiently and also assisted with the stability of the solution. The prism layers at the interfaces between the fuel compact and the moderator graphite, and the between the moderator graphite and the coolant channel can be seen in **Figure 5**. The conformal mapping across the interfaces can also be seen.

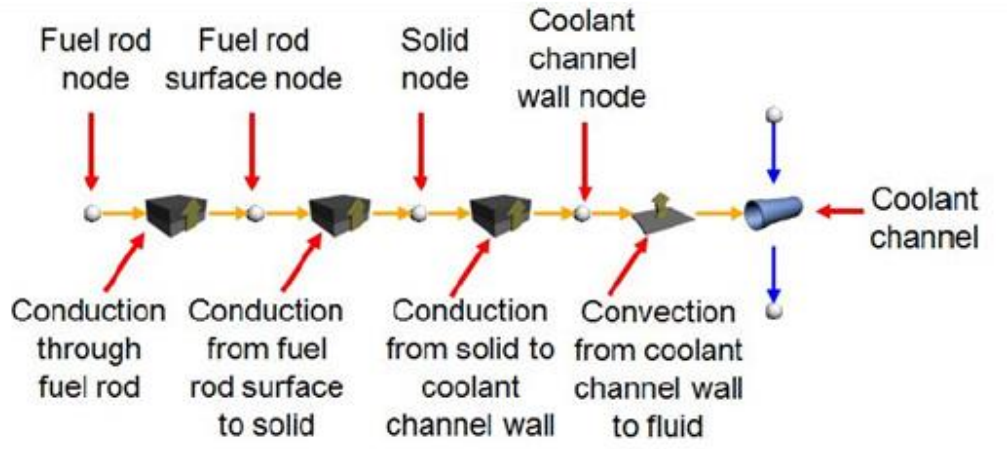

Figure 3 Flownex network for heat transfer from fuel rod and coolant channel

The total length of the 1/6th SCFM model required for the simulations is 9200 mm to account for the top reflector and the height of 8000 mm of the heated section as shown in **Figure 1(a**). Travis & El-Genk (2013b) commented that the 1200 mm length of the reflector is 75 coolant channel diameters which are sufficient for fully developed turbulent flow to occur at the entrance to the heated section.

An extruded mesh was implemented for the $1/6^{th}$ of the SCFM in the full 3D model. The models constructed accounts for three different layer heights for the extrusion that accounts for 1200 mm reflector and the 8000 mm heated section. In the work done by Nel (2018), 11500 layers were extruded with a layer height of 0.8 mm which gives the required 9.2 m of the SCFM. In addition to the 0.8 mm layer height extrusion model

two additional layer height extrusion models of which the heights are 1.6 mm and 0.4 mm were considered. The additional models with different layer heights add up to 5750 and 23000 layers respectively that accounts for the 9200mm height of the 1/6th SCFM. Thus, the coarse grid represents 5750 layers, the medium grid 11500 layers and the fine grid represents 23000 layers.

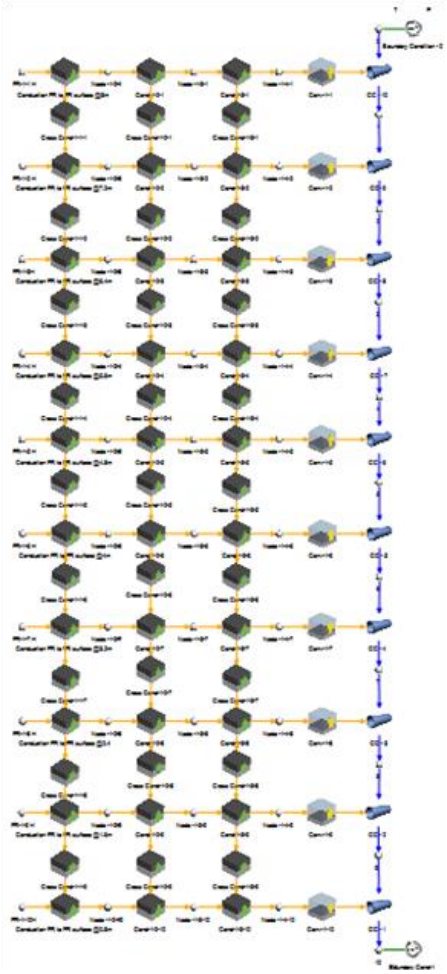

Figure 4 800 mm x 10 increment Flownex model

At the top of the coolant channel, an inlet temperature of 914 K was specified, whilst an outlet pressure of 7.022 MPa was prescribed at the bottom of the coolant channel. The simulation was initialized by specifying a velocity inlet boundary condition of 41.5114 m/s which corresponded to the specified mass flow rate of 0.0051 kg/s. This helped to stabilize the solution during the initial phase of the simulation. Once the solution has stabilized the velocity boundary condition was replaced with the specified mass flow rate condition. The outside surfaces of the fuel compact and the moderator graphite were specified to be adiabatic and the outside surfaces of the coolant channel as symmetry planes.

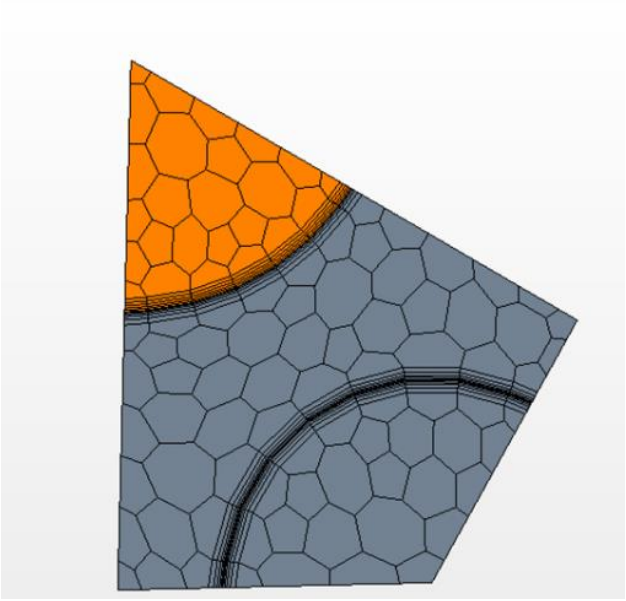

Figure 5 Cross section of STAR CCM+ (Full 3D) mesh.

RESULTS

In the 1D Flownex models the pressure and temperature at the inlet boundary were specified as 7.07 MPa and 914 K respectively. The outlet boundary condition is specified as a mass flow of which the flow rate is 0.0051 kg/s. As for the full 3D STAR CCM+ models the inlet boundary condition is set to be the mass flow rate and inlet temperature and the outlet boundary condition was set to be the outlet pressure. The required results were extracted from the different Flownex and STAR CCM+ models and compared with each other.

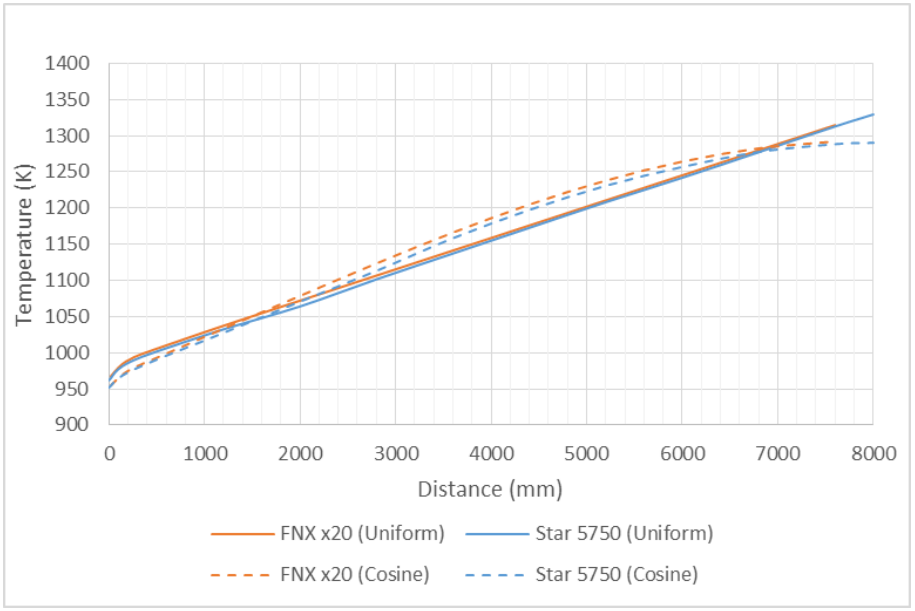

Figure 6 Fuel Compact Center Temperature (Coarse Grid)

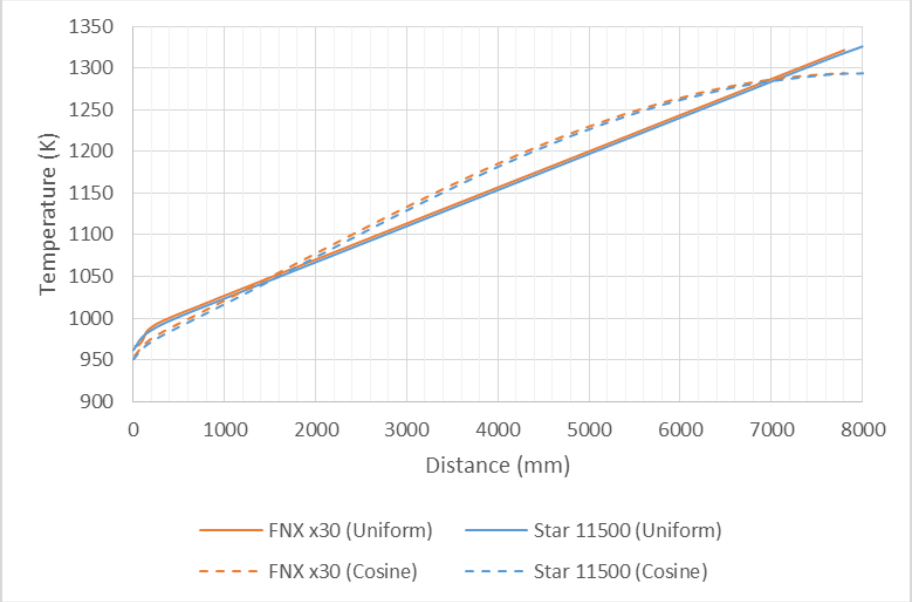

Figure 7 Fuel Compact Center Temperature (Medium Grid)

In **Figure 6**, **Figure 7** and **Figure 8** the comparison of the temperature distributions in the center of the fuel compact for the coarse, medium and fine grids respectively are shown for the uniform and cosine power profiles. The graphs also compares the results of the temperature distribution results obtained by Flownex and STAR CCM+ with each other. As can be seen the results from Flownex and STAR CCM+ are in good agreement with each other for both the uniform and cosine power profile models.

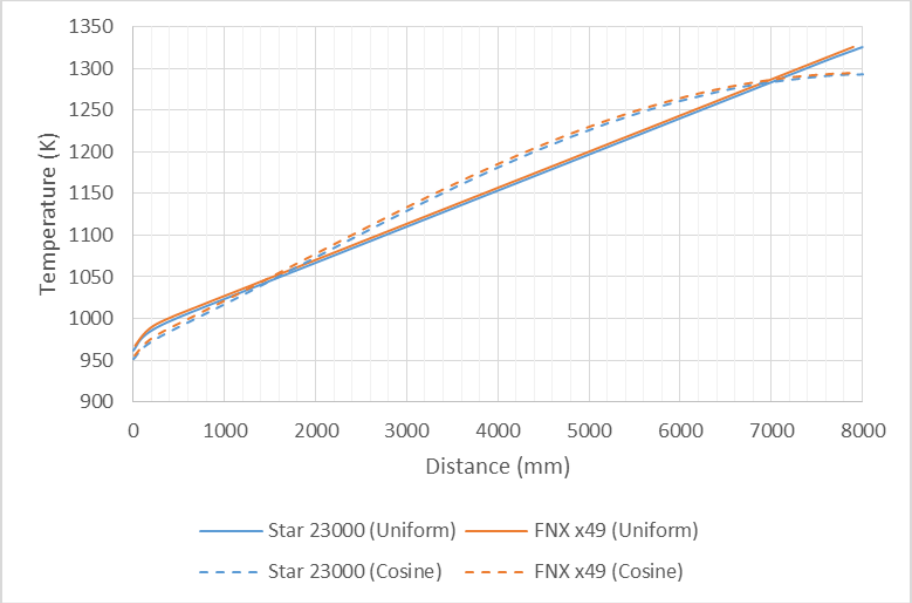

Figure 8 Fuel Compact Center Temperature (Fine Grid)

The next results considers the temperature distribution results for the fuel compact wall at the interface between the fuel compact and the moderator graphite. In **Figure 9** the results are shown for the Flownex and STAR CCM+ models which use a coarse grid for the simulation of the two different power profiles through the SCFM. These results are in very good agreement with each other. It should also be noted that as Travis & El-Genk (2013b) no gap or resistance between the fuel compact and the moderator graphite was considered.

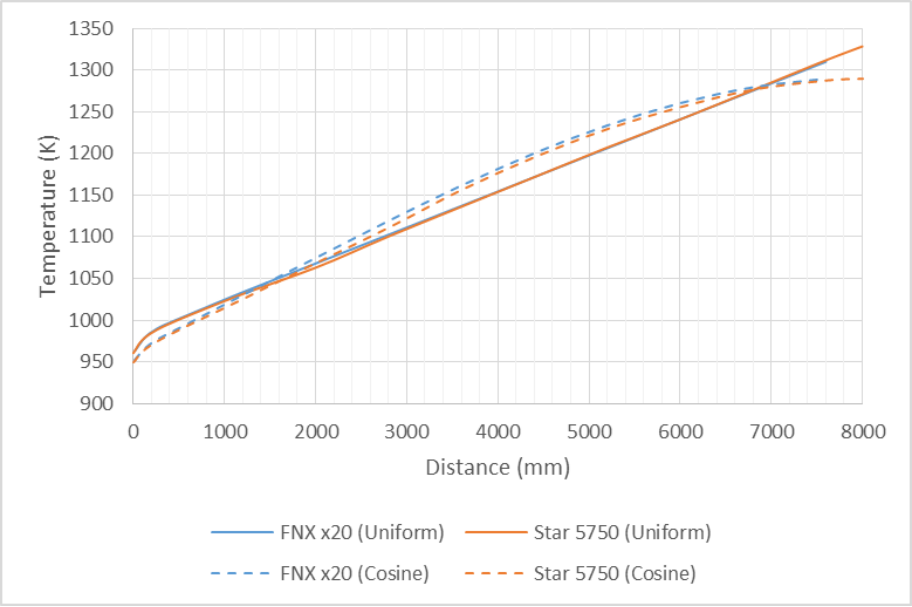

Figure 9 Fuel Compact Wall Temperature (Coarse Grid)

Figure 10 shows the results obtained by the Flownex and STAR CCM+ medium sized mesh model for the uniform and cosine power profiles. These results are also in very good agreement. The results obtained by Flownex and STAR CCM+ for the fine grid sized model for the uniform and cosine power profiles are shown in **Figure 11**. Again, the corresponding results are in very good agreement.

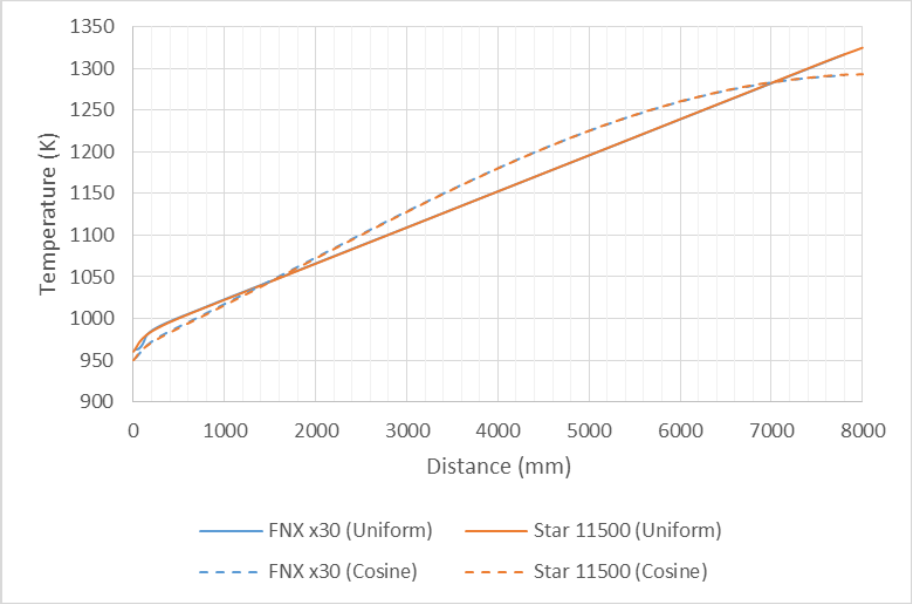

Figure 10 Fuel Compact Wall Temperature (Medium Grid)

Although not shown in the paper, it was found that the bulk temperatures of the fluid predicted by the Flownex and STAR CCM+ models were also in very good agreement.

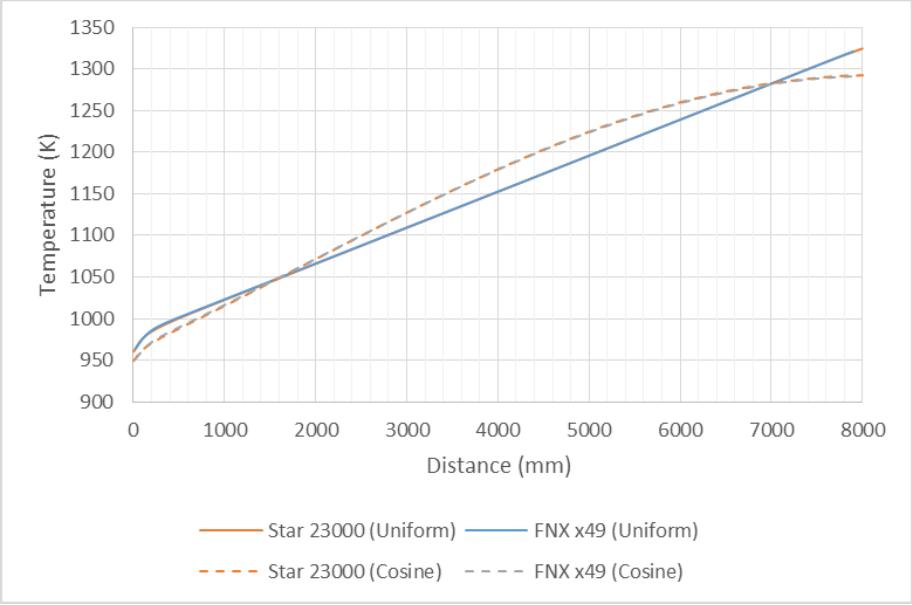

Figure 11 Fuel Compact Wall Temperature (Fine Grid)

With the results obtained by the full 1D and full 3D simulations the temperature distribution results at both the center and the wall of the fuel compact differed by less than 1%. It can therefore be concluded that the 1D Flownex models can predict the temperature distributions in the fuel compact to a very good accuracy.

CONCLUSION

In this paper the development of a full 1D Flownex model and a full 3D STAR CCM+ model of 1/6th of a single-channel fuel module (SCFM) of a prismatic fuel block of a VHTR was discussed. The study is based on work done by Travis & El-Genk (2013b) and Nel & du Toit (2018). A uniform and a cosine power profile were considered in the study. With the results obtained it is was found that the values predicted by Flownex and STAR CCM+ for the temperature distributions at the center of the fuel compact and the wall of the fuel compact are in good agreement with each other. With the difference between the results predicted by the two codes being less than 1%, it can be concluded that the 1D Flownex models can predict the temperature distribution in the fuel compact with sufficient accuracy.

ACKNOWLEDGEMENTS

This work is based on the research supported by the South African Research Chairs Initiative of the Department of Science and Technology and the National Research Foundation of South Africa (Grant No 61059).

Any opinion, findings and conclusion or recommendation expressed in this material is that of the authors and the NRF does not accept any liability in this regard.

NOMENCLATURE

A	Area
Ai	Aicher number
C_p	Specific heat
D	Diameter
k	Thermal conductivity
Nu	Nusselt number
Nu_{FD}	Nusselt number for fully developed flow
P	Pressure
PD	Power density
PD_{max}	Maximum power density
Pr_b	Prandtl number based on bulk fluid temperature
Ra	Rayleigh number
Re	Reynolds number
Re_b	Reynolds number based on bulk fluid temperature
R_g	Gas constant
r	Radial position
T	Temperature
T_b	Bulk fluid temperature
T_w	Wall temperature
z	Axial position
Δz	Length of increment
μ	Dynamic viscosity
ρ	Density

REFERENCES

Travis, B.W., El-Genk, M.S.(2013b) 'Numerical Simulation and Turbulent Convection Heat Transfer Correlation for Coolant Channels in a Very-High-Temperature Reactor', Heat Transfer Engineering, 34, no 1, pp. 1–14

Sambureni, P. (2015) 'Thermal fluid network model for a prismatic block in a gas-cooled reactor using FLOWNEX', Masters Dissertation, North-West University.

M-Tech Industrial (2017), Flownex SE Version 8.8.1.3243, http://www.flownex.com

Nel, G.J., du Toit, C.G. (2018) ‘A System CFD model of a Single-Channel Fuel Module in a Prismatic Block VHTR’, SACAM, vol. 11.

SIEMENS, STAR CCM+ (2018). https://mdx.plm.automation.siemens.com/star-ccm-plus.

Nel, G.J. (2018) ‘Numerical modelling of the flow and heat transfer in a prismatic block VHTR single-channel fuel module’, Masters Dissertation, North-West University.

Johnson, R.W., Sato, H.(2012) ‘Bypass flow computations using a one-twelfth symmetric sector for normal operation in a 350 MWth prismatic VHTR’, Nuclear Engineering and Design, vol. 251, p. 84–91.

Tak, N.I., Kim, M.H., Lee, W.J. (2008) ’Numerical investigation of a heat transfer within the prismatic fuel assembly of a very high temperature reactor’, Annals of Nuclear Energy, vol. 35, p. 1892–1899.

Tung ,Y.H., Ferng, Y.M., Johnson, R.W., Chieng, C.C. (2013) ‘Chieng. Study of natural circulation in a VHTR after a LOFA using different turbulence models’, Nuclear Engineering and Design, vol. 263, p. 206–217.

Tung, H., Ferng, Y.M., Johnson, R.W., Chieng, C.C. (2016) ‘Transient LOFA computations for a VHTR using one-twelfth core flow models’, Nuclear Engineering and Design, vol. 301, p. 89–100.

CHAPTER 3: NUMERICAL SIMULATION OF A REPRESENTATIVE PMR200 REACTOR MODEL IN FLOWNEX (PART 1)

Numerical simulation of a representative PMR200 Reactor model in Flownex (Part 1)

GJ Nel*, CG du Toit

Unit for Energy and Technology Systems

North-West University

Private Bag X6001

Potchefstroom 2520

South Africa

Tel: +27 18 299 1322

Fax: +27 18 299 1320

Cell: +27 82 856 4200

Corresponding author email: Jat.DuToit@nwu.ac.za

ABSTRACT

The heat transfer through the core of a Very High Temperature Reactor (VHTR) is important in the normal operation of the reactor. The two main types of VHTR's are a PBMR (Pebble Modular Reactor) and a PMR (Prismatic Modular Reactor). In this study, the PMR200 reactor without the attached RCCS (Reactor Cavity Cooling System) is used with a multi-hole prismatic block core with integrated bypass and cross flow channels and with helium as cooling fluid. The heat transfer considered will consist of Conduction, Convection and Radiation heat transfer. With the development of different simulation models in different computational codes there is still a need for representative simulation models that incorporates a full reactor and that is still computationally feasible with accurate approximate results. The paper will discuss a system CFD (Computational Fluid Dynamics) model that simulates the different heat transfer elements and fluid flow. A representative Flownex model of the whole PMR200 reactor is constructed and used to obtain temperature distributions and fluid distributions. Results are extracted and compared to research of similar nature. The representative system CFD model uses much fewer resources compared to partial fuel block models in 1D/3D and 3D simulation models. The current model is compared to other research done on different sections of the core that is modelled in different simulation codes, 1D and 3D models alike.

Keywords:

PMR200; Prismatic fuel block; heat transfer; conduction; convection; 1D modelling

1. Introduction

Very High Temperature Gas-Cooled Reactors are included in the generation IV design category for nuclear reactors/plants (World Nuclear Association (2020)). These reactors can reach up to 600 MW_{th} and can produce an outlet helium temperature of between 900-1000℃. Operating pressures can also vary between 4 MPa to 9 MPa. There are two types of VHTR reactor designs considered, namely the PBMR (Pebble Bed Modular Reactor) and the PMR (Prismatic Modular Reactor) designs (IAEA 2010). The reactor model considered for the current study is the PMR200 model (Jo et al., 2008) with a multi hole prismatic block core configuration (Ribeiro et al., 2013). The core of the reactor is made up of prismatic fuel blocks stacked on top of each other with the height per layer/block being 0.793 m. On top of the active core assembly a Top Reflector and Top Head Plenum is placed whilst at the bottom of the assembly a Bottom Reflector, Bottom Plenum and Bottom Support is used. TRISO Particles are embedded in the fuel compacts that make up the fuel rods that are used in the reactor.

Different thermal-fluid phenomena will occur within the different components of a prismatic reactor, with such components including the fuel compacts, coolant channels, graphite blocks and the bypass and cross flow gaps between the different graphite blocks. Due to the amount of associated detail that is considered (geometric features, fluid flow, temperature distributions, heat transfer, etc), 3-dimensional simulations of the full reactor require extensive computational resources that are not generally available. Therefore, much research has been done by employing 3D explicit models (Ribeiro et al., 2013; Tak et al., 2008), which account for only parts of a reactor and generate detailed results but only for the partial reactor, fuel block or fuel assembly models simulated. A 1D system simulation approximation of a full or partial reactor, core, fuel block or fuel assembly generates results that are representative of the thermal hydraulic characteristics of the reactor or core (Sambureni, 2015; Khoza, 2019). Although the results are not as detailed as in the case of 3D simulations, the results that are obtained are very informative, and the computational resources needed for the full 1D representative reactor is much less than that required for the full and partial 3D simulations.

Travis et al. (2013) performed a 3D numerical simulation using STAR CCM+ of a single flow channel module of a prismatic VHTR core. Results obtained were used to develop a turbulent convection heat transfer correlation. The correlation accounts for the entrance mixing length that increases the local heat transfer coefficient. When the fluid flow in the coolant channel is represented in a 1D simulation code and the conduction/solid elements are represented in a 3D code, the two models can then be coupled to represent one model to account for the fluid flow, convection and conduction heat transfer. The developed convection heat transfer correlation is used in the 1D code for the fluid flow characteristics calculations. With the combination of the 1D and 3D codes for the model simulation the meshing time and computational time decrease without a significant effect on the accuracy of the numerical results.

Travis et al. (2013) also studied the thermal flow characteristics of a VHTR and the corresponding fuel elements. The analysis includes and excludes the bypass flow between different fuel blocks, as well as between control rods and their corresponding graphite containment hole of the VHTR and fuel elements. Results from a $1/6^{th}$ VHTR core single layer height (0.793 m) with and without bypass flow were extracted. More results were also extracted from a model that accounted for the full height (9.93 m) of the $1/6^{th}$ VHTR core without bypass flows. A more efficient methodology was also followed by coupling the 1D helium flow in the coolant channels with the more detailed conduction components in the 3D Star CCM+ model. They extracted accurate results from the 1D/3D coupling analysis and the computational power required was also reduced using this methodology.

Ribeiro et al. (2013) used the CFD code ANSYS CFX 14.0 to numerically evaluate prismatic multi-hole and annular VHTR fuel elements. A $1/12^{th}$ of a fuel element/block was used to generate the results and the results of the assemblies were compared with each other and the numerical validation was done through the energy balance. The numerical results generated are in good agreement with the theoretical values of both the multi-hole and annular models.

Tak et al. (2008) considered $1/12^{th}$ of a fuel assembly to evaluate fluid flow and temperature distribution employing a 3D CFD simulation. A Unit cell approach to evaluate heat transfer and other thermal phenomena is widely applied in the different analysis of the prismatic VHTR (Tak et al., 2008; Du Toit et al, 2015). The results from the 3D analysis are compared with the results obtained using a unit cell analysis and it is observed that the unit cell approach under predicts the maximum fuel temperature as the bypass gaps are increased in size. Thus, the more detailed partial 3D analysis is more accurate to predict different thermal-fluid variables than that of a unit cell analysis. But the unit cell analysis can provide reasonable approximations for practical situations.

Tak et al. (2011) developed a practical method for the analysis of a core of a prismatic gas cooled reactor. This method entails using a combination of CFD and a system approach that uses far less computational resources than a full 3D CFD approach. The CFD part accounts for the conduction part of the system and the one-dimensional approach accounts for the fluid flow in the system. The complex geometries are represented by a collection of purposed designed unit cells. The approach that is followed provided accurate results. Calculation time and computational resources were also reduced significantly using this approach.

Jun et al. (2007) performed steady state and limiting accident analyses on a $200MW_{th}$ PMR which is one of the scale down prototype reactor models proposed for an NHDD (Nuclear Hydrogen Development and Demonstration) plant. The analysis for the steady-state conditions was done using the GAMMA+ code (Lim et al., 2006). Key design parameters of the steady-state conditions are provided, such as the peak fuel

temperatures, RPV temperature, control rod (CR) bypass flow, reactor cooling system flow rates and the heat that is lost to the RCCS.

Steady state and transient state analyses were performed by Jun et al. (2009) on the PMR200 reactor system. The steady state and transient analyses were done at LPCC (Low Pressure Conduction Cooling) and HPCC (High Pressure Conduction Cooling) conditions. A prismatic core is used with 6 layers of fuel blocks and with an air cooled RCCS system and VCS (Vessel Cooling System) system. The thermal-fluid analysis of the 200 MW^{th} reactor was performed using GAMMA+ (Lim et al., 2006). Gamma+ was able to simulate 11 of the 66 fuel assemblies, as the core cross section has a symmetry of 1/6, to reduce the number of flow paths. Maximum temperature results are extracted from the fuel elements and the RPV, as well as other flow characteristics in the coolant flow components.

Sambureni (2015) studied time dependence with regards to the validity of the Fourier and Biot numbers on a rectangular block using Flownex and Star CCM+. A good comparison was achieved between the results obtained by the two codes which verified that Flownex can give good results for pure radial conduction. The different grid sizes of a triangular block were also tested in Flownex and an optimal grid size of 11 radial direction nodes and 5 tangential direction nodes were chosen for her models. A unit cell was developed to characterise the heat transfer from the wall of a fuel rod hole to the wall of the adjacent coolant channel wall. Sambureni also studied to see if a system CFD model can be constructed to simulate one-sixth of a single hexagonal prismatic fuel block of an HTR (High Temperature Reactor). The results obtained with the integrated system CFD model of the $1/6^{th}$ of a prismatic block were compared with the corresponding results of a 3D model of a $1/12^{th}$ prismatic block that was simulated in Star CCM+. The heat transfer and temperature distributions were compared, and it was found that the results were in good agreement. Thus, Sambureni concluded that Flownex can be used to build advanced integrated models of a prismatic block reactor.

A $1/6^{th}$ of a standard fuel block, a complete fuel block and an assembly of three standard fuel blocks) of an HTR were the main models to be simulated in Flownex by Khoza (2019. For the construction of the $1/6^{th}$ of a fuel block Khoza (2019) made use of data from the unit cell for heat transfer between the fuel rods and coolant channels developed by Sambureni (2015). With the grid size of the model, only a maximum of three standard fuel blocks could be stacked in Flownex due to memory and GUI restrictions. Temperature distribution results were extracted and was compared to similar results obtained by the CORONA (Core Reliable Optimization and thermo-fluid Network Analysis) system CFD code (Tak et al., 2014). For the modelling of the fuel block/s, the plugs of the block were not modelled in Flownex, and the bypass and cross flows were included in the models. The maximum temperatures of the fuel, coolant channel and graphite increased as the gap width was increased. Khoza (2019) concluded that Flownex can solve the fundamental conservation and heat transfer relations as applied to a prismatic core fuel block.

Nel et al. (2018) modelled 1/6th of an SCFM (Single Channel Fuel Module) which consists of 1/6th of a coolant channel and a third of a fuel rod. For the construction of the 1/6th of an SCFM. Nel et al. (2018) made use of data from the unit cell for heat transfer between the fuel rods and coolant channels developed by Sambureni (2015). They studied the heat transfer coefficient and temperature distribution in the SCFM applying uniform and cosine power profiles. They used different Nusselt number correlations (Travis et al. (2013)) in their 1D Flownex simulations and compared the results to the corresponding results obtained from a 3D CFD Star CCM+ simulation model. This 1D model is one of the most basic fluid flow simulations that can be performed in the study of a prismatic fuel block.

In this study, a new one-dimensional SCFD (System Computational Fluid Dynamics) axi-symmetric model is constructed in Flownex of the PMR200 reactor. The model that is constructed will be a representation of the full PMR200 reactor which includes all six layers of the active fuel core, as well as the top head plenum, top reflector, the bottom reflector, bottom plenum and bottom support. The model representation of the axi-symmetric model is based on the representative SCFM model constructed by Nel et al. (2018 & 2019). The model also accounts for the central and side reflectors, as well as the core barrel (CB) and reactor pressure vessel (RPV). Bypass flows and cross flows between the different assembly blocks and the fuel elements are also included in the model. Although the reactor model will have the capability to be linked to a model of the reactor cavity cooling system (RCCS), it will not be done in this study.

The study progressed from an SCFM to a single representative fuel block, then a single fuel assembly and finally to a full representative core, allowing selected fluid flow characteristics and temperature distributions to be extracted from the calculated results and relevant details to be presented and evaluated Nel et al. (2018 & 2019). With the different flow paths for the helium fluid through the coolant, control rod and bypass channels the mass flow rates are extracted and compared with similar results obtained by (Jun et al., 2009). Maximum temperatures from different sections of the reactor such as the fuel compacts and the coolant of the reactor are also extracted. Average temperature distributions from the core barrel, vessel cooling cavity/system and reactor pressure vessel are also obtained and presented.

2. PMR200 Overview

The PMR200 reactor, illustrated in Fig. 1, generates 200 MWth heat which correlates to a power density of 25.9925 MW/m^3 within the fuel compacts. The inlet boundary conditions for the helium coolant are a mass flow rate of 83.38 kg/s at an inlet temperature of 490°C with and a corresponding inlet pressure of 7 MPa. The nominal outlet temperature of the coolant is 950°C.

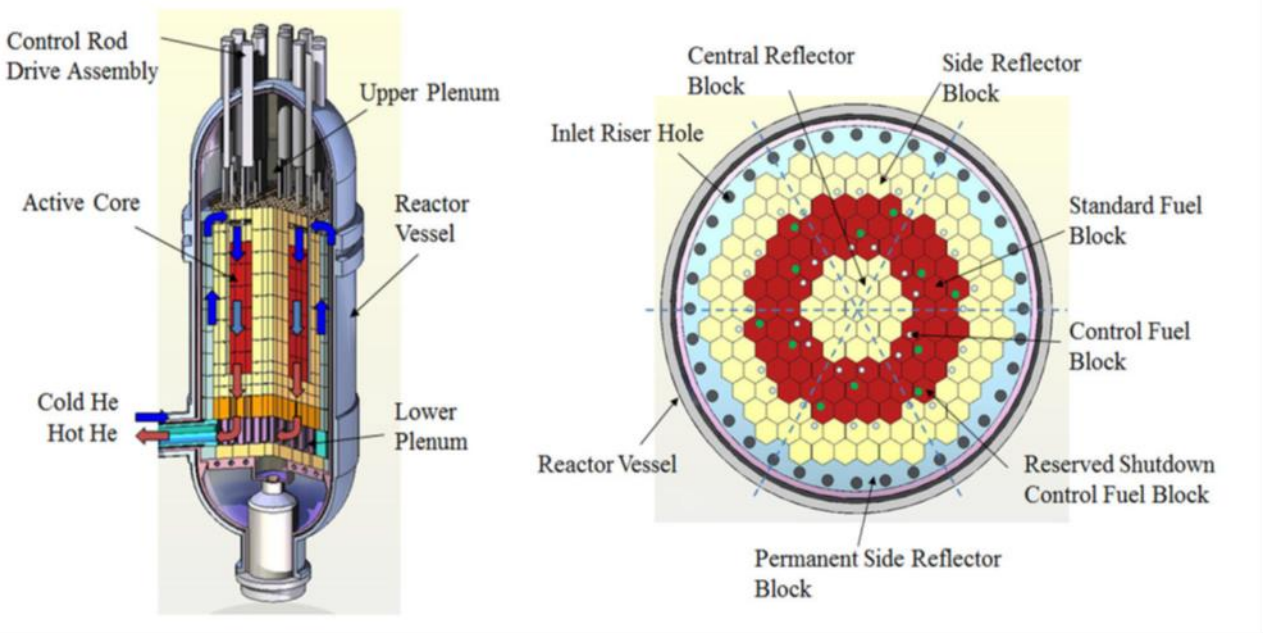

Fig. 1: Layout of PMR200 reactor and cross-section through active core (Tak et al., 2014).

The PMR200 reactor is part of the VHTR design category that is based on the GT-MHR (Gas Turbine Modular Helium Reactor). The PMR can make use of two different types of designs of the prismatic fuel blocks namely an annular design or a multi-hole design (Ribeiro et al., 2013). In the multi-hole fuel block design, the helium flows in separate coolant channels parallel to the fuel rods whereas in the annular design the helium flows in annular channels around the fuel rods. For the current study, only the multi-hole prismatic fuel block design shown in Fig. 2 is considered.

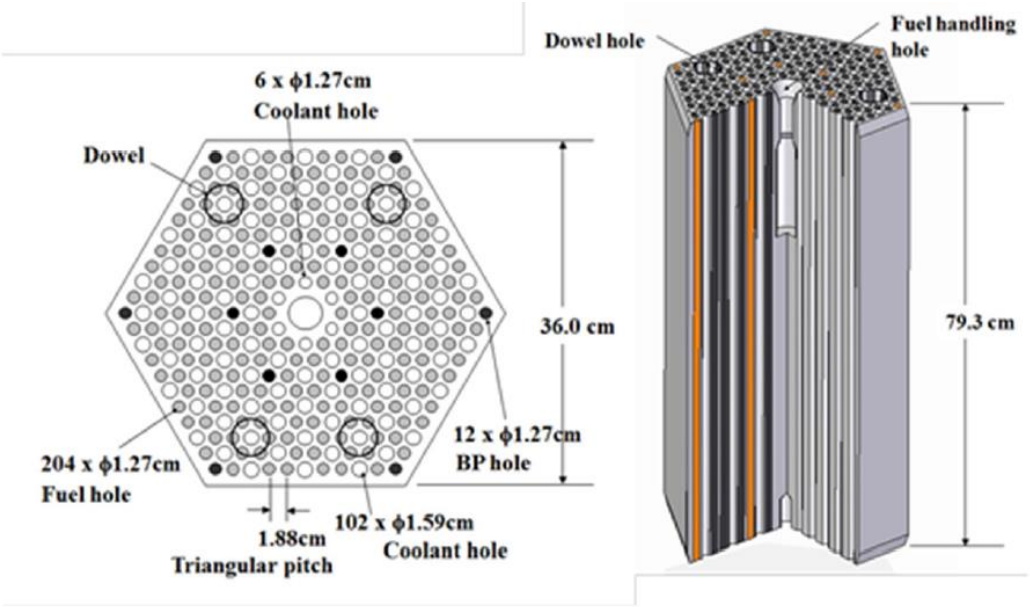

Fig. 2: Typical Prismatic Reactor Fuel Block (Tak et al., 2014).

The core of the PMR200 reactor consists of hexagonal fuel blocks that are stacked to form multiple fuel assemblies for the active core and multiple non-fuel graphite block assemblies for the inner and outer reflectors of the core as seen in Fig. 1. In the PMR200 the helium coolant enters the reactor at the bottom and flows upwards through inlet riser tubes situated in the outer permanent reflector to the top of the reactor. Then the helium flows downwards through the different coolant, bypass and control rod channels to the bottom of the reactor and then it exits through the lower plenum (Tak et al., 2011).

The core of the reactor is enclosed in the core barrel which in turn is enclosed in the RPV (Reactor Pressure Vessel). Between the core-barrel and the RPV is a helium gap known as the VCC (Vessel Cooling Cavity) when the flow is assumed to be stagnant, and the VCS (Vessel Cooling System) if the flow is assumed to be active. The VCS assists in cooling the core-barrel and the RPV along with the RCCS to maintain the temperature of the RPV to below its maximum allowable operating temperature of 371°C (Jun et al., 2009). The VCS operates with inlet conditions set at 140°C for the inlet temperature and inlet mass flow of 2.0 kg/s.

3. Flownex

A reactor such as the PMR200 can be represented by a network model consisting of a collection of one-dimensional components (Du Toit and Rousseau, 2012). The different Flownex components (M-Tech Industrial, 2021) that can be used to model the relevant thermal-fluid phenomena present in the PMR200 reactor are depicted in Fig. 3.

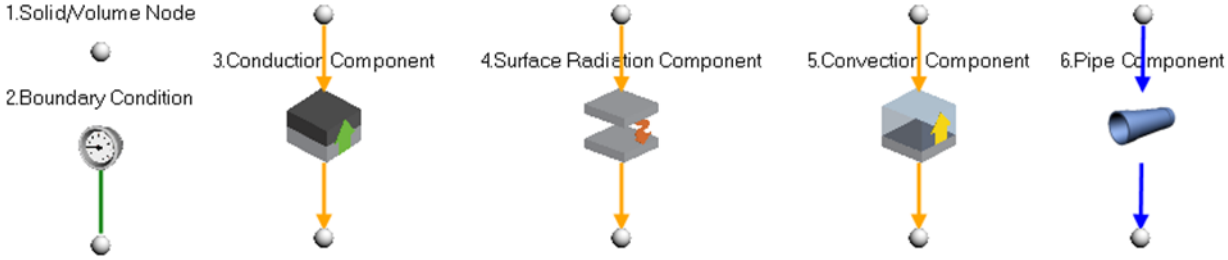

Fig. 3: Different Flownex Components

The flow in the inlet risers, coolant channels, bypass and cross flow gaps and vessel cooling system can be represented by pipe components (Fig. 3(6)). The equation for the conservation of mass in the pipe components is given as (M-Tech Industrial, 2021):

$$\frac{\partial \bar{\rho}}{\partial t} \forall + \dot{m}_e - \dot{m}_i = 0 \qquad (1)$$

Where $\bar{\rho}$ is the averaged density in the pipe, $\forbidden{V}$ the volume of the pipe, $\dot{m}$ the mass flow rate and *e* and *i* respectively denote the exit and inlet of the pipe. Secondly, the equation for the conservation of momentum in the pipe is expressed as (M-Tech Industrial, 2021):

$$\frac{L}{A}\frac{\partial}{\partial t}\left(\dot{m}\right)+\left(p_{0,e}-p_{0,i}\right)+\bar{\rho}g\left(z_e-z_i\right)+\left[\left(\frac{fL}{D_H}+K\right)\cdot\frac{\left|\dot{m}\right|\dot{m}}{2\bar{\rho}A^2}\right]=0 \qquad (2)$$

Here *L* is the length and *A* the cross-sectional area of the pipe, p_0 is the total pressure, *g* the gravitational acceleration, *z* the elevation, D_H the hydraulic diameter and *K* the form loss factor. The Darcy-Welsbach friction factor *f* is obtained using the modified Colebrooke-White (Streeter and Wylie, 1979). Lastly the equation for the conservation of energy for the pipe is given as (M-Tech Industrial, 2021):

$$\frac{\partial}{\partial t}\left(\bar{\rho}h_0\right)\forbidden{V}+\dot{m}\left(h_{0,e}-h_{0,i}\right)=\dot{Q}-\dot{m}g\left(z_e-z_i\right)+\frac{\partial p}{\partial t}\forbidden{V}+\Delta p_L\cdot\frac{\dot{m}}{\bar{\rho}} \qquad (3)$$

Where h_0 is the total enthalpy, *p* the static pressure and Δp_L the frictional loss. The second term on the right-hand-side represents the gravitational work and the last term the frictional work respectively done by the moving fluid.

The convection heat transfer between the fluid in the pipe components and the associated solid structures is represented by the convection component (Fig. 3(5)). The convection heat transfer $\dot{q}_{conv}$ to the fluid is given as (M-Tech Industrial, 2021):

$$\dot{q}_{conv}=-hA\left(T_f-T_s\right) \qquad (4)$$

Here *T* is the temperature and *s* and *f* refer respectively to the surface of the solid and fluid. *A* is the contact area and *h* is the heat transfer coefficient. The heat transfer coefficient is obtained from the Nusselt number Nu with $h=\mathrm{Nu}\,k_f/D_H$ where k_f is the thermal conductivity of the fluid. The Nusselt number is calculated using the Gnielinski correlation (Incropera and DeWitt, 1996).

The conduction heat transfer through the solids is represented by the conduction component (Fig. 3(3)). The conduction heat transfer $\dot{q}_{cond}$ is obtained using (M-Tech Industrial, 2021):

$$\dot{q}_{cond} = -\frac{k_s A}{L}\left(T_e - T_i\right) \qquad (5)$$

Where *A* and *L* are respectively the conduction area and length and k_s is the thermal conductivity of the solid.

The radiation heat transfer across the gaps between the fuel rods and the fuel hole and the radiation heat transfer across the gap between the core barrel (CB) and the reactor pressure vessel (RPV) is represented by the radiation component (Fig. 3(4)). The surface-to-surface radiation heat transfer from surface A_i to surface A_e is given by (M-Tech Industrial, 2021):

$$\dot{q}_{rad} = -\frac{\sigma\left(T_e - T_i\right)}{\frac{1-\varepsilon_i}{\varepsilon_i A_i} + \frac{1}{A_i F_{ie}} + \frac{1-\varepsilon_e}{\varepsilon_e A_e}} \qquad (6)$$

Here σ is the Stefan-Boltzmann constant, ε the emissivity and F_{ie} the view factor from surface *i* to surface *e*.

Flownex employs a finite volume-based implicit pressure correction method (Greyvenstein, 2002) to obtain the solution of the conservation equations. Flownex has been certified as being ASME NQA-1 compliant (Flownex, 2019). The relevant helium and solid properties are calculated by Flownex using the information provided by Jun (2020), and values of the fluid properties are based on the local temperatures.

4. Single- Channel Fuel Module

Looking closely at the cross-section of the prismatic fuel block in Fig. 2 it can be observed that typically a coolant channel is surrounded by six fuel holes containing the fuel rods, each made up of several fuel compacts. A small gap exists between a fuel rod and the wall of the associated fuel hole. Travis and El-Genk (2013) depicted the coolant channel and the surrounding six 1/3rd rods as a single channel fuel module (SCFM) as indicated by the dashed hexagon in Fig. 4. The SCFM can be divided into six identical quadrilaterals as indicated by the inner dashed lines. A quadrilateral defines the unit cell described by Sambureni (2015) to characterise the heat transfer between the wall of a fuel hole and the wall of an adjacent coolant channel. The unit cell can be duplicated to represent a full representative fuel block.

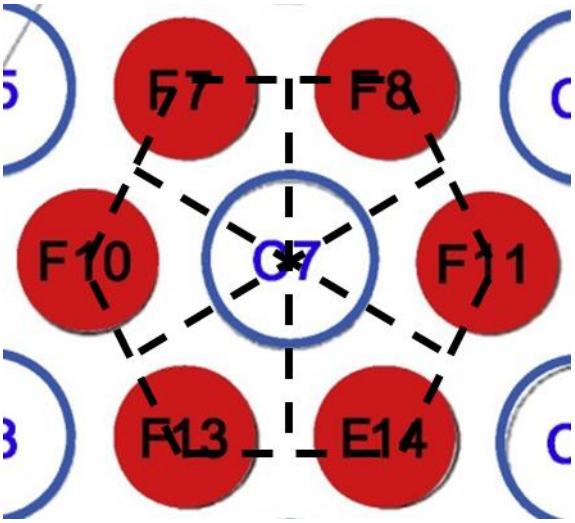

Fig. 4: Single Channel Fuel Module. Adapted from Sambureni (2015).

Calculating the conduction form factors for the conduction heat transfer from the fuel hole wall to the graphite and from the graphite to the coolant channel wall, Sambureni (2015) found that for a PMR200 fuel block the heat transfer $\dot{q}_{fg}$ from the fuel hole wall to the graphite can be expressed as:

$$\dot{q}_{fg} = -\frac{k_s A_{fg}}{L_{fg}}\left(T_g - T_{fw}\right) \qquad (7)$$

Where $A_{fg} = 8.8321\times10^{-3}\ \mathrm{m}^2/\mathrm{m}$ are the equivalent conduction area per unit axial length and $L_{fg} = 1.6309\times10^{-3}\ \mathrm{m}$ the conduction length. The graphite is denoted by *g* and the fuel hole wall by *fw*. The heat transfer $\dot{q}_{gc}$ from the graphite to the coolant channel wall is expressed as:

$$\dot{q}_{gc} = -\frac{k_s A_{gc}}{L_{gc}}\left(T_{cw} - T_g\right) \qquad (8)$$

Here $A_{gc} = 8.8321\times10^{-3}\ \mathrm{m}^2/\mathrm{m}$ is the equivalent conduction area per unit axial length and $L_{gc} = 2.8691\times10^{-3}\ \mathrm{m}$ the conduction length. The coolant wall is denoted by *cw*. It can be seen that a fuel rod has three-unit cells associated with it and that a coolant channel has six-unit cells associated with it.

Fig. 5 shows a network of conduction, radiation, convection and pipe components to model the heat transfer from a fuel rod to a coolant channel. The fuel rod is discretized into three concentric increments.

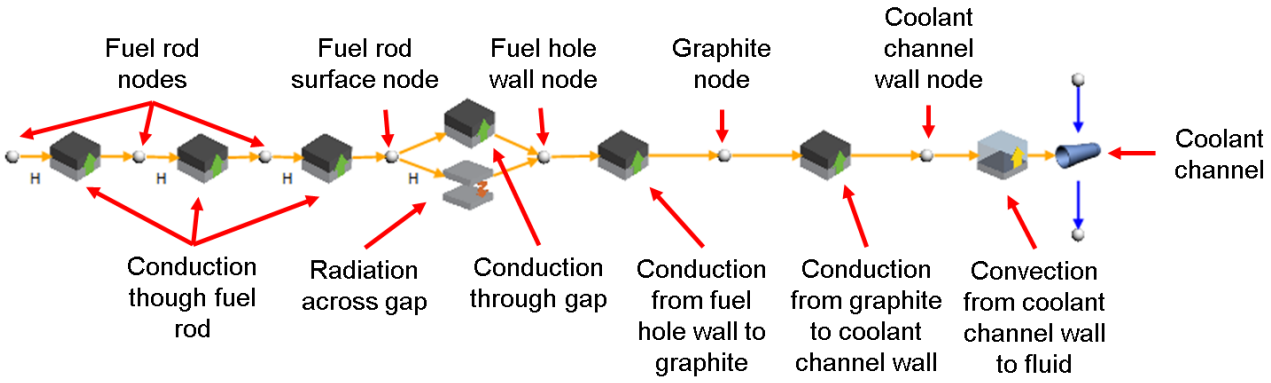

Fig. 5: Network for heat transfer from fuel rod to coolant channel.

5. Single Prismatic Fuel block

Sambureni (2015) created a 2D network model of a sixth of a fuel block by discretizing the block in the radial and tangential directions and employing a single increment in the axial direction. Fig. 6 shows a schematic of a 3 (radially) x 3 (tangentially) network. The solid nodes represent the graphite control volumes (CV) and conduction elements (components) that account for the conduction heat transfer between the graphite CVs. The flow elements represent the bypass gap and the convection elements account for the convection heat transfer from the graphite to the bypass gap.

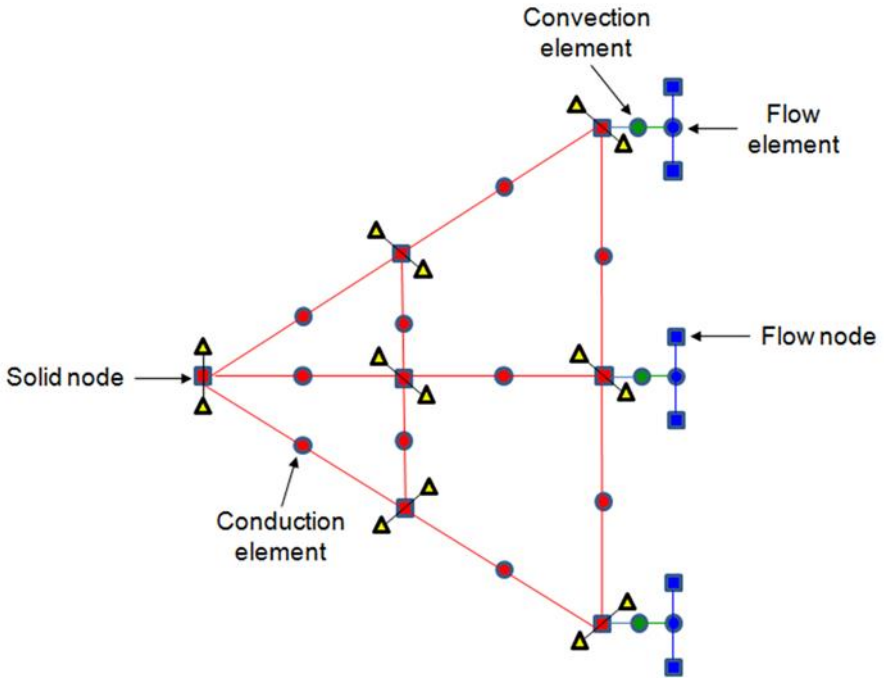

Fig. 6: Schematic layout of network for sixth of a fuel block

One of the triangles linked to a solid node represents the conduction, convection and pipe components for the heat transfer from the graphite to the coolant shown in Fig. 5. The other triangle represents the conduction and radiation components for the heat transfer from the fuel rods to the graphite shown in Fig. 5. Sambureni (2015) assumed the coolant channels and fuel holes to be uniformly distributed over the cross-section of the fuel block. The pipe component associated with a solid node is thus representative of the coolant channels contained in the CV. Similarly, the fuel rod or hole is representative of the fuel rods or holes contained in the CV. Sambureni (2015) did not model the fuel rods but applied the heat released by the fuel rods directly to the node representing the fuel hole wall. The temperatures obtained by Sambureni (2015) represent the axially average temperatures for a fuel block. Sambureni (2015) found that a sufficiently grid independent solution could be obtained using an 11 x 5 network.

Khoza (2019) extended the fuel block model of Sambureni (2015) by discretizing the sixth of a fuel block into three axial increments, thus creating a 3D network model, to also account for the axial temperature distribution and the associated axial heat transfer. Khoza (2019) modelled the fuel rods and found that discretizing the fuel rods into three concentric increments provided sufficiently accurate results. A uniform volumetric heat source was applied to the rods. The temperatures obtained by Sambureni (2015) and Khoza (2019) were compared with the temperatures obtained by a 3D simulation of one twelfth of a fuel block. The three sets of results were in good agreement with the 3D simulation providing finer detail.

Khoza (2019) extended the sixth of a fuel block model to simulate a full fuel block, as well as an assembly of three fuel blocks. Due to the complexity of constructing the models, Khoza (2019) could only construct a PMR200 fuel assembly consisting of six fuel blocks by stacking six of the sixth of fuel block models. Although Khoza (2019) demonstrated that Flownex could be used to construct 3D network models of fuel blocks, the complexity of the models renders them impractical in the context of Flownex to create a network model of a full reactor that could be incorporated efficiently into a systems model of a nuclear power plant.

To address this issue a 1D network model of a fuel block was developed in this study. The 1D model consists of three axial increments each representing a CV. Each CV contains only one graphite node as shown in Fig. 7 with the axial conduction components accounting for the heat transfer between the CVs.

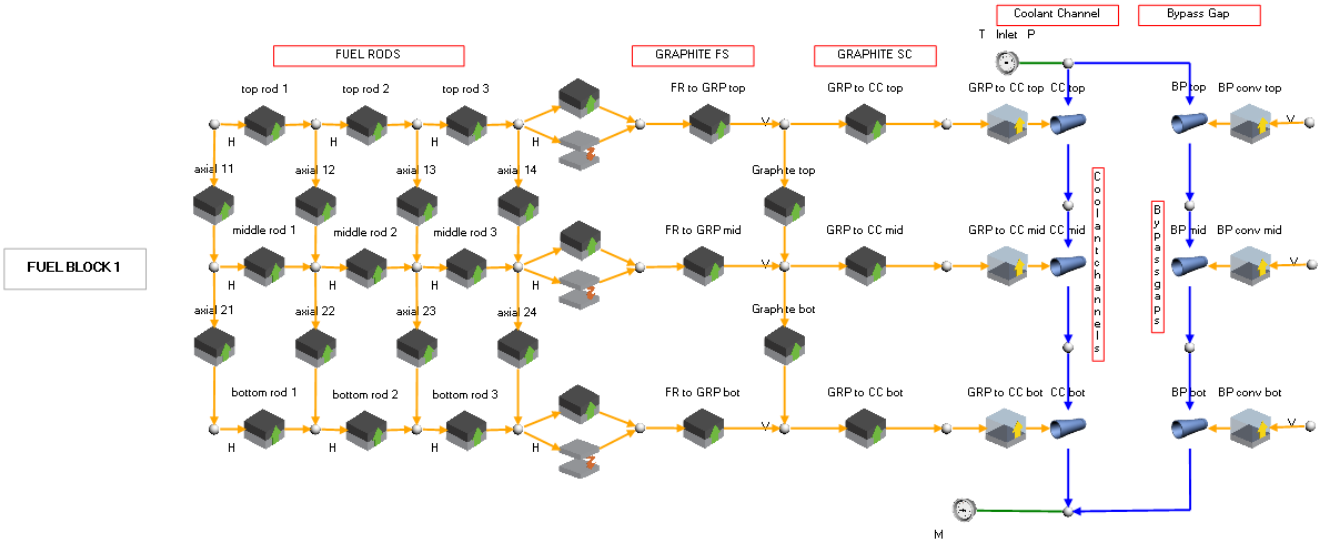

Fig. 7: Single Representative Fuel Block.

On the left-hand side of the graphite nodes and conduction components in Fig. 7 are the radial and axial conduction components (top rod, middle rod & bottom rod) of a discretized representative fuel rod, the conduction and radiation components for the heat transfer across the fuel rod gap and the conduction components for the heat transfer from the fuel hole wall to the graphite. The 210 fuel rods in a fuel block are represented by one representative fuel rod. The representative fuel rod is discretized into three conduction components in the radial direction and three conduction components in the axial direction. A volumetric heat source is applied at each representative fuel rod node to account for the heat generated by the 210 fuel rods. On the right-hand side of the graphite nodes and conduction components are the conduction and convection components for the heat transfer from the graphite to the coolant and the pipe components to model the representative coolant channel. The coolant channel represents the 108 coolant channels in the fuel block. On the far right hand side are the pipe components to represent the bypass gap and the convection components for the convection heat transfer from the graphite nodes to the bypass gap. The nodes on the right-hand side are copies or views, as indicated by the "v" next to each node, of the graphite nodes. The boundary condition components (Fig. 3(2)) are employed to specify the pressure and temperature at the inlet and the mass flow leaving the domain at the outlet. Table 1 gives a summary of the comparison between selected average temperatures at mid-level in the fuel block as obtained by the 1D, 2D and 3D Flownex models. The case considered is similar to a fuel block situated in the top layer of the active core of the PMR200 reactor.

Table 1: Average temperatures for mid-level of fuel block.

	1D	2D	3D
Fuel centre (°C)	604.5	-	605.7

Fuel hole wall (°C)	599.1	602.0	601.6
Graphite (°C)	595.1	597.9	596.2
Coolant channel wall (°C)	515.6	516.1	517.2

The agreement between the three sets of results is very good with the maximum difference being 0.5%. These results confirm the ability of the 1D fuel model to simulate the heat transfer in a fuel block.

6. Single fuel assembly

As further validation of the 1D fuel block model, a model of the single fuel assembly consisting of six stacked fuel blocks simulated by Tak et al. (2014) and Khoza (2019) was constructed. Along with the bypass gap, the crossflow gaps between successive fuel blocks were included in the model. The fuel assembly model was constructed by stacking six of the fuel blocks shown in Fig. 7. The cross gaps were modelled by linking the coolant channel nodes between fuel blocks with appropriate pipe components to the corresponding bypass gap nodes as shown in Fig. 8. It should be noted that following Khoza (2019) the length of the fuel rods were assumed to be the same as the height of the fuel block. The graphite plugs at the top and bottom of the fuel rods (Tak et al., 2014) were therefore not accounted for.

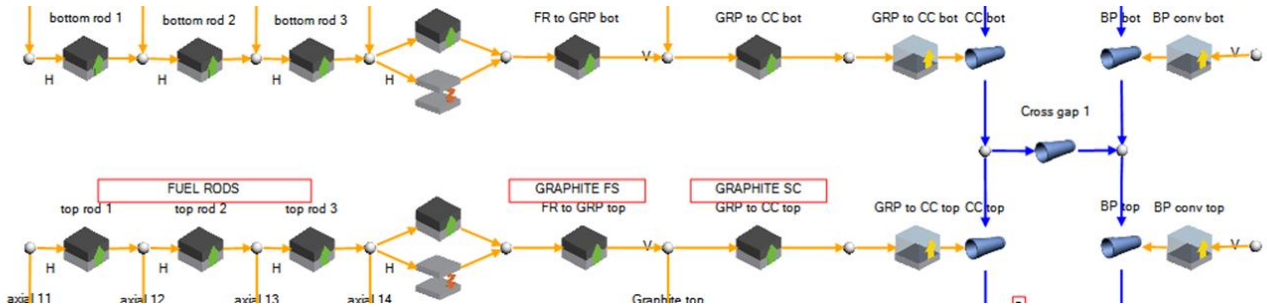

Fig. 8: Cross gap between adjacent fuel blocks.

Tak et al. (2014) modelled the fuel assembly employing the commercial code CFX and the in-house code CORONA. They found the agreement between corresponding results predicted by CORONA and CFX very good and concluded that the conjugate heat transfer in fuel blocks could be simulated using CORONA.

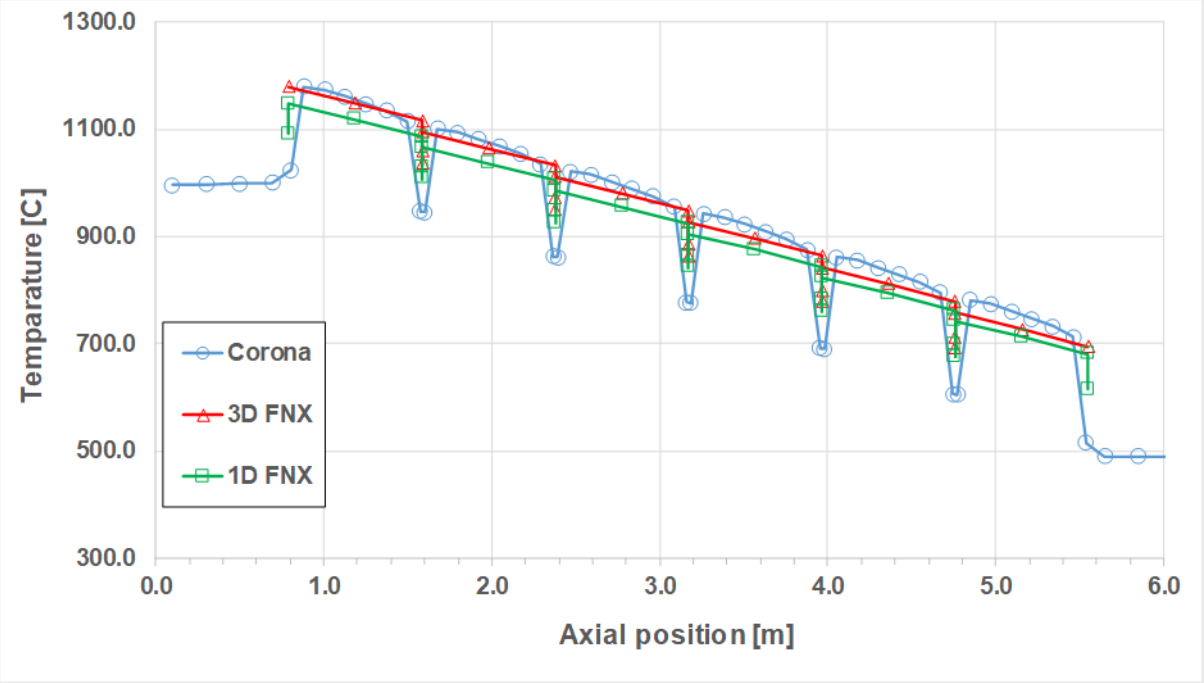

Fig. 9: Axial distribution of the temperature at the centre of the hottest fuel rod.

The axial distribution of the temperature at the fuel rod centre obtained by the 1D fuel assembly simulation is compared with the axial temperature distribution obtained by Tak et al. (2014) for the hottest fuel rod and the corresponding axial temperature distribution obtained by Khoza (2019) for the fuel rod centre of the hottest CV. It is important to remember that the coolant flows from the top to the bottom of the fuel assembly. The dips in the profile obtained by Tak et al. (2014) is due to the graphite plugs. The dips in the 1D profile are due to the inclusion of the graphite temperatures at the bottom and top of adjacent fuel blocks. The agreement between the three sets of results is good with the difference between the highest Corona and 1D temperatures being 2.8%. When the graphite plugs were accounted for in the 1D model, the difference between the highest Corona and 1D temperatures was reduced to 2.3%. It can be concluded that the 1D representative fuel block model provides results of sufficient accuracy so that it can be used as a building block along with the relevant Flownex components to construct a representative reactor model of a prismatic block gas-cooled reactor such as the PMR200.

7. Axi-Symmetric PMR200 Reactor Model

A schematic layout of the axi-symmetric model of the full PMR200 reactor that was simulated in this study is shown in Fig. 10. The layout should be interpreted along with the layout of the PMR200 reactor and the cross-section through the active core depicted in Fig. 1. Each ring per layer is represented by one representative block within the Flownex model.

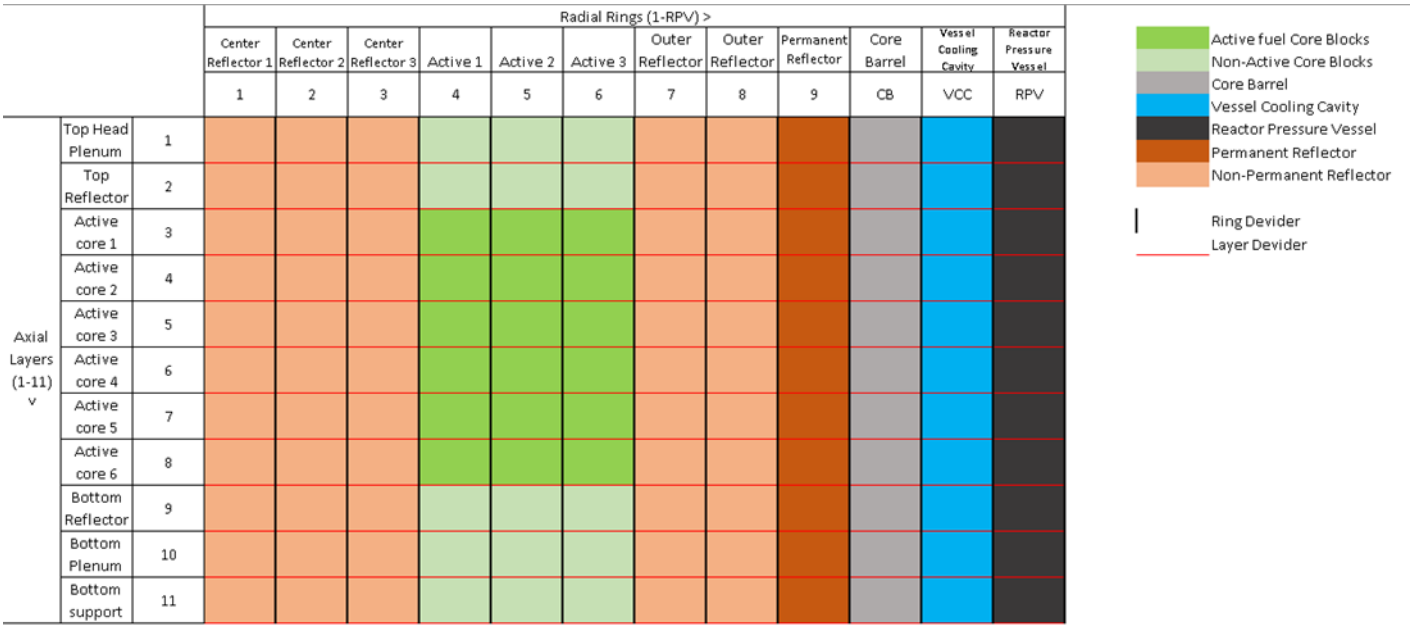

Fig. 10: Schematic layout of axial layers and radial rings of PMR200 model.

The representative fuel block shown in Fig. 7 (and Fig. 8) was used to construct the eighteen rings of fuel blocks in the active core (layers 3 to 8 and rings 4 to 6). Heat transfer between adjacent layers was modelled by implementing axial conduction components consisting of the helium in the cross gaps between the layers. It is assumed that the helium gap between the layers is the means of how heat is transferred and thus is used with a solid conduction component and the helium used is used as a solid element. The heat transfer in the radial direction between adjacent rings was modelled through the convection heat transfer through the bypass gap between the rings. The control rod channels present in the three rings were modelled by a representative control rod channel in each ring using pipe components (Fig. 3 (6)) to account for the flow and convection components (Fig. 3(5)) to account for the convection heat transfer between the control rod channels and the graphite.

The non-active core blocks in the bottom reflector (layer 9 and rings 4 to 5) were constructed using the representative fuel block (Fig. 7) with the fuel rod components, radiation and conduction components in the gap between the fuel hole wall and the graphite, and the conduction components for the heat transfer from the fuel hole wall to the graphite omitted. The heat transfer across the cross gaps between adjacent layers was again modelled using helium conduction components, and the radial heat transfer between adjacent rings through the convection heat transfer through the bypass gap between rings.

The inner reflector blocks (layers 1 to 9 and rings 1 to 3) and the outer reflector blocks (layers 2 to 9 and rings 7 to 8) were also constructed using the representative fuel block (Fig. 7) as a basis. In the case of the reflector blocks the fuel rod components, radiation and conduction components in the gap between the fuel

hole wall and the graphite, and the conduction components for the heat transfer from the fuel hole wall to the graphite were omitted. Further, the conduction components between the graphite and the coolant channel wall, the convection component for the convection heat transfer between the coolant channel wall and the coolant channel, and the pipe component representing the coolant channel, were also omitted. The heat transfer across the cross gaps between adjacent layers was again modelled using helium conduction components, and the radial heat transfer between adjacent rings through the convection heat transfer through the bypass gap between rings. The control rod channels present in the first outer reflector ring (layers 3 to 8 and ring 7) were modelled by a representative control rod channel using pipe components (Fig. 3 (6)) to account for the flow and convection components (Fig. 3(5)) to account for the convection heat transfer between the control rod channels and the graphite.

The permanent reflector blocks (layers 2 to 9 and ring 9) were also constructed using the representative fuel block (Fig. 7) as a basis. The components associated with the fuel rods and heat transfer to the graphite were omitted from the model. The conduction components from the graphite to the coolant channel wall were also omitted and the convection components were linked directly to the graphite nodes. The pipe component representing the coolant channels was adapted to represent the inlet risers. No cross gaps were assumed to occur between adjacent permanent reflector blocks and no bypass gap was assumed to occur between the permanent reflector blocks and the core barrel (Jun, 2020).

The bottom plenum (layer 10 and rings 1 to 9) was modelled using axial conduction components (Fig. 3(3) to account for axial conduction heat transfer, pipe components (Fig. 3(6)) to account for the collection and outflow of the hot helium, as well as the inflow of cold helium to the inlet risers, and convection components to account for the convection heat transfer between the helium and the graphite structures. The inlet boundaries conditions for the cold helium and the outlet boundary conditions for the hot helium are associated with the bottom plenum.

The bottom support (layer 11 and rings 1 to 9) consist only of conduction components (Fig. 3(3)) to account for the axial and radial heat transfer in the bottom support. No gap is assumed to occur between the solid structures of the bottom plenum and bottom support and the layers thus share the nodes lying on the interface.

As in the case of the bottom plenum, the non-active, outer reflector and permanent reflector blocks in the top reflector (layer 2 and rings 4 to 9) were modelled axial conduction components (Fig. 3(3)) to account for the axial heat transfer. The distribution of the helium from the inlet risers through the voids in the blocks to the coolant channels and bypass gaps were modelled using pipe components (Fig. 3(6)) and the convection heat transfer between the graphite structures and the helium was accounted for using the convection components (Fig. 3(5)).

The volume in the top head plenum (layer 1 and rings 1 to 9) was modelled using a single volume node (Fig. 3(1)) the account for the volume in the top head. Convection components (Fig. 3(5)) account for the convection heat transfer from the top of the top reflector and the radiation component for the radiation heat transfer between the top reflector and the core barrel.

The core barrel (layer 1 to 11 and ring CB) and reactor pressure vessel (layer 1 to 11 and ring RPV) were modelled using the conduction components (Fig. 3(3)) to account for the conduction in the radial direction through the CB and RPV, as well as for the conduction heat transfer in the axial direction along with the CB and RPV. As mentioned previously it was assumed that there is no gap between the permanent reflector and the BC (Jun, 2020) and they, therefore, share the nodes lying on the interface.

Finally, the gap between the CB and the RPV, namely the vessel cooling cavity (VCC) or vessel cooling system (VCS) is modelled using pipe components (Fig. 3(6)) to account for the flow of the cooling helium. Convection components (Fig. 3(5)) is used to model the convection heat transfer between the CB and the helium and between the RPV and the helium. Radiation components are employed to account for the radiation heat transfer between the outer surface of the CB and the inner surface of the RPV.

The layout of the complete Flownex reactor model is illustrated in Appendix A.

The approach outlined to construct the model of the PMR200 prismatic block reactor can be implemented and adapted, as required, to construct a 1D model of a similar prismatic block reactor.

8. Results

Distributing the 200 MW power generated by the PMR200 reactor uniformly over the volume of the fuel rods (or compacts) gives rise to a volumetric heat source of 25.9925 MW/m^3 to be applied to nodes associated with the fuel rods. At the inlet of the inlet risers the helium enters the reactor at a temperature of 490°C and a pressure of 7 MPa. The helium leaves the reactor at the hot outlet at a mass flow rate of 83.38 kg/s (Jun, 2020). Jun et al. (2009) specified a helium coolant mass flow rate of 82.79 kg/s which is 0.71% less than the helium mass flow rate given by Jun (2020). At the inlet of the vessel cooling system the helium enters the system at a temperature of 140°C and a pressure of 7 MPa, whilst at the outlet of the vessel cooling system the helium leaves the system at a mass flow rate of 2.0 kg/s.

In their whole core analysis considering one sixth of the core, Tak et al. (2012) applied a fixed temperature boundary condition at the outside surface of the permanent reflector of 490 ^{o}C. They did not include the core barrel and RPV in the analysis. Lommers et al. (2014) represented the reactor cavity heat transfer by a simplified model with radiation and convection from the outer surface of the RPV to the RCCS with the RCCS assumed to be at a constant temperature of 65 ^{o}C. No detail of the simplified model is given. Jun et

al. (2009) included the RCCS in their model which therefore in an integrated manner accounted for the heat transfer from the cavity surface of the RPV and the associated temperature of the RPV surface. In the absence of a coupled RCCS model and relevant detail, the cavity surface of the RPV was, as a first approximation, assumed to be adiabatic in the current study.

The purpose of the current study is to establish the validity of the 1D model of the PMR200 reactor and, therefore, only steady-state results are considered.

8.1. Fuel rod power and temperature distributions

To determine whether the heat sources had been applied correctly at the fuel nodes, the amount of heat generated in each ring of fuel blocks in each of the layers of the active core was extracted. We have that in each layer there are 18 fuel blocks in the first active core ring (Fig. 10, ring 4) and in the second (Fig. 10, ring 5) and third (Fig. 10, ring 6) active core rings each layer consists of 24 fuel blocks. The power produced by each of the three rings of fuel blocks in each layer is summarized in Table 2. The total power produced by all the layers in each, as well as the overall power produced by all the fuel blocks, are also given in Table 2. All the values given in Table 2 are in exact agreement with the corresponding analytical values. The results are also a confirmation that the volumes associated with each of the fuel rod nodes have been calculated correctly by the Flownex model.

Table 2: Power generated by each ring of fuel blocks.

	Ring 4	Ring 5	Ring 6
Layer	8762,87	12286,1	12286,06
Layer	8762,38	12285,42	12285,4
Layer	8762,39	12285,42	12285,4
Layer	8762,39	12285,42	12285,39
Layer	8762,39	12285,42	12285,40
Layer	8762,09	12284,97	12285,09
Ring	52574,53	73712,74	73712,74
Total		200000	

The axial distributions of the temperature at the centres of the representative fuel rods for the first fuel block ring (FC1), the second fuel block ring (FC2) and the third fuel block ring (FC3) are shown in Fig. 11. It can be observed in Fig. 11 that the temperatures associated with FC2 are higher than the corresponding temperatures for FC1 and FC3. Moving from the top to the bottom of the active core the temperature differences between the profiles gradually become larger. At the bottom of the core, the temperature for FC2 is 0.99% larger than the temperature for FC1 and 1.93% larger than the temperature for FC3. The

temperature profiles and the values of the temperatures are also in good agreement with the 1D profile and associated values of the temperatures shown in Fig. 9. The maximum temperature recorded in the active core fuel components at the bottom of FC3 (Fig. 10, layer 8, ring 5) is 1134.66℃ and is below the 1250℃ for the operating limit of the fuel assembly (Jun et al., 2009). Jun et al. (2009) recorded a peak temperature of 1138℃ at BOC which is also within the fuel operating temperature range limit. However, Jun et al. (2009) used an unspecified non-uniform power distribution with the peak temperature occurring at the top of the core. The appropriate non-uniform power distribution specified by Jun et al. (2009) needs to be obtained and applied in the current model to be able to make a more comprehensive comparison.

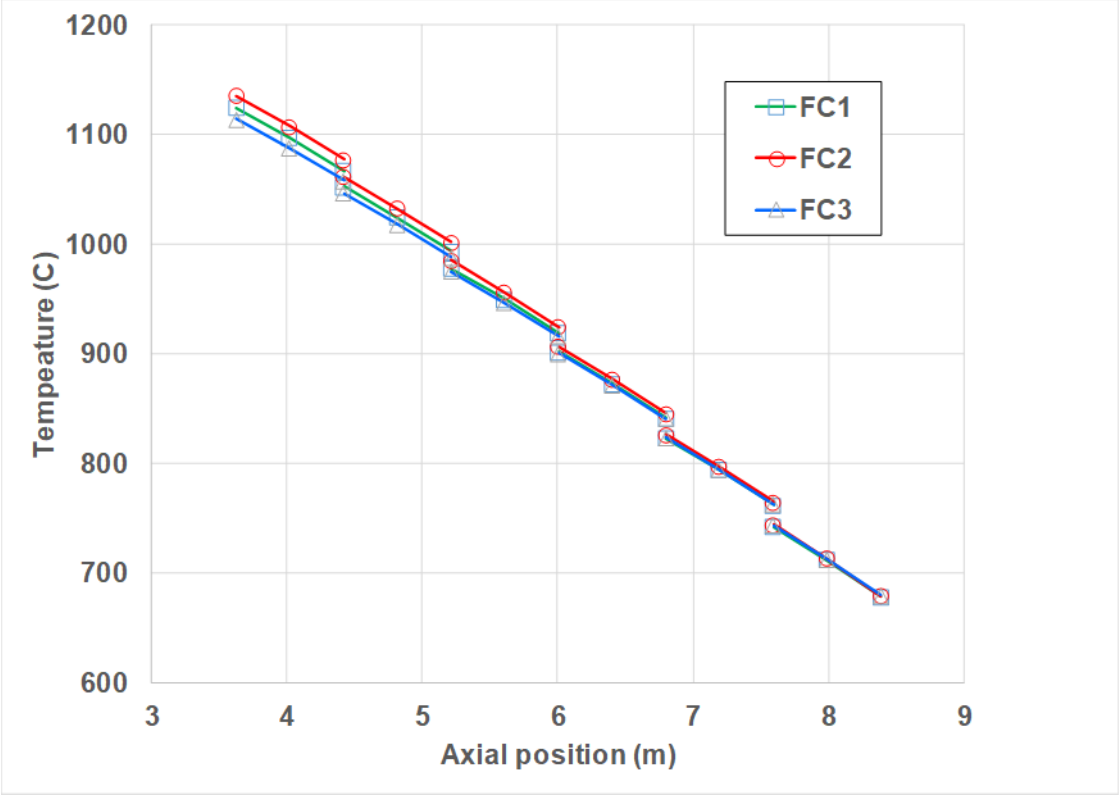

Fig. 11: Axial distribution of temperature at fuel centre for fuel block rings.

8.2. Coolant distribution

The mass flow rate of 83.38 kg/s prescribed at the inlet boundary is split between the different flow channels that include the coolant channels, control rod flow channels and the different bypass flow channels. The mass flow rate of coolant channel 1 (CC1) is 18.61 kg/s and for coolant channels, 2 (CC2) and 3 (CC3) the mass flow rates are 26.21 kg/s and 26.11 kg/s respectively as seen in Table 3. These mass flow rates represent 22.33%, 31.44% and 31.32% of the total mass flow rate and are in good agreement with the mass flow distributions of 23%, 32% and 32% for CC1, CC2 and CC3 obtained by Jun et al. (2009). The

combined mass flow rate of the bypass gaps is 5.8 kg/s and for the control rod flow channels it is 6.63 kg/s. Thus, the percentages of the bypass, coolant and control rod channels compared to the total inlet mass flow rate is 6.96%, 85.09% and 7.95%. The combined flow of 14.91% through the bypass and control rod channels is slightly larger than the 13% obtained by Jun et al. (2009).

The temperature of the coolant at the hot outlet is 949.8 °C which is in very good agreement with the nominal coolant outlet temperature of 950 °C. The maximum temperature of the helium coolant is found to be 1043,97 °C at the bottom of the second fuel ring (Fig. 10, ring 5, layer 8) in the bypass gap representing the bypass gaps occurring between the blocks of the second ring. Jun et al. (2009) provide no information regarding the temperatures of the coolant in the bypass gaps.

Table 3: Mass flow rate distribution for flow channels.

Flow Channels	%	kg/s	Coolant	%	kg/s
Bypass	6,95	5.79	CC1	22,33	18,61
Coolant	85,09	70,94	CC2	31,44	26,21
Control Rod	7,95	6.63	CC3	31,31	26,11
Total	100	83,38	Total	85,09	70,94

8.3. Effect of mass flow rate of coolant in VCS

For the specified VCS mass flow rate of 2.0 kg/s (Jun et al., 2009) the maximum temperature on the outer surface of the RPV is 438.5 °C. This exceeds the design limit of 371 °C for the SA508 steel proposed for the RPV. The outlet temperature of the VCS is 239.1 °C and the VCS removes 1028.6 kW which represents 0.51% of the heat generated by the reactor.

Table 4: Effect of VCS mass flow rate on selected parameters.

	VCS mass flow rate (kg/s)				
	1.0	2.0	4.0	8.0	16.0
RPV T_{max} (°C)	476.9	438.5	394.2	336.4	273.4
FC1 T_{max} (°C)	1124.3	1123.4	1122.4	1121.1	1119.5
FC2 T_{max} (°C)	1135.4	1134.5	1133.6	1132.3	1130.7
FC3 T_{max} (°C)	1114.0	1113.1	1112.0	1110.6	1108.8
Coolant T_{out} (°C)	950.9	949.8	948.6	947.1	945.1
VCS T_{out} (°C)	247.8	239.1	214.5	193.2	176.6
VCS Q (kW)	559.2	1028.6	1546.3	2208.4	3040.1
VCS Q %	0.28	0.51	1.00	1.00	1.52

In order to determine the effect of the VCS mass flow rate on the reactor in addition to the 2.0 kg/s, mass flow rates of 1.0 kg/s, 4.0 kg/s, 8.0 kg/s and 16.0 kg/s were also investigated. The values obtained in the

respective simulation for the maximum RPV temperature, maximum fuel centre temperatures, coolant outlet temperature, VCS outlet temperature and the heat removed by the VCS are summarized in Table 4.

In Table 4 it can be observed that the maximum temperature of the RPV decreases by 42.7% as the mass flow rate increases from 1.0 kg/s to 16.0 kg/s. In contrast, the maximum temperatures of the fuel centres only decrease on average by 0.44%. The coolant outlet temperature also only decreases by 0.6%. The VCS outlet temperature at the same time decreases by 28.7% whilst the heat removed by the VCS increases by 443.7% from 0.28% to 1.52% of the heat generated by the reactor. For steady-state conditions and the adiabatic boundary condition assumed for the RPV surface, the VCS mass flow rate must be larger than 5.4 kg/s to ensure that the maximum temperature of the outer surface is less than the design limit of 371 ^{o}C.

The results in listed Table 4 shows that the VCS mass flow rate has a significant impact on the maximum temperature of the RPV, the outlet temperature of the VCS and the heat removed by the VCS. However, the VCS mass flow rate has a negligible impact on the maximum fuel centre temperatures and the outlet temperature of the coolant.

In order to get a more complete understanding of the thermal-hydraulic performance of the PMR200 reactor, the reactor must be coupled to the associated RCCS (Jun et al., 2009; Kim et al., 2010). This can be achieved by adapting the RCCS model simulated by Rousseau et al. (2015) and Du Toit et al. (2016). The relevant power profile should also be assigned so that a more appropriate comparison can be made with the steady-state and transient results presented by Jun et al. (2009).

With an HP Z8 PC that utilizes an Intel Xeon Gold 6140 CPU at 2.30 GHz and with 64 GB of RAM Flownex solved the energy, mass and momentum equations for the model in 32 steady state iterations in 1,61s. It can be concluded that the specific results that are obtained and displayed from the full representative SCFD model of the PMR200 reactor are in good agreement with other results found in the literature. Thus, it can be stated that a full representative core of a VHTR can be modelled and simulated in Flownex in a reasonable time frame and that the model can give good representative results.

9. Conclusion

As the different types of heat transfer in a full core of a PMR200 reactor are very important for the optimal operation of the VHTR, different thermal characteristics are needed to assure the core can be utilised in a proper, safe and efficient manner. This paper discussed a representative System CFD (network) model of the PMR200 reactor and its different thermal characteristics.

Several studies were done on the PMR200 reactor and on different sections of the reactor for various thermal characteristics. These studies utilized Single Channel Fuel Modules (Nel and du Toit, 2018), 1/12th

of a fuel block (Ribeiro et al., 2013) and a 1/6th of the PMR200 reactor by Travis and El-Genk (2013). These studies considered their specified sections of the core with and without bypass and cross flow gaps for the stacked fuel blocks. However, some of the studies only used the active core up to the permanent reflector and did not include the core barrel, vessel cooling cavity/system and the reactor pressure vessel. They also excluded the top head plenum and top reflector for the top of the core as well as the bottom reflector, bottom plenum and bottom support at the bottom of the core.

This study considered a full representative core of the PMR200 that includes each section from the top head plenum down to the bottom support and from the inner reflector through the active core to the RPV of the reactor. Bypass gaps and cross flow gaps are also included in the model to get more accurate results of the thermal characteristic. In this study, the reactor cavity cooling system was not coupled to this model of the PMR200. Several thermal characteristic results are calculated and extracted but only a certain selection of necessary characteristics are displayed in the results represented.

With an inlet mass flow rate of 83.38 kg/s and an inlet temperature and pressure of 490℃ and 7 MPa, the outlet temperature of the helium is 949.8℃ at a pressure of 6,9923 MPa. The maximum fuel temperature extracted is 1134.66℃ and is compared to the 1138℃ calculated by Jun, J.S. et al. (2009) and both results are within the limit range of 1250℃. As for the fluid components of the study, the maximum fluid temperature in the core is recorded at 1043.97 ℃ whereas the fluid mass flow rate distribution between the three coolant channels is respectively 22.33%, 31.44% and 31.32% which is in good agreement with the results obtained by Jun, J.S. et al. (2009).

With the specified mass flow rate of 2 kg/s the outlet temperature of the coolant in the VCS is 239.1℃ and the corresponding maximum RPV temperature is 438.5 ℃. The VCS extracts 1028.6 kW worth of heat from the reactor core. As the VCS mass flow rate is increased from 1 kg/s to 16 kg/s the RPV maximum temperature decreases by 42.7%. For the RPV to remain under the maximum design limit of 371℃ the mass flow rate within the VCS needs to be 5.4 kg/s. With the increase in the flow rate of the coolant in the VCS, there is little change in the temperature distribution within the active core

10. Recommendation

The inclusion of the RCCS system into the PMR200 core system model will allow a more comprehensive evaluation of the performance of the PMR200 system under various conditions. With the RCCS added to the system effect that RCCS has on the heat dissipation and other thermal characteristics of the core can be determined and compared with the results obtained by Jun et al. (2009) and other research. The effect on the full system of flow disturbances that could occur in the RCCS can also be investigated.

11. Acknowledgements

This work is based on the research supported by the South African Research Chairs Initiative of the Department of Science and Technology and the National Research Foundation of South Africa (Grant No 61059).

Any opinion, findings and conclusion or recommendation expressed in this material is that of the authors and the NRF does not accept any liability in this regard.

A sincere thanks to Dr JS Jun and Dr NI Tak for providing the necessary data of the PMR200.

Abbreviations

HTGR	High-temperature gas-cooled reactor
HTR-10	10 MW High Temperature Gas Cooled Reactor of Tsinghua University, China
PBMRs	Pebble bed modular reactors
TRISO	TRi-structural ISOtropic
HTR	High Temperature Reactor
VHTR	Very High Temperature Reactor
PMR	Prismatic Modular Reactor
MW_{th}	Mega Watt Thermal
MPa	Mega Pascal
SCFM	Single Channel Fuel Module
HPCC	High Pressure Conduction Cooling
LPCC	Low Pressure Conduction Cooling
RCCS	Reactor Cavity Cooling System
VCS	Vessel Cooling System
CFD	Computational Fluid Dynamics
SCFD	System Computational Fluid Dynamics
CB	Core Barrel
VCC	Vessel Cooling Cavity
RPV	Reactor Pressure Vessel
NQA-1	Nuclear Quality Assurance
PBMR	Pebble Bed Modular Reactor
NWU	North West University
NNR	National Nuclear Regulator
BOC	Beginning of Cycle

List of Symbols

$\bar{\rho}$	Average density
$\forall$	Volume
$\dot{m}$	Mass flow
e	Exit
i	Inlet
L	Length
A	Cross-sectional area
p_0	Total pressure
g	Gravitational acceleration
z	Elevation
D_H	Hydraulic diameter
K	Form loss factor
f	Friction factor
h_0	Total enthalpy
P	Static pressure
Δp_L	Frictional loss
$\dot{q}_{conv}$	Convection heat transfer
T	Temperature
s	solid
f	Fluid
h	Heat transfer coefficient
Nu	Nusselt number
k_f	Thermal conductivity
$\dot{q}_{cond}$	Conduction heat transfer
k_s	Thermal conductivity of the solid
σ	Stefan-Boltzmann constant
$\dot{q}_{rad}$	Radiation heat transfer
ε	Emissivity
F_{ie}	View factor

References

Du Toit, C.G., Rousseau, P.G. (2012) Modeling the flow and heat transfer in a packed bed high temperature gas-cooled reactor in the context of a systems CFD approach, Journal of Heat Transfer, 134, pp 031015-1 – 031015-12.

Du Toit, C.G.; Rousseau, P.G.; Sambureni, P; le Grange, L.A., (2015) 'A System CFD model of the heat transfer in a Prismatic Block of a VHTR Core', ICAPP 2015, Nice (France).

Du Toit, C.G., Rousseau, P.G., Jun, J.S., Kim, M.H. (2016) Numerical simulation of break flows occurring in the reactor cavity cooling system of a very high temperature reactor using a system CFD approach, Proceedings of HTR 2016, Las Vegas, USA.

Flownex, Bringing nuclear quality and standards to system simulation, https://www.flownex.com/about-us/certification, (accessed: 27 November 2019).

Greyvenstein, G.P. (2002) An implicit method for the analysis of transient flows in pipe networks, International Journal for Numerical Methods in Engineering, 53, pp 1127 – 1143.

IAEA (2010) 'HIGH TEMPERATURE GAS COOLED REACTOR FUELS AND MATERIALS', IAEA, Vienna, ISBN 978-92-0-153110-2

Incropera, F.P., DeWitt, D.P. (1996) Fundamentals of heat and mass transfer, New York: John Wiley & Sons.

Jo, C.K; Lim, H.S.; Noh, J.M., (2008) Pre conceptual Designs of the 200MW_{th} Prism and Pebble-type VHTR Cores', PHYSOR 2008, Switzerland, Interlaken.

Jun, J.S.; Lim, H.S.; Lee, W (2007) 'The Steady State Performance and Limiting Accident Analysis for a PMR 200MWth Prototype Reactor', Transactions of the Korean Nuclear Society Spring Meeting,

Jun, J.S.; Lim, H.S.; Jo, C.K.; Noh, J.M., (2009) 'Thermal-Fluid Analysis of the PMR 200MW_{th} Reactor System at the Steady State and Transient Conditions', Transactions of the Korean Nuclear Society Spring Meeting,

Jun, J.S. (2020) GAMMA+ input sheets for PMR600 and PMR200, unpublished document.

Khoza, S.N. (2019) 'An integrated thermal hydraulic system CFD model of a prismatic block HTR core using Flownex', North-West University, South Africa

Kim, M.H., Tak, N.I, Lim, H.S. (2010) Thermal-fluid assessment of the design options for reactor vessel cooling in a prismatic core VHTR, Annals of Nuclear Energy, 37, pp. 1774 – 1782.

Kim, M and Lim, H, (2011) 'Evaluation of the influence of bypass flow gap distribution on the core hot spot in a Prismatic VHTR core', Nuclear Engineering and Design, 241, 3076-3085.

Lim, H.S.; No, H.C,. (2006) ' GAMMA Multidimensional Multicomponent Mixture Analysis to Predict Air Ingress Phenomena in an HTGR', Nuclear Science and Engineering, 152, 1-11.

Lommers, L.J., Mays, B.E., Shahrokhi, F. (2014) Passive heat removal impact on AREVA HTR design, Nuclear Engineering and Design 271, pp. 569–577.

M-Tech Industrial, (2021) Flownex SE Version 8.12.17.4334, http://www.flownex.com.

Nel, G.J. and du Toit, C.G. (2018) 'A System CFD Model of a Single-Channel Fuel Module in a Prismatic Block VHTR', South African Conference on Computational and Applied Mechanics 2018, South Africa.

Ribeiro, F.L.; Santos, A.A.C.; Pinto, J.P.C.A.; Mesquita, A.Z.; de Mattos, J.R.L., 'Numerical simulations of helium flow through prismatic fuel elements of very high temperature reactors', International Nuclear Atlantic Conference 2013, Brazil.

Rousseau, P.G., Du Toit, C.G., Jun, J.S., Noh, J.M. (2015) Code-to-code comparison for analysing the steady-state heat transfer and natural circulation in an air-cooled RCCS using GAMMA+ and Flownex, Nuclear Engineering and Design, 291, pp 72 – 89.

Sambureni, P (2015) 'Thermal fluid network model for a prismatic block in a gas-cooled reactor using FLOWNEX', North-West University, South Africa.

Streeter, V.L., Wylie, E.B. (1979) Fluid Mechanics, Tokyo: McGraw-Hill.

Tak, N; Kim, M; Lee, W.J. (2008) 'Numerical investigation of a heat transfer within the prismatic fuel assembly of a very high temperature reactor', Annals of Nuclear Energy, 35, pp. 1892-1899.

Tak, N.; Kim, M; Lim, H.S.; Noh, J.M., (2011) 'A Practical Method for Whole-Core Thermal Analysis of a Prismatic Gas Cooled Reactor', Nuclear Technology, 177, pp. 352-365.

Tak, N.; Lee, S.N.; Kim, M; Lim, H.S.; Noh, J.M., (2014) 'DEVELOPMENT OF A CORE THERMO-FLUID ANALYSIS CODE FOR PRISMATIC GAS COOLED REACTORS', Nuclear Engineering and Technology, 46 No.5, 641-654.

Travis, B.W. and El-Genk, M.S. (2013) 'Thermal-hydraulics analysis for 1/6 prismatic VHTR core and fuel element with and without bypass flow, Energy Conversion and Management, 67, pp. 325-341.

Travis, B.W. and El-Genk, M.S. (2013) 'Numerical Simulation and Turbulent Convection Heat Transfer Correlation for Coolant Channels in a Very-High-Temperature Reactor', Heat Transfer Engineering, 34(1), 1-14.

World Nuclear Association (2020) 'Generation IV Nuclear Reactors', https://world-nuclear.org/information-library/nuclear-fuel-cycle/nuclear-power-reactors/generation-iv-nuclear-reactors.aspx

Yoon, S; Lee, J; Kim, M; Park, G, (2012) 'The effects of cross flow gap and axial bypass gap distribution on the flow characteristics in prismatic VHTR core', Nuclear Engineering and Design, 250, 465-479.

CHAPTER 4: NUMERICAL SIMULATION OF AN INTEGRATED RCCS WITH A FULL REPRESENTATIVE PMR200 IN FLOWNEX (PART 2)

Numerical simulation of an integrated RCCS with a full representative PMR200 Reactor in Flownex.

(Part 2)

GJ Nel*, CG du Toit

Unit for Energy and Technology Systems

North-West University

Private Bag X6001

Potchefstroom 2520

South Africa

Tel: +27 18 299 1322

Fax: +27 18 299 1320

Cell: +27 82 856 4200

Corresponding author email: Jat.DuToit@nwu.ac.za

ABSTRACT

Heat transfer within a nuclear power plant system is of plays an important role in normal and upset operating conditions of the nuclear reactor system. A 1D air-cooled Reactor Cavity Cooling System (RCCS) model is constructed and integrated with a reactor system to avoid high temperatures during accident conditions by means of heat extraction from the reactor pressure vessel wall. With the development of different models of the RCCS in different simulation packages, there is still a need for integrated representative models of a reactor and an RCCS. In this study, the integrated PMR200 (Prismatic Modular Reactor) Reactor and RCCS system is simulated using the 1D system network code Flownex. The simulation investigates the heat transfer between the reactor and the RCCS, as well as the effects breaks in the RCCS manifold, will have on the different characteristics and performance of the representative reactor and RCCS. Results are extracted and compared to relevant research of similar nature.

Keywords:

PMR200; Prismatic fuel block; Reactor Cavity Cooling System; heat transfer; conduction; convection; 1D modelling

1. Introduction

Under normal operating conditions a generation IV reactor can produce up to 600MW_{th} worth of heat with an outlet temperature between 900℃ and 1000℃ (World Nuclear Association (2020)). During normal operating conditions heat needs to be removed from the reactor cavity to protect the reactor pressure vessel (RPV) and citadel, whilst during accident conditions decay heat needs to be removed to avoid further degradation of the nuclear system. In these accident or normal operating conditions, the RCCS (Reactive Cavity Cooling System) is imperative for the heat removal process of the reactor system. The RCCS operates naturally and is driven by buoyancy forces and is constructed to work as a water cooled, air-cooled or as a combined water-air-cooled driven system (Hassan, 2013; Du Toit et al., 2016).

The PMR200 reactor is part of the generation IV design category with an inlet temperature of 490℃ and an outlet temperature of 950℃. Apart from the coolant flowing through the core of the reactor system and the Vessel Cooling System (VCS), the RCCS is also needed to remove the heat released by the RPV from the reactor cavity for normal operations. There are several experimental programs and numerical research that support the feasibility and cooling performance of the reactor cavity cooling system (Kim et al., 2010; Du Toit et al., 2014; Lisowski, 2013; Frisani, 2010).

Lisowski (2013) investigated the boiling mechanisms and thermal hydraulic behaviour present in a scaled down version of a Reactor Cavity Cooling System (RCCS). The 1/4th scale model of an RCCS model is a water based RCCS that is designed to remove decay heat from an advanced nuclear reactor. With different conditions applied to the experimental scaled RCCS, Lisowski's (2013) research suggests that the RCCS examined will successfully remove decay heat during accident conditions.

The computational fluid dynamics tool Star CCM+ was used by Frisani (2010) to compare numerical simulation results with results of an experimental 180º section of a VHTR RCCS. The experimental bench test of the partial RCCS was performed at Texas A&M University. Two types of fluids namely, air and water, were considered for the cooling fluid of the RCCS that was needed to cool the RCCS concrete walls. The scaled analysis of the RCCS produced satisfactory results that were in good agreement with the temperature distributions inside the RCCS cavity medium.

Jun et al. (2007) performed steady state and limiting accident analyses on a 200MW_{th} PMR which is one of the scale down proto type reactor models proposed for an NHDD (Nuclear Hydrogen Development and Demonstration) plant. The analysis for the steady-state conditions was done with the GAMMA+ code (Lim et al., 2006). Key design parameters of the steady-state conditions are provided, such as the peak fuel temperatures, RPV temperature, control rod (CR) bypass flow, reactor cooling system flow rates and the heat that is lost to the RCCS.

A steady state and transient state analyses were performed by Jun et al. (2009) on the PMR200 reactor system. The steady state and transient analyses were done at LPCC (Low Pressure Conduction Cooling) and HPCC (High Pressure Conduction Cooling) conditions. A prismatic core is used with 6 layers of fuel blocks and with

an air cooled RCCS system and VCS (Vessel Cooling System) system. The thermal-fluid analysis of the 200 MW_{th} reactor was performed using GAMMA+ (Lim et al., 2006). Maximum temperature results are extracted from the fuel elements and the RPV, as well as other flow characteristics in the coolant flow components.

KAERI (Korea Atomic Energy Research Institute) and the NWU (North West University of South Africa) had an established program of "Joint Research Collaboration in the System Analysis of the Passive Safe Small Modular High Temperature Gas-Cooled Reactor" where the two organizations compared benchmark calculations of the natural circulation in an air-cooled RCCS. KAERI performed calculations using GAMMA+ and the NWU used the code Flownex for their calculations. Common input data such as the geometry and the material properties was given by KAERI for the 200MW_{th} PMR (Prismatic Modular Reactor) design that has been used by both KAERI and the NWU for the benchmarking of the RCCS (Jun, 2012; Rousseau et al., 2015).

A study was done by Sehoana (2014) to establish a methodology to create an integrated system level process model of a typical air-cooled RCCS in Flownex. The RCCS design that was used in the study was the conceptual design of KAERI (Jun, 2012). The study was performed to simulate and analyse different scenarios of the operational characteristics of the system. It was found that the RCCS model in Flownex removed enough heat from the reactor to the atmosphere so that the concrete wall maintained a temperature below the limit value for the different boundary conditions that were applied. With three quarters of the risers in the RCCS blocked or if a break occurs in the chimney ducts the RCCS was found to maintain its functionality.

With an RPV inner surface temperature set at 350℃/250℃ and the inlet atmospheric temperature at 40℃, Rousseau (2015) determined multiple output characteristics of the RCCS model under review. The total heat that is removed by the RCCS and the natural convection mass flow rate through the RCCS was extracted. The heat that was removed by the RCCS with the respective boundary condition is 0.819 MW for the 250℃ PRV wall temperature and 1.58 MW for the 350℃ RPV wall temperature, whilst the corresponding mass flow rates are 11.11 kg/s and 13.08 kg/s respectively. Also, the corresponding outlet air temperatures are 113℃ and 159℃ respectively.

Rousseau et al. (2015) used GAMMA+ and Flownex which is both based on a 1D flow network modelling approach to simulate different heat transfer phenomena in an air-cooled RCCS. There were different noticeable differences in some modelling aspects between the two codes but regardless of the differences the analysis and results obtained from the codes were in good agreement with each other. Radiation heat transfer was also the main source of the heat that was transferred from the RPV (Reactor Pressure Vessel) surface. It was also found that the reversal of fluid flow in the RCCS will result in a high temperature surface for the concrete wall. With the good comparison between the results obtained by the two different codes, the two codes have the ability to solve the different thermal phenomena within the RCCS system.

Du Toit et al. (2014) simulated an air-cooled RCCS system with a U-tube configuration in the two 1D network codes, GAMMA+ and Flownex. A manifold system is used to connect the downcomers and risers to the atmosphere. A section of the reactor cavity was modelled in a 3D simulation package STAR CCM+. The 3D

simulation package is used to extract the results for the heat transfer coefficients in the reactor cavity. GAMMA+ and Flownex are used to study the performance of the RCCS subjected to the radiative and convective heat transfer with atmospheric conditions. Results between the two different codes were in good agreement with each other which serves as verification of the methodologies that were followed.

In addition to the study by Du Toit et al. (2014), Du Toit et al. (2016) investigated the effects that breaks within the manifold of the RCCS will have on the performance of the RCCS. The breaks that occur in the manifold of the RCCS causes a short circuit between one section of the cold inlet manifold and the corresponding hot outlet manifold. When a break reached a critical size the fluid flow direction reversed in the relevant half of the manifold. With the reversal of the fluid flow direction, they observed a 10% decrease in the heat removal capability. Results within the study obtained by the two codes (GAMMA+ and Flownex) were in good agreement with each other.

In this study, the full representative PMR200 reactor constructed in Flownex by Nel and Du Toit (2021) is integrated with an adapted version of the RCCS model constructed in Flownex by du Toit et al. (2016). The integrated Flownex model will account for the heat generated by the reactor, as well the reactor that is cooled down by the coolant flow through the core and the heat extraction process by the VCS and RCCS. All the different characteristics that were present in the reactor itself that was included in the study by Nel and Du Toit (2021) are retained. Several adaptations are done on the RCCS model constructed by du Toit et al. (2016) to correlate with the reactor model by Nel and Du Toit (2021). The RCCS is integrated with the full representative reactor model by means of coupling it to the outside wall of the RPV. Different characteristics of the reactor, VCS and the RCCS will be extracted and evaluated. With different break sizes at selected positions in the manifold (Du Toit et al., 2016) the temperature and mass flow rates are also obtained and evaluated. The heat transfer capacity of the RCCS when various breaks occur is also examined.

2. PMR200

The PMR200 reactor, illustrated in Fig. 1, generates 200 MW_{th} worth of heat which correlates to a power density of 25.9925 MW/m^3 within the fuel compacts. The inlet boundary conditions for the helium coolant are a mass flow rate of 83.38 kg/s at an inlet temperature of 490℃ with and a corresponding inlet pressure of 7 MPa.

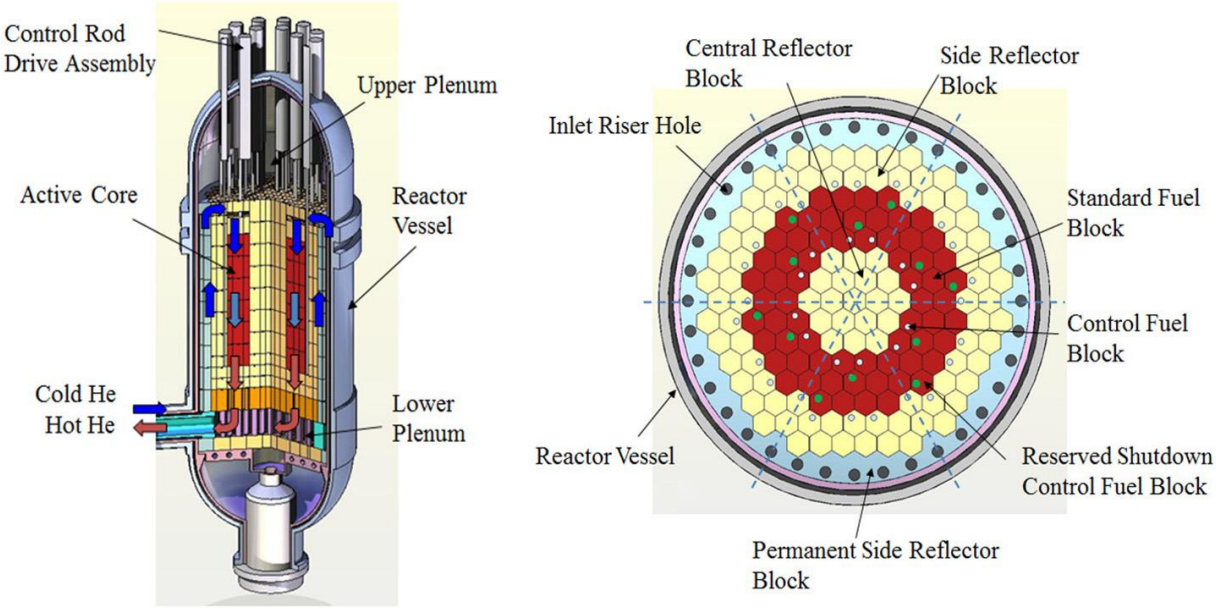

Fig. 1: Layout of PMR200 reactor and cross-section through active core (Tak et al., 2014).

The PMR200 reactor is part of the VHTR design category that is based on the GT-MHR (Gas Turbine Modular Helium Reactor). A multi-hole prismatic fuel block is used in this instance for the PMR 200. The core of the PMR200 reactor consists of hexagonal fuel blocks that are stacked to form multiple fuel assemblies for the active core and multiple non-fuel graphite block assemblies for the inner and outer reflectors of the core as seen in Fig. 1. In the PMR200 the helium coolant enters the reactor at the bottom and flows upwards through inlet riser tubes situated in the outer permanent reflector to the top of the reactor. Then the helium flows downwards through the different coolant, bypass, and control rod channels to the bottom of the reactor and then it exits through the lower plenum (Tak et al., 2011).

The core of the reactor is enclosed in the core-barrel which in turn is enclosed in the RPV (Reactor Pressure Vessel). The helium gap between the core-barrel and the RPV is known as the VCS (Vessel Cooling System) as the flow is assumed to be active. The VCS assists in cooling the core-barrel and the RPV along with the RCCS to maintain the temperature of the RPV to below its maximum allowable operating temperature of 371℃ (Jun et al., 2009). The VCS operates with inlet conditions set at 140℃ for the inlet temperature and inlet mass flow of 2.0 kg/s and a working pressure of 7MPa.

Flownex was used by Nel and Du Toit (2021) to construct a full representative reactor system network model of the PMR200. The representative model includes the whole reactor from the top head plenum to the bottom support of the reactor. All six layers of the active fuel core of the PMR200 are also included, as well as the

VCS between the core barrel and the reactor pressure vessel (RPV). Bypass gaps and cross flow gaps between the different representative prismatic blocks are also included in the model. The different representative coolant and control rod flow channels are also accounted for. This representative PMR200 model is used to integrate the current 2021 RCCS model with the representative reactor model. Details on the full representative PMR200 reactor constructed in Flownex can be found in Nel and Du Toit (2021)

3. Reactor Cavity Cooling System (RCCS)

A Reactor Cavity Cooling System is a system that is designed to remove heat that is released from the RPV wall through convection and radiation to the reactor cavity. The RCCS can be a buoyancy water-cooled or air-cooled driven system (Du Toit, 2016). An RCCS is able to operate in active operating conditions as well as in passive operating conditions. In active operating conditions, the flow is can be driven by a pump system and in passive operating conditions, the flow is driven naturally by the fluid buoyancy effects.

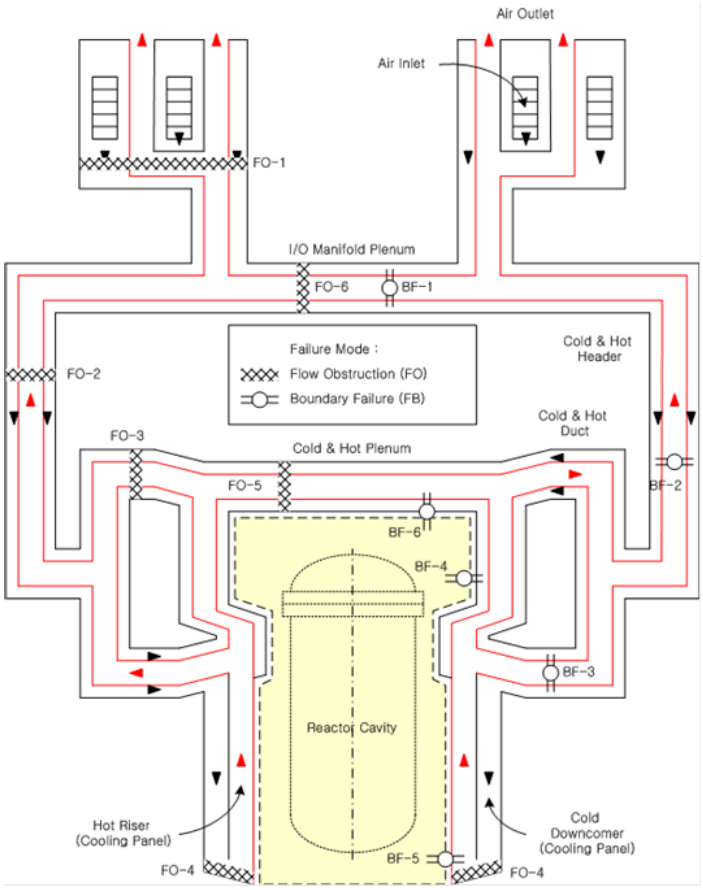

Fig. 2: Flow Path in the Air-Cooled RCCS (Jun, 2012).

An air-cooled RCCS consists of the following basic components: cold downcomer, hot riser tubes and the manifold which provides the cold inlet air from the atmosphere and rejects the hot air to the atmosphere (Niemand, 2021). A U-tube configuration is used for the current RCCS model depicted in Fig. 2, where the annular downcomer is connected via a bottom-header to 220 riser tubes (Du Toit, 2016). The thermal radiation heat that is radiated from the RPV wall as well as the convection heat that is transferred heats up the air within

the risers which induce the buoyancy forces that in turn drives the whole system. With cool air entering the manifold and downcomer the hotter air within the risers are forced up the risers and out through the manifold as the density of the cold air is higher than that of the hot air. As the hot air is pushed up the risers and out of the manifold the warm air is expelled to the atmosphere and the whole cycle restarts with cold air that enters the inlet manifold and downcomers as seen in Fig. 2. This heat that is extracted and expelled to the atmosphere endeavours to keep the RPV wall under the maximum allowable operating temperature during normal operating conditions, and during accident conditions also endeavours to restrict the core temperatures.

4. Flownex

A reactor such as the PMR200 can be represented by a network model consisting of a collection of one-dimensional components (Du Toit and Rousseau, 2012). The different Flownex components (M-Tech Industrial, 2021) that can be used to model the relevant thermal-fluid phenomena present in the PMR200 reactor and the RCCS are depicted in Fig. 3.

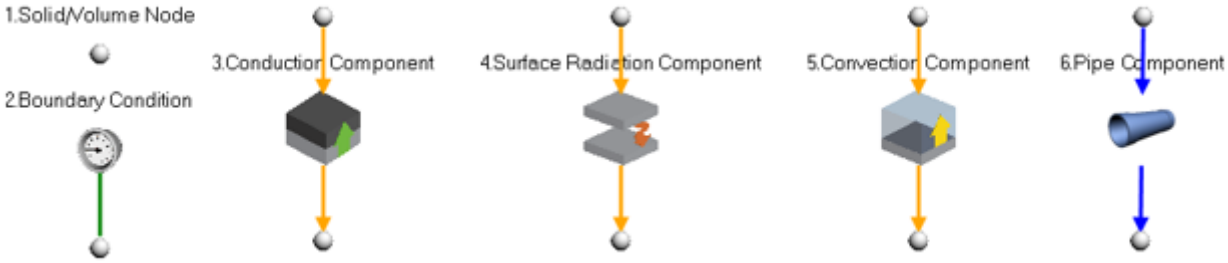

Fig. 3: Different Flownex components.

The flow in the manifolds, downcomer and risers, as well as the flow paths in the reactor (Nel and Du Toit, 2021). The equation for the conservation of mass in the pipe components is given as (M-Tech Industrial, 2021):

$$\frac{\partial \bar{\rho}}{\partial t}\forall + \dot{m}_e - \dot{m}_i = 0 \qquad (1)$$

Where $\bar{\rho}$ is the averaged density in the pipe, $\forall$ the volume of the pipe, $\dot{m}$ the mass flow rate and *e* and *i* respectively denote the exit and inlet of the pipe. Secondly, the equation for the conservation of momentum in the pipe is expressed as (M-Tech Industrial, 2021):

$$\frac{L}{A}\frac{\partial}{\partial t}(\dot{m}) + (p_{0,e} - p_{0,i}) + \bar{\rho} g (z_e - z_i) + \left[\left(\frac{fL}{D_H} + K\right)\cdot\frac{|\dot{m}|\dot{m}}{2\bar{\rho}A^2}\right] = 0 \qquad (2)$$

Here L is the length and A the cross-sectional area of the pipe, p_0 is the total pressure, g the gravitational acceleration, z the elevation, D_H the hydraulic diameter and K the form loss factor. The Darcy-Welsbach

friction factor f is obtained using the modified Colebrooke-White (Streeter and Wylie, 1979). Lastly the equation for the conservation of energy for the pipe is given as (M-Tech Industrial, 2021):

$$\frac{\partial}{\partial t}\left(\bar{\rho}h_0\right)\cancel{V} + \dot{m}\left(h_{0,e} - h_{0,i}\right) = \dot{Q} - \dot{m}g\left(z_e - z_i\right) + \frac{\partial p}{\partial t}\cancel{V} + \Delta p_L \cdot \frac{\dot{m}}{\bar{\rho}} \qquad (3)$$

Where h_0 is the total enthalpy, p the static pressure and Δp_L the frictional loss. The second term on the right-hand-side represents the gravitational work and the last term the frictional work respectively done by the moving fluid.

The convection heat transfer between the fluid in the inside walls of risers and downcomer, as well as the outside walls of the risers and the outside wall of the RPV and the cavity air, is represented by the convection component (Fig. 3(5)). The convection heat transfer $\dot{q}_{conv}$ to the fluid is given as (M-Tech Industrial, 2021):

$$\dot{q}_{conv} = -hA\left(T_f - T_s\right) \qquad (4)$$

Here T is the temperature and s and f refer respectively to the surface of the solid and fluid. A is the contact area and h is the heat transfer coefficient. The heat transfer coefficient is obtained from the Nusselt number Nu with $h = \mathrm{Nu}\,k_f / D_H$ where k_f is the thermal conductivity of the fluid. The Nusselt number is calculated using the Gnielinski correlation (Incropera and DeWitt, 1996).

The conduction heat transfer through the solids, such as the walls of the risers and the downcomer, is represented by the conduction component (Fig. 3(3)). The conduction heat transfer $\dot{q}_{cond}$ is obtained using (M-Tech Industrial, 2021):

$$\dot{q}_{cond} = -\frac{k_s A}{L}\left(T_e - T_i\right) \qquad (5)$$

Where A and L are respectively the conduction area and length and k_s is the thermal conductivity of the solid.

The radiation heat transfer between the reactor pressure vessel (RPV) surface and outside surfaces in the risers, as well as between the inside surfaces of the risers, is represented by the radiation component (Fig. 3(4)). The radiation heat transfer q_i from surface i is given by (M-Tech Industrial, 2021):

$$q_i = \frac{E_{bi} - J_i}{(1-\varepsilon_i)/(\varepsilon_i A_i)} = \sum_{j=1}^{N} \frac{J_i - J_j}{\left(A_i F_{ij}\right)^{-1}} \qquad (6)$$

Here E_{bi} is the emissive power of surface i, J_i the radiosity associated with the surface, ε the emissivity, A_i the area of the surface, F_{ij} the view factor from the surface i to surface j and N are the number surfaces that

surface *i* is radiating to. In Flownex the left-hand side of eq. (6) is represented by the radiation component (Fig. 3(4)) specified as a surface radiation component. The right-hand side of eq. (6) is represented by the radiation component (Fig. 3(4)) specified as a spatial radiation component.

Flownex employs a finite volume-based implicit pressure correction method (Greyvenstein, 2002) to obtain the solution of the conservation equations. Flownex has been certified as being ASME NQA-1 compliant (Flownex, 2019). The relevant helium and solid properties are calculated by Flownex using the information provided by Jun (2020), and values of the fluid properties are based on the local temperatures.

5. RCCS Flownex Model

The RCCS model is set up in Flownex using 1D elements and their associated nodal elements discussed in section 4 and illustrated in Fig. 3. The two top increments of the RCCS, not yet integrated with the reactor model, are shown in Fig. 4. There are 23 increments each associated with a corresponding increment in the PMR200 reactor model described by Nel and Du Toit (2021). Each riser pipe component is representative of the 220 riser tubes that are in parallel and accounts for the combined flow area, wetted perimeter and surface areas of the 220 riser tubes. The conduction components account for the conduction heat transfer through the RPV wall, riser wall, insulation on the inner wall of the downcomer, downcomer walls and the concrete containment. Although convection heat transfer to the air in the cavity is considered and the variation in the temperature of the air accounted for, the air is assumed to be stagnant (Rousseau et al., 2015).

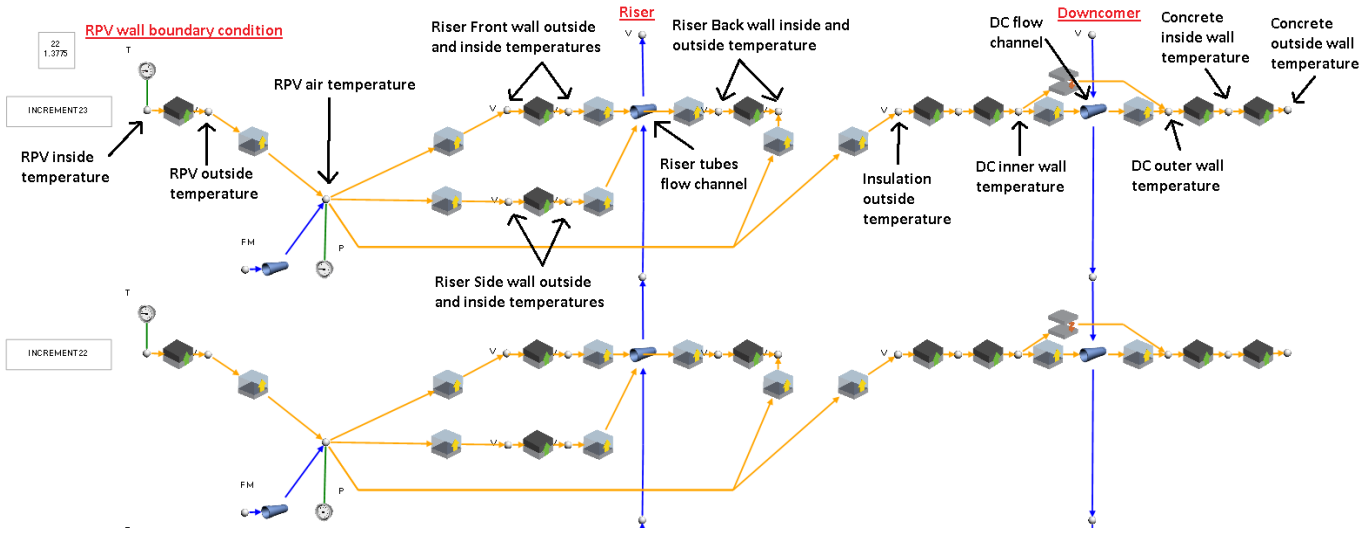

Fig. 4: RCCS riser and downcomer and the associated heat transfer components layout in Flownex not integrated with reactor model.

The radiation network for the radiation heat transfer between the RPV outer surface, the front, side and back surfaces of the representative riser, and the cavity surface of the insulation in the inner downcomer wall is shown in Fig. 5(a). Fig. 5(b) shows the radiation network for the radiation heat transfer between the inner

surfaces of the representative riser. The radiation heat transfer components to account for the radiation heat transfer between the inside surfaces of the downcomer are shown in Fig. 4.

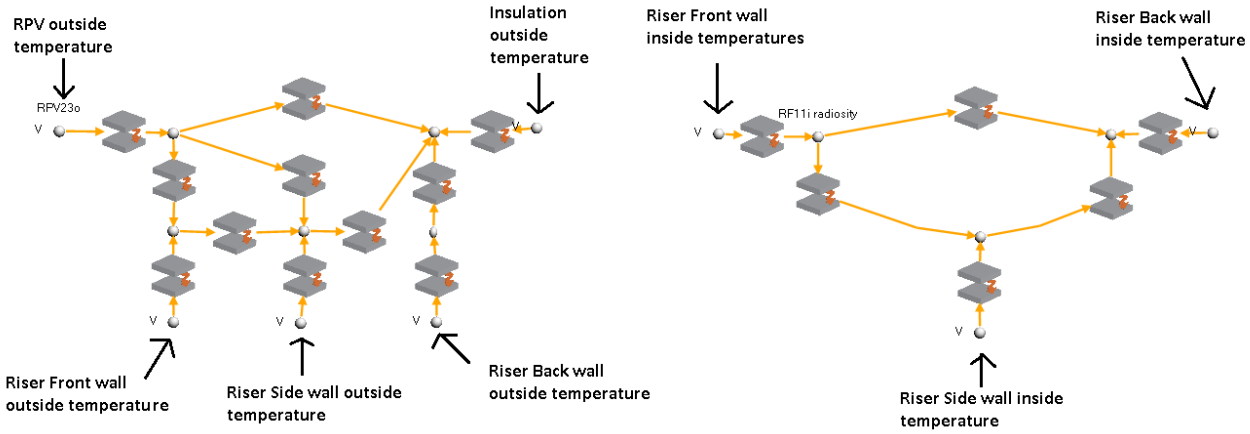

Fig. 5: Radiation networks for (a) radiative heat transfer between cavity surfaces, and (b) inside surfaces of riser.

The top of the riser and the downcomer are connected to the inlet and outlet flow manifold structures of the RCCS which are displayed in Fig. 9, i.e. the top nodes of the riser and downcomer are merged with the bottom nodes of the outlet manifold and the inlet manifold respectively. Further detailed description of the construction of the RCCS, the components used and the details used for specific components in Flownex can be obtained from du Toit et al. (2014) and Rousseau et al. (2015).

The layout for the RCCS coupled to the PMR200 reactor given by Jun (2020) consists only of the radii of the inner (RPV) and outer (steel) walls of the cavity, the dimensions and placing of the riser tubes, and the thicknesses of the steel wall and the concrete wall of the containment. No down-comer is described. The PMR200 RCCS described by Rousseau et al. (2015) was therefore adapted to be coupled to the PMR200 reactor model. Thus, added to the inner and outer radii of respectively 3.2476 m and 4.6316 m given by Jun (2020), are an insulation layer with a thickness of 0.0762 m, the inner steel wall of down-comer with a thickness of 0.0127 m, down-comer width of 0.254 m, the outer steel wall of down-comer with a thickness of 0.0127 m and the concrete wall of the containment with a thickness of 1.5 m. The height of the riser tubes and down-comer is 14.068 m compared to the height of 18.5 m in the case of Rousseau et al. (2015) as the current RCCS model is adjusted to fit the data used for the conceptual design of KAERI PMR-200 reactor. The riser tubes have inner dimensions of 0.254 m x 0.0508 m with a wall thickness of 0.0048 m. The cavity view factors given by Jun (2020) was employed in the study. The inlet and outlet manifolds were taken to be the same as those defined by Du Toit et al. (2016). The RPV is made of SA508 steel, the risers and downcomer of SS304 steel and Microtherm insulation are used (Jun 2012, 2020). The emissivity of RPV, riser and downcomer surfaces is assumed to be 0.8 and the emissivity of the insulation to be 0.1.

The heat transfer coefficients specified in the current RCCS model are the averages of the values obtained from the GAMMA+ model (Du Toit et al., 2016) and are 8.0 W/m^{2}K, 3.0 W/m^{2}K, 6.0 W/m^{2}K, 6.0 W/m^{2}K

and 4.0 W/m^{2}K for the RPV wall, the front face of the riser tubes, side faces of the riser tubes, back face of the riser tubes and the back wall of the cavity respectively. The convection heat transfer coefficients for the inside surfaces of the riser and the downcomer are calculated using the Dittus-Boelter correlation (Incropera and DeWitt, 1996).

6. Integration of PMR200 Reactor and RCCS model

When integrating the RCCS Flownex model with the full representative model of the PMR200 the conduction components representing the RPV wall and the associated input boundary conditions as seen in Fig. 4 are removed. The nodes in the RCCS model representing the outside surface of the RPV are merged with the corresponding nodes in the PMR200 reactor model as indicated by the circled nodes in Fig. 6. Not shown in Fig. 6 are the radiation components, as described in section 5, which is also connected to the outside surface of the RPV.

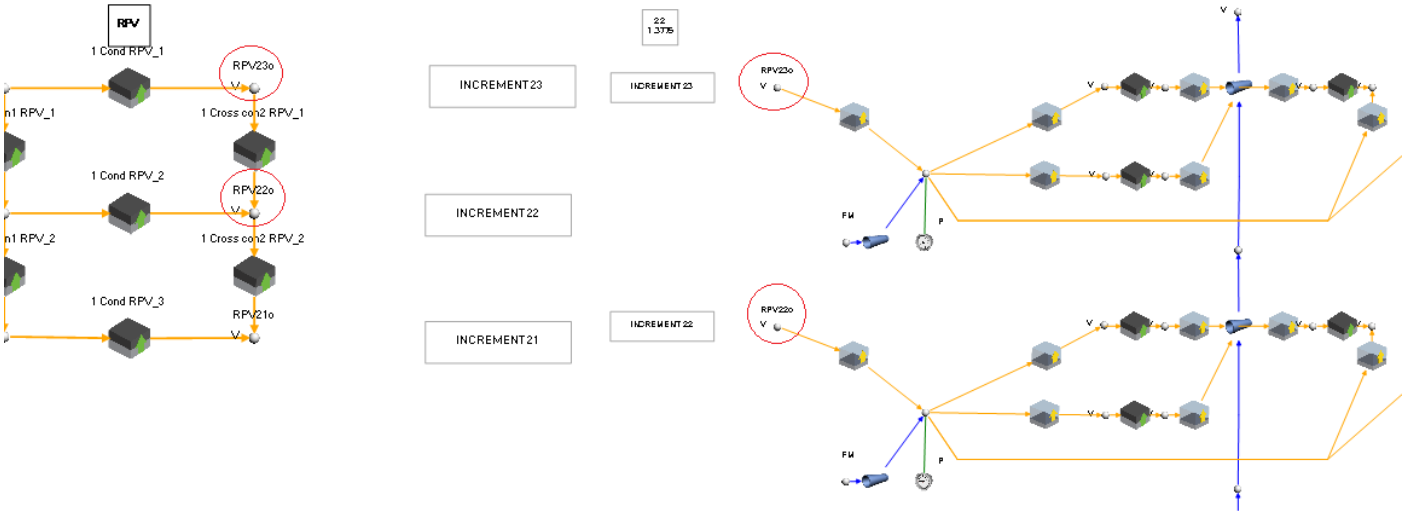

Fig. 6: RPV wall and riser increment allocation for integration.

The integration of the reactor and RCCS models therefore ensures that the effect that they have on each other is directly accounted for and that the overall performance of the system can be simulated.

7. Results

An atmospheric pressure of 100 kPa is applied to the inlets and outlets of the manifold (Fig. 9), whilst the temperature of the atmospheric air entering the RCCS is assumed to be 40 ^{o}C. The outer surface of the concrete containment is considered to be adiabatic (Du Toit et al., 2016).

Du Toit et al. (2016) studied the PMR200 RCCS system (Jun, 2012) employing the 1D network codes GAMMA+ and Flownex. The models did not include the reactor but included the RPV wall. A steady-temperature of 250 ^{o}C was applied to the inside surface of the RPV wall for normal operating conditions, and a steady-state temperature of 350 ^{o}C was applied to the inside surface of the RPV for accident conditions. The

height of the risers and downcomers is 18.5 m (Jun, 2012). Note that GAMMA+ (Lim and No, 2006) models the circulation of air in the cavity using coarse axi-symmetric 2D mesh. Du Toit et al. (2016) extracted the total heat loss at the RPV surface, the radiation heat transfer at the RPV surface, the convection heat transfer at the RPV surface, mass flow rate of the air in the RCCS, the temperature of the air at the outlet of the RCCS, and the maximum wall temperatures of the riser tubes, downcomer and concrete from the GAMMA+ and Flownex simulation results. The relevant values are summarized in Table 1 in the columns GAMMA+ 2016 and FNX 2016. The results are for the case where the temperature of the inside surface of the RPV was specified to be 250 ºC. From similar results presented by Rousseau et al. (2015), it was concluded that in general there is very good agreement between the results generated with the two codes.

Table 1: Steady-state operation results.

		RCCS only		**Integrated**
Parameter	**GAMMA+ 2016**	**FNX 2016**	**FNX 2021a**	**FNX 2021b**
Total Heat Loss at RPV Surface (MW)	0.930	0.949	0.792	0.888
Radiation Heat Transfer at RPV Surface (MW)	0.628	0.632	0.527	0.619
Convection Heat Transfer at RPV Surface (MW)	0.302	0.317	0.265	0.269
Chimney Air Flow rate in RCCS (kg/s)	10.46	10.44	12.04	12.46
Chimney Exit Temperature (ºC)	127.31	129.79	105.01	110.33
Maximum Temperature of Riser Tube (ºC)	165.36	167.41	149.49	173.26
Maximum Temperature of Downcomer Wall (ºC)	155.06	152.77	133.39	144.99
Maximum Temperature of Concrete Wall (ºC)	42.82	42.87	42.07	42.48

In the current study, two initial simulations were performed. In the first simulation the adapted RCCS model not integrated with the reactor model, as depicted in Fig. 4, was considered. A temperature of 250 ºC was applied to the inside surface of the RPV wall. The corresponding results obtained from this simulation are summarized in Table 1 in the column FNX 2021a. In the second simulation the RCCS model integrated with the reactor model, as depicted in Fig. 6, was considered. The summary in column FNX 2021b given in Table 1 is the corresponding results obtained from this simulation.

The effect of the difference in height of the risers/downcomer between the FNX 2016 and FNX 2021a models, i.e. 18.5 m versus 14.068 m, can be observed in Table 1. This difference in height leads to a reduction of 8.86 m in the length of the flow path between the top of the downcomer and the top of the riser in the FNX 2021a model compared to the FNX 2016 model. The heat removed by the RCCS in the FNX 2021a model is 0.157 kW less than the heat removed by the RCCS in the FNX 2016 model. However, the mass flow rate in the case of the FNX 2021a model is 1.6 kg/s more than the mass flow rate in the case of the FNX 2016 model. As a first assumption, it could be expected that the mass flow rate should decrease as the heat transferred to the RCCS decreases. However, it can be deduced that the reduction in frictional resistance due to the reduction in the length of the flow path is larger than the effect of the reduction in the heat transferred leading to the increase

in the mass flow rate. This needs to be evaluated in greater detail. The higher heat transferred and lower mass flow rate in the case of the FNX 2016 model leads to a higher RCCS outlet air temperature compared to the corresponding value for the FNX 2021a models associated with a lower heat transferred and higher mass flow rate. No anomalies are observed in the FNX 2021a results compared to the FNX 2016 results and it can therefore be concluded that the FNX 2021a model is a valid model and when integrated with the reactor model (FNX 2021b) should provide representative results for the performance of the integrated reactor-RCCS system.

From the results in Table 1, it can be observed that 96 kW more heat is transferred in the case of the FNX 2021b model compared to the FNX 2021a model. In the case of the FNX 2021b model, the radiative heat transfer comprises 69.7% of the total heat transfer compared to 66.5% in the case of the FNX 2021a model. As expected, the RCCS mass flow in the case of the FNX 2021b model is larger than the corresponding value for the FNX 2021a model. In this case, the larger heat transfer and the larger mass flow rate result in a larger RCCS outlet air temperature for the FNX 2021b model compared to the FNX 2021a model.

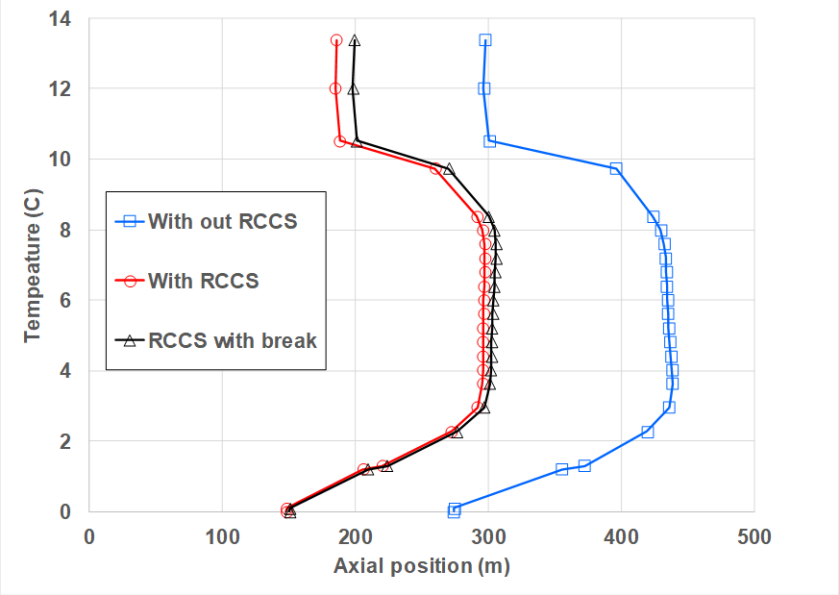

Fig. 7: Temperature distribution on RPV outer wall.

The temperature distribution on the outside surface of the RPV is shown in Fig. 8. The cases without RCCS and with RCCS are discussed in this section. When the RCCS model is not integrated with the reactor model, the outside surface of the RPV is considered to be adiabatic and the only cooling for the RPV is provided by the vessel cooling system (VCS). With the VCS mass flow rate prescribed as 2.0 kg/s with an inlet temperature of 140 ^{o}C, the maximum RPV surface temperature is found to be 438.5°C and the average surface temperature is 394.3 °C. These values exceed the maximum allowable value of 371 ^{o}C (Jun et al., 2009). In the case of the integrated reactor-RCCS model with VCS flow maintained the maximum RPV surface temperature is found to be 297.7 ^{o}C and the average surface temperature is 259.1 ^{o}C. These values are well below the maximum allowable value for the temperature and the maximum temperature is in good agreement with the corresponding value of 295 ^{o}C obtained by Jun et al. (2009).

The maximum fuel centre temperatures for the first, second and third rings of fuel blocks occur at the bottom of the active core and is respectively 1122.3 ºC, 1133.5 ºC and 1111.9 ºC. These are respectively 0.10%, 0.09% and 0.11% lower than the corresponding values obtained by Nel and Du Toit (2021) when the RPV is only cooled by the VCS. It can therefore be concluded that the RCCS has a significant impact on the temperatures of the RPV, but virtually no impact on the maximum fuel temperatures under normal steady-state operating conditions.

7.1 Effect of mass flow rate of coolant in VCS

The heat removed by the VCS in the case of the integrated reactor-RCCS model when the VCS is mass flow rate is 2.0 kg/s is 713.6 kW compared to the 887.9 kW removed by the RCCS giving a total of 1601.5 kW. The maximum RPV surface temperature and heat removed by the VCS and RCCS as functions of the VCS mass flow rate are shown in Fig. 8.

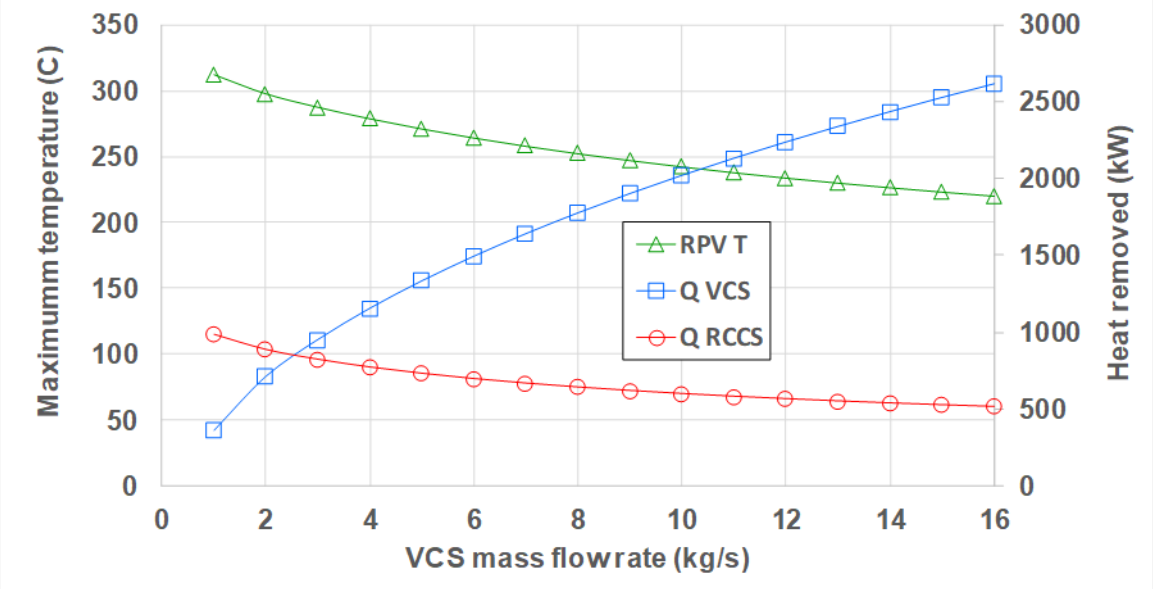

Fig. 8; Maximum RPV temperature and heat removed by VCS and RCCS as functions of VCS mass flow rate.

The heat removed by the VCS exceeds the heat removed by the RCCS when the VCS mass flow rate is larger than 2.5 kg/s. When the VCS mass flow rate is 1.0 kg/s the RCCS removes 73.2% of the heat, whilst for VCS mass flow rate of 16.0 kg/s the RCCS removes only 16.5% of the heat. The core outlet temperature changes from 949.1 ºC for a VCS mass flow rate of 1.0 kg/s to 947.7 ºC when the VCS mass flow rate is 16.0 kg/s. This represents a change of 1.5%.

7.2 Effect of a break on the performance of the RCCS

Du Toit et al. (2016) studied the effect that breaks occurring between the cold and hot flow streams may have on the performance of the RCCS. In this paper, the study was extended to evaluate the effect of the postulated

breaks on the performance of the integrated reactor-RCCS system. With the RCCS_InHead and RCCS_OutHead, see Fig. 9, identified to be the most vulnerable with regards to the surface area, pressure differences and volume flow rate the different breaks are assumed to occur between the walls of one of the RCCS_InHead ducts and the corresponding RCCS_OutHead duct (Du Toit et al., 2016). Five positions were selected for the postulated breaks between the InHead and the OutHead of the RCCS. The five locations are indicated in Fig. 9 and numbered from 1 through 5. The first break position is located at the end of the horizontal section of the RCCS_InHead/RCCS_OutHead. In the middle of the horizontal leg, the second break position is located, and the third break position is located and the end/bend/beginning of the horizontal/vertical leg. The fourth break position is located in the middle of the vertical leg of the RCCS_InHead/RCCS_OutHead and the fifth break position is located at the top end of the vertical leg.

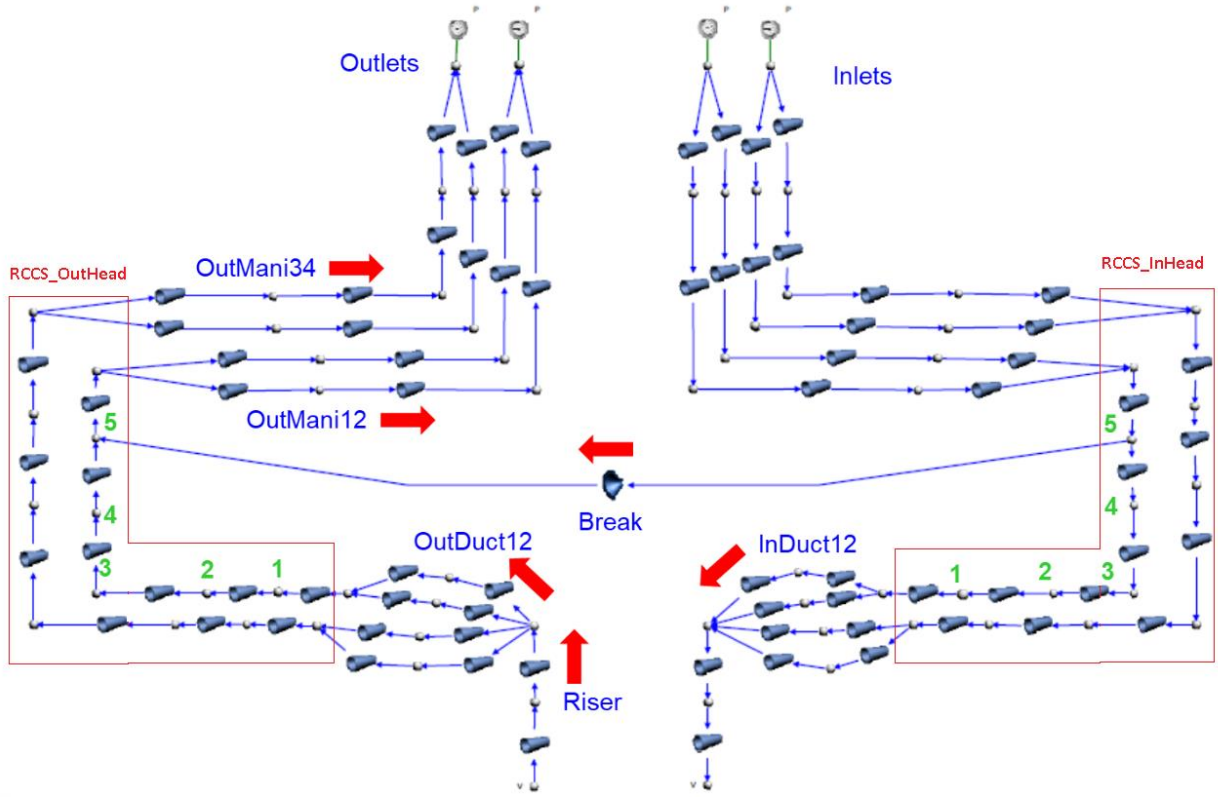

Fig. 9: RCCS Manifold with Break allocation.

In the Flownex model, a break is represented by an orifice with a discharge coefficient of 0.6. To simulate a selected break, the end points of the orifice fibres were connected to the relevant nodes (Fig. 10 illustrates the break at position 5). The size of the breaks is assumed to be 1%, 2%, 4%, 5%, 10%, 30%, 50%, 70%, 90% and 100% of twice the flow area of the RCCS_OutHead (Du Toit et al., 2016). To evaluate the effect of a break the mass flow rates through selected components are monitored. The selected components are the Break component itself, the OutDuct12, OutMani12, OutMani34 and the InDuct12 as well as the Outlets and the Inlets as indicated in Fig. 9. The positive flow direction through the components is indicated by the red arrows in Fig. 9. Note that in the case of OutDuct12, OutMani12, OutMani34 and InDuct12 the combined mass flow in the two legs is considered.

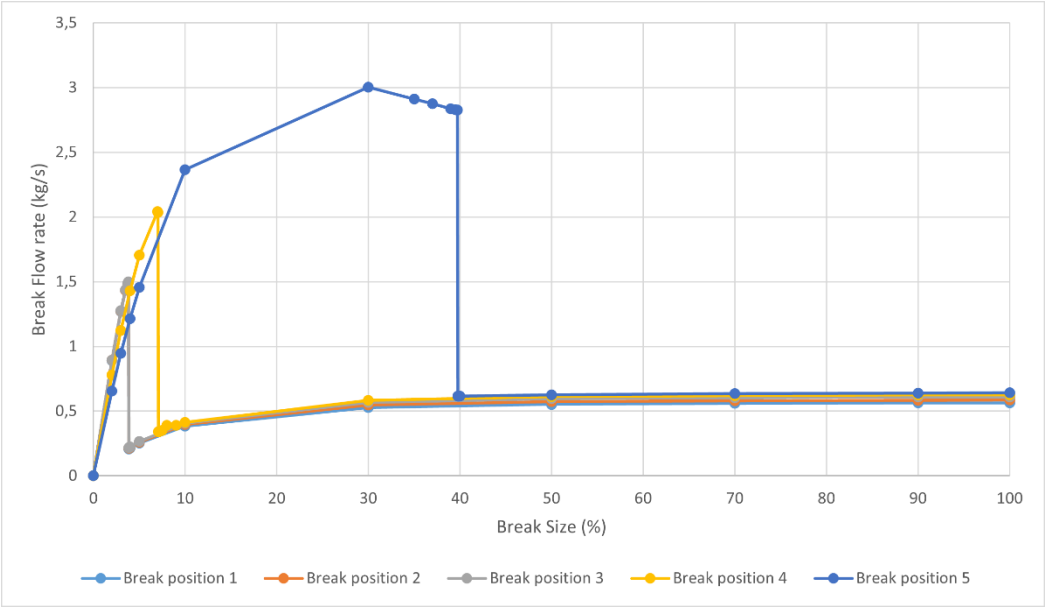

Fig. 10: Break mass flow for FNX 2016 model.

When a break occurs in the manifold, air flows through the break between the RCCS_InHead and the RCCS_OutHead. In Fig. 10 the break mass flow rates for each break position as a function of break size obtained by the FNX 2016 model are shown. For a given break position, it can be observed that the break mass flow increases with increasing break size until the break size reaches a critical value. At the critical break size, the mass flow decreases sharply but remains in the positive direction. For all break positions, the mass flow rate through the break reaches an asymptotic value when the break size is larger than 50%. At the critical break size, Du Toit et al. (2016) found that the direction of the flow through OutDuct12 and OutMani12 is reversed.

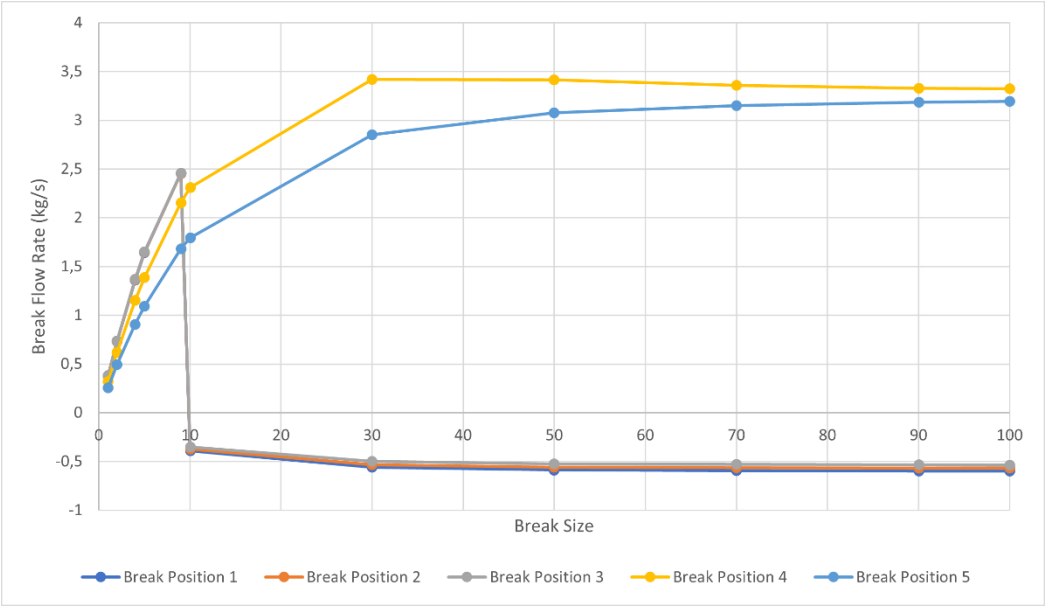

Fig. 11: Break mass flow rate for FNX 2021a model.

The corresponding break mass flow rates obtained by the FNX 2021a and FNX 2021b models are shown in Fig. 11 and Fig. 12 respectively. It can be seen in Fig. 11 that the break flow rate for break positions 1, 2 and 3

increases as the break size increases until the break reaches the critical break size and then the flow direction through the break reverses. After the critical break size, the break mass flow rate becomes independent from the break size when the break size is larger than 50%. In Fig. 12 it can be seen that for the FNX 2021b model the same trends are followed for the break mass flow rates as shown for the FNX 2021a model in Fig. 11. It is found that in both the FNX 2021a and FNX 2021b models the break flow direction changes at the same instant as the flow in the OutDuct12 and OutMani12 changes direction. For the break positions of 1, 2 and 3, the critical break size remains between 9% and 11% for both the FNX 2021a model and the FNX 2021b model. For break positions 4 and 5, it can be seen that flow direction within the break does not reverse. It is also found that the flow direction in OutDuct12 and OutMani12 does not reverse. The flow reversal at break positions 1, 2 and 3 follow the same trend, due to the fact that the break positions are on the same vertical level and differ from the trends followed by the breaks at positions 4 and 5 is because they are at different vertical positions. It is also interesting to note that in the case of the FNX 2016 model the break mass flow rate after the critical break size approaches the asymptotic mass flow from above. In the case of the FNX 2021a and FNX 2021b models, the break mass flow rate approaches the asymptotic value from below. The fundamental underlying physical phenomena that are responsible for the differences in behaviour should be studied in more detail in order to develop a thorough understanding of the interacting forces that determine the behaviour of the RCCS.

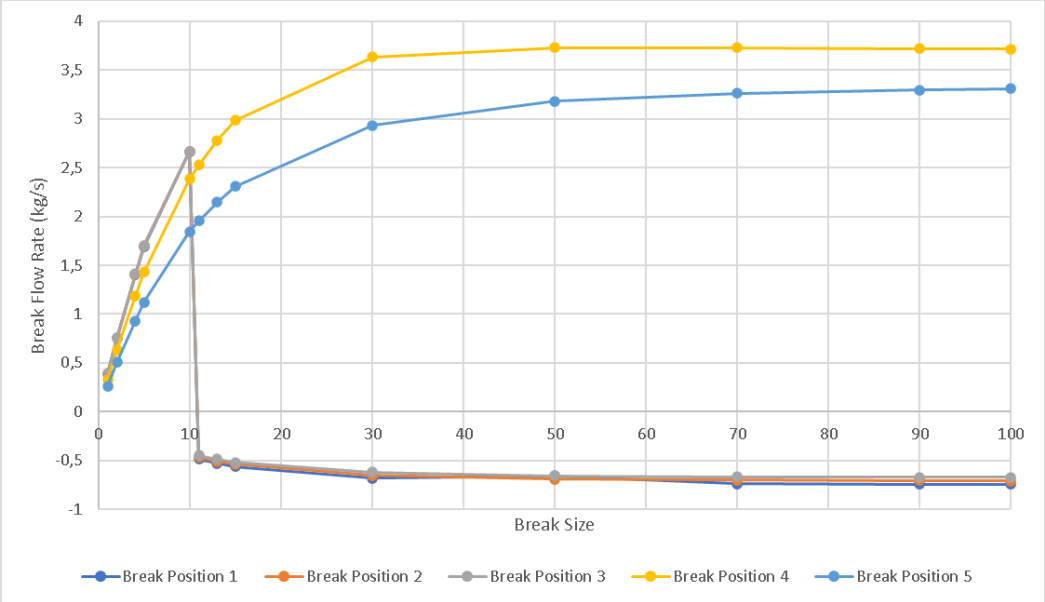

Fig. 12: Break mass flow rate for FNX 2021b model.

In Fig. 13 the mass flow rates for break position 2 through the Break, OutDuct12, OutMani12, OutMani34 and the Riser as a function of the break size are shown. Before a break occurs within the manifold system the mass flow rates through the OutDuct12, OutMani12 and OutMani34 are the same and equal to half of the mass flow rate through the Riser. As the break size grows the airflow through the break from the cold inlet stream to the hot outlet stream increases and the mass flow rates through OutDuct12 and OutMani12 decrease. At the same time, the mass flow rate through the risers decreases because of the mass flow short-circuiting through the Break. Note that the difference between the mass flow rates through OutDuct12 and OutMani12 is equal to the mass flow rate through the Break. While the mass flow rates through OutDuct12 and OutMani12 decrease, the mass flow rate through

OutMani34 increases. Thus before the critical break size is reached, an increasing part of the mass flow through the risers is diverted to OutMani34. As the critical break size is reached the flow directions through OutDuct12, OutMani12 and the Break reverse. All the mass flow from the risers is now diverted to OutMani34 along with the reversed mass flow through OutDuct12. Also, part of the mass flow flowing down OutMani12 is diverted through the Break which is then through InDuct12 (Fig. 9) directed to the top of the downcomer. After the break size has reached its critical size, the mass flow rates through the selected ducts and the Break stabilize and become independent of break size.

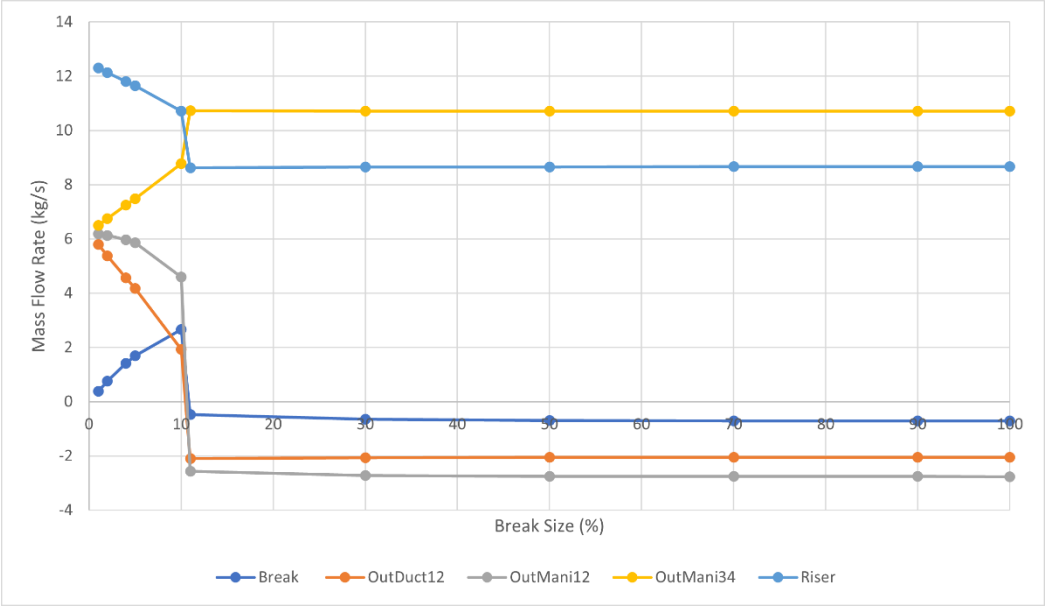

Fig. 13: Mass flow rate through selected ducts at break position 2 for FNX 2021b model.

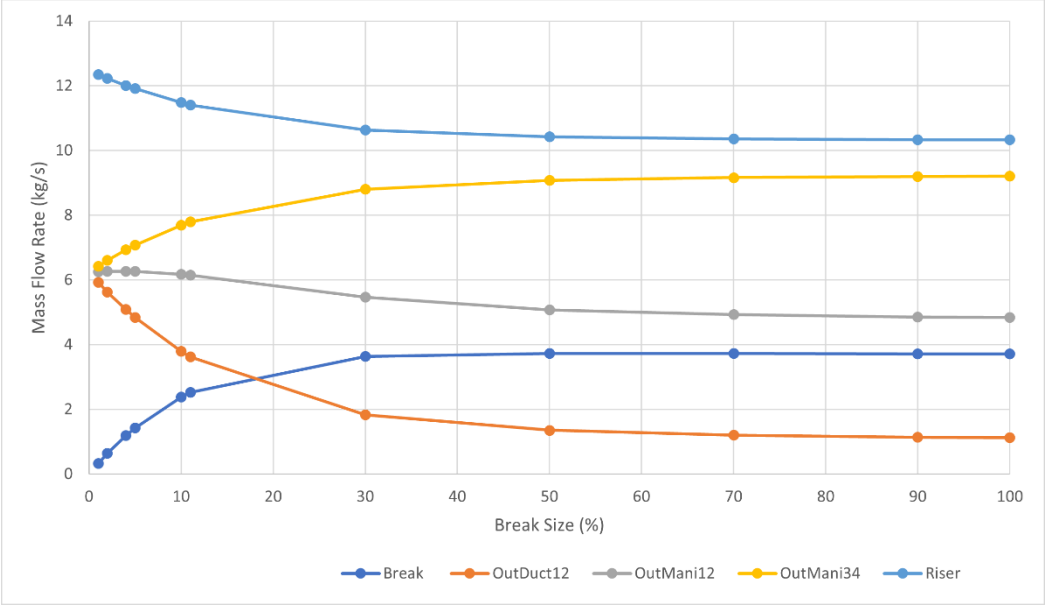

Fig. 14: Mass flow rate through selected components at break position 4 for FNX 2021b model.

In Fig. 14 the mass flow rates for break position 4 through the Break, OutDuct12, OutMani12, OutMani34 and the Riser as a function of the break size are shown. A noticeable difference between Fig. 13 and Fig. 14 is that it can be observed that in none of the selected ducts the flow reverses. As the break size at position 4 grows the mass flow rate through the break increases and at a break size of 50% reaches an asymptotic value. The mass through the break from the cold inlet stream to the hot outlet stream results in a reduction in the mass flow OutDuct12. Although the mass flow through OutMani12 initially appears to remain unchanged, the mass flow rate also decreases to reach an asymptotic value. The mass flow rate through OutMani34 increases which indicates that an increasing part of the mass flow through the risers is diverted to OutMani34. Because part of the cold inlet stream is short-circuited through the Break, the mass flow rate through the risers decreases to reach an asymptotic value along with the other flow streams.

The critical break sizes as a function of break position are shown in Fig. 15. As shown in Figs. 11 and 12 for both the FNX 2021a and FNX 2021b models critical break sizes only occur for breaks at positions 1,2 and 3. At the 4th and 5th break positions no flow reversal occurs in the selected ducts and there are thus no critical break sizes associated with the break positions. The critical break sizes at the different break positions from the FNX 2016 model (Du Toit et al., 2016) are also included in Fig. 15. It can be seen that there are critical break sizes associated with all the break locations. The critical break sizes of the FNX 2021a and FNX 2021b models range between 9% and 10%. In the FNX 2016 model, the critical break sizes at positions 1, 2 and 3 vary between 3% and 4% and at position 4 the critical break size is 7.1%. For the critical break size at position 5 the percentage break is significantly higher than that of the other break positions and comes to 39.75%.

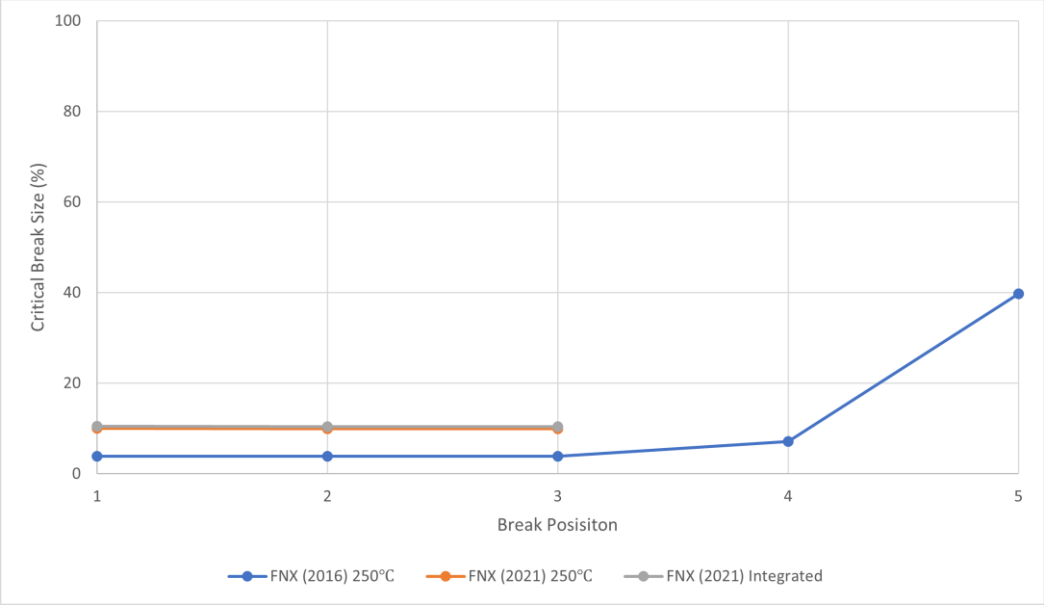

Fig. 15: Critical break size as function of position (2021 integrated).

To determine the cause of the reversal of flow in sections of the RCCS manifold the balance in gravitational forces, stagnation pressure forces and resistance forces between the break and the OutMani12 section of the manifold was investigated. Eq. (7) gives the balance of the forces used in the investigation.

$$\sum_k(\Delta p_0)_k + \sum_k(\Delta\bar{\rho}gz)_k = \sum_k(\Delta p_L)_k \qquad (7)$$

With:

$$\sum_k(\Delta p_0)_k = \sum_k(p_{0i} - p_{0e})_k$$

$$\sum_k(\Delta\bar{\rho}gz)_k = \sum_k(\Delta\bar{\rho}g[z_i - z_{e]})_k$$

$$\sum_k(\Delta p_L)_k = \sum_k(\frac{fL}{D_h}\bar{\rho}|\bar{V}|\bar{V})_k + \sum_k(K\frac{1}{2}\bar{\rho}|\bar{V}|\bar{V})_k$$

Where *k* is the counter over the pipe elements and $\bar{V}$ the average velocity in a pipe element. The variation in the resistance force as a function of break size for break positions 3, 4 and 5 as from the FNX 2021b model is shown in Fig. 16. As seen in Fig. 16 the resistance force for break position 3 declines as the break size increases until the critical break size is reached and then the resistance force term becomes negative. It should be kept in mind that the stagnation pressure term is positive upwards, whilst the gravitational force term is always negative downwards. When the resistance force term becomes negative, the gravitational force downward is larger than the stagnation pressure force upwards. Thus, when the resistance force term is negative the flow has reversed. The observed trend correlates with the trend seen in Fig. 12.

The cold air flowing through the break mixes with the hot air flowing through OutDuct12 when the break occurs. As a result, the density of the air above the break increases and thus the gravitational force above the break also increases. As the break size grows, the mass flow rate through the break increases, as well as the density of the air above the break. At the critical break size, the density of the air above the break is large enough for the gravitational force to overcome the stagnation pressure force and the flow direction in OutMani12 reverses. Because the elevations of break positions 1, 2 and 3 are the same, the critical break sizes for these positions are the same. In the case of break positions 4 and 5, the increase in density is not large enough for the gravitational force to overcome the stagnation pressure force.

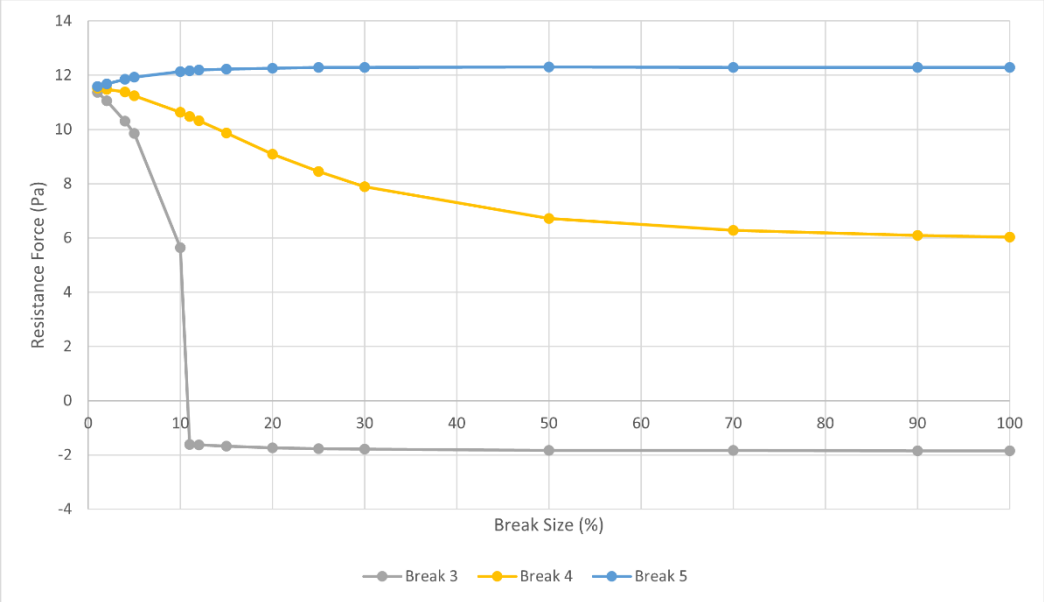

Fig. 16: Resistance force as a function of break size for FNX 2021b model.

The performance of the heat removal capacity of the RCCS as a function of break size and break position as extracted from the FNX 2021b model is shown in Fig. 17. In any instance where a break occurs the heat removal performance of the RCCS deteriorates as the mass flow through the risers decreases. It can be seen in Fig. 17 that when a break occurs the lowest value of the heat removal capacity is reached when the flow in ManiOut12 reverses. With a break size of 1% at all the break positions, the mass flow rates in the riser are between 12kg/s and 13kg/s. For break positions 1, 2 and 3 the critical break size is reached between 9% and 11% and the mass flow through the riser drops to between 10kg/s and 11kg/s with a flow reversal in the OutDuct12 and OutMani12 sections. For Break positions 4 and 5 at the same break size as the critical break size for break 1, 2 and 3, the mass flow through the riser is between 11kg/s and 12kg/s. As the mass flow through the riser is more for break positions 4 and 5 than that of the flow rate through break positions 1, 2 and 3 the heat removal capacity is more for breaks 4 and 5 than that of break positions 1, 2 and 3.

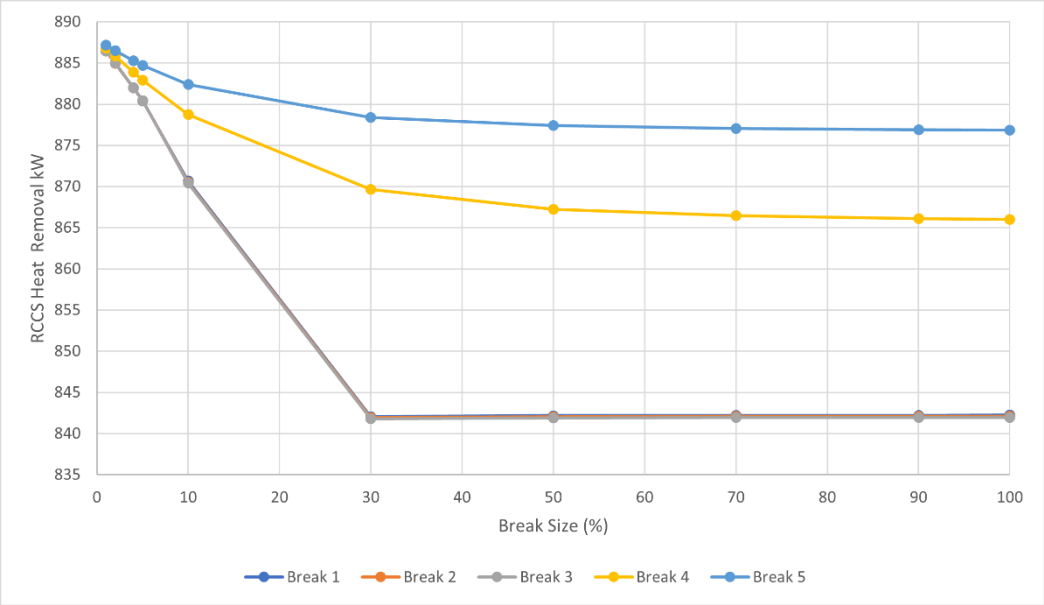

Fig. 17: RCCS heat removal as a function of break size (2021 integrated).

In Fig. 7 the temperature distribution on the surface of the RPV when a break size of more than 30% occurs at break position 3. The maximum temperature on the RPV surface is 306.0 ºC and the average temperature is 266.4 ºC. The maximum temperature is 8.3 ºC larger than the corresponding temperature in the case of the fully operational RCCS. The maximum fuel centre temperatures for the first, second and third rings of fuel blocks occur at the bottom of the active core increase respectively by 0.004%, 0.004% and 0.005%. It can therefore be concluded that the effect of the breaks under steady-state conditions on the reactor is minimal.

8. Conclusions

Three different RCCS Flownex (1D system network code) models were investigated, the 18.5m high riser RCCS model (FNX 2016) from Du Toit et al. (2016) with an RPV wall temperature boundary condition of 250℃ and an adapted RCCS version (FNX 2021a) of the RCCS from Du Toit et al. (2016) with the riser height of 14.068m and an RPV wall temperature boundary condition of also 250℃. The input temperature boundary conditions assigned for the FNX 2016 and FNX 2021a models is applied uniformly at the inside wall of the RPV section. A third Flownex model (FNX 2021b) where the 14.068m high adapted RCCS model was integrated with a full representative PMR200 reactor model was also studied. In this model, the RCCS extracts heat generated by the active fuel core of the reactor released by the RPV.

With the VCS included in the integrated Flownex model of the PMR200 and the RCCS, a total of 713.61 kW worth of heat is extracted by the VCS itself. The RCCS extracts 887.87 kW worth of heat from the reactor system. The maximum outer wall temperature for the RPV is 297.68℃ which is below the maximum allowable temperature for the RPV of 371℃. When the flow rate is increased in the VCS, the outlet temperature of the reactor coolant is nearly unchanged and thus the VCS flow rate has a negligible effect on the outlet temperature of the reactor coolant.

In the Flownex models that were constructed, postulated breaks were introduced between one half of the inlet and the corresponding outlet manifold of the RCCS and the effects of the break on the RCCS were investigated. The results from the different models were compared with each other and elaborated on as some trends/results within the models correlate with each other and other differs from one another. For certain break positions in the evaluated models, flow reversal is observed as the break size exceeds a certain value. In the integrated model the reversal of flow at break positions 1, 2 and 3 leads to the RCCS' heat removal capacity to drop between 3% and 4%. The amount of heat that is removed by the RCCS from the Reactor without a break in the manifold is 888 kW and varies from 887 kW to 842 kW when breaks are introduced to the system. It can thus be said that if a break occurs between the InHead and OutHead of the RCCS the impact to heat removal capacity of the RCCS is not critical. With the RCCS integrated into the representative PMR200 reactor model, the RCCS cools down the RPV wall to below the maximum allowed operating temperature. The effect that the breaks have on the temperature of the outside surface of the RPV and the maximum fuel temperatures in the active core of the reactor is minimal.

The integrated PMR200 reactor-RCCS model can be coupled with the balance of the primary loop and the secondary loop to study and evaluate the performance and behaviour of the complete plant. The uniform power profile applied to the active core should be replaced with an appropriate non-uniform power profile.

9. Acknowledgements

This work is based on the research supported by the South African Research Chairs Initiative of the Department of Science and Technology and the National Research Foundation (NRF) of South Africa (Grant No 61059).

Any opinion, findings and conclusion or recommendation expressed in this material is that of the authors and the NRF does not accept any liability in this regard.

The authors wish to thank Dr JS Jun for providing the data of the PMR200 reactor (Jun, 2020).

Abbreviations

HTGR	High-temperature gas-cooled reactor
RCCS	Reactor cavity cooling system
VCS	Vessel Cooling System
NHDD	Nuclear Hydrogen Development and Demonstration
CR	Control rod
CB	Core Barrel
PMR	Prismatic Modular Reactor
RPV	Reactor Pressure Vessel
CFD	Computational Fluid Dynamics
SCFD	System Computational Fluid Dynamics
MW_{th}	Mega Watt Thermal
NWU	North West University
HPCC	High Pressure Conduction Cooling
LPCC	Low Pressure Conduction Cooling
GT-MHR	Gas Turbine Modular Helium Reactor

List of Symbols

$\bar{\rho}$	Average density
$\forall$	Volume
$\dot{m}$	Mass flow
e	Exit
i	Inlet
L	Length
A	Cross-sectional area
p_0	Total pressure
g	Gravitational acceleration
z	Elevation
D_H	Hydraulic diameter
K	Form loss factor
f	Friction factor
h_0	Total enthalpy
P	Static pressure
Δp_L	Frictional loss
$\dot{q}_{conv}$	Convection heat transfer
T	Temperature
s	solid
f	Fluid
h	Heat transfer coefficient
Nu	Nusselt number
k_f	Thermal conductivity of the fluid
$\dot{q}_{cond}$	Conduction heat transfer
k_s	Thermal conductivity of the solid
σ	Stefan-Boltzmann constant
$\dot{q}_i$	Radiation heat transfer
ε	Emissivity
F_{ie}	View factor
E_{bi}	Emissive power
J_i	Radiosity
N	Number of surfaces
$\bar{V}$	Average velocity

k Counter

References

Du Toit, C.G., Rousseau, P.G. (2012) Modeling the flow and heat transfer in a packed bed high temperature gas-cooled reactor in the context of a systems CFD approach, Journal of Heat Transfer, 134, pp 031015-1 – 031015-12.

Du Toit,C.G.; Rousseau, P.G.; Jun,J.S.; Noh, J.M. (2014) '1D AND 3D NUMERICAL SIMULATION OF THE REACTOR CAVITY COOLING SYSTEM OF A VERY HIGH TEMPERATURE REACTOR', IHTC 15, Japan, August 2014.

Du Toit,C.G.; Rousseau, P.G.; Jun,J.S.; Kim, M-H (2016) ' NUMERICAL SIMULATION OF BREAK FLOWS OCCURING IN THE REACTOR CAVITY COOLING SYSTEM OF A VERY HIGH TEMPERATURE REACTOR USING A SYSTEM CFD APPROACH', HTR 2016, Las Vegas NV, November 2016.

Flownex, Bringing nuclear quality and standards to system simulation, https://www.flownex.com/about-us/certification, (accessed: 27 November 2019).

Frisani, A. (2010) 'Analysis of the Reactor Cavity Cooling System for Very High Temperature Gas-Cooled Reactors using Computational Fluid Dynamic Tools', Texas A&M University, United States of America

Greyvenstein, G.P. (2002) An implicit method for the analysis of transient flows in pipe networks, International Journal for Numerical Methods in Engineering, 53, pp 1127 – 1143.

Hassan, Y (2013) 'CFD Model Development and Validation for High Temperature Gas Cooled Reactor Cavity Cooling System (RCCS) Applications' Texas A&M University, Project No. 09-817

Incropera, F.P., DeWitt, D.P. (1996) Fundamentals of heat and mass transfer, New York: John Wiley & Sons.

Jun, J.S.; Lim, H.S.; Lee, W (2007) 'The Steady State Performance and Limiting Accident Analysis for a PMR 200MWth Prototype Reactor', Transactions of the Korean Nuclear Society Spring Meeting,

Jun, J.S.; Lim, H.S.; Jo, C.K.; Noh, J.M., (2009) 'Thermal-Fluid Analysis of the PMR 200MW_{th} Reactor System at the Steady State and Transient Conditions', Transactions of the Korean Nuclear Society Spring Meeting,

Jun J.S. (2012) 'Common Input Data Lists of KAERI-NWU Joint GAMMA+/FLOWNEX Code-to-Code Benchmark Study of the Natural Circulation in the Air-cooled RCCS, Korea Atomic Energy Research Institute, NHDD-RD-CA-12-016, Rev 01.

Jun, J.S. (2020) 'Main Design Data of the PMR 200MW_{th} Reactor', KAERI (unpublished)

Kim, M-H; Tak, N; Lim, H-S.(2010) ' Thermal-fluid assesment of the design options for reactor vessel cooling in a prismatic core VHTR', Annals of Nuclear Energy, 37, pp. 1774-1782

Lim, H.S.; No, H.C. (2006) ‘ GAMMA Multidimentional Multicomponent Mixture Analysis to Predict Air Ingress Phenomena in an HTGR’, Nuclear Science and Engineering, 152, 1-11.

Lisowski, D.D. (2013) ‘ Thermal Hydraulic Analysis of an Experimental Reactor Cavity Cooling System with Water: Performance and Stability’, University of Wisconsin, Madison, United States of America

M-Tech Industrial, (2021) Flownex SE Version 8.12.17.4334, http://www.flownex.com.

Nel, GJ (2021) ‘Numerical simulation of a representative PMR200 Reactor model in Flownex (Part 1)’, North-West University, South Africa

Niemand, P.F. (2021) ‘1D and 3D simulation of a water-cooled reactor cavity cooling system experimental facility’, North-West University, South Africa

Rousseau, P.G. (2015) ‘Natural Circulation in the Aircooled RCCS – Flownex Code Model and Calculation Results’, KAERI/NWU Workshop, South Africa, July 2015

Rousseau, P.G.; du Toit, C.G.; Jun, J.S.; Noh, J.M. (2015) ‘Code-to-Code comparison for analysing the steady-state heat transfer and natural circulation in an air-cooled RCCS using GAMMA+ and Flownex’, Nuclear Engineering and Design, 291, pp. 71-89

Sehoana, K.A. (2014) ‘ Simulation of natural circulation in air cooled Reactor Cavity Cooling System using Flownex’, North-West University, South Africa

Streeter, V.L., Wylie, E.B. (1979) Fluid Mechanics, Tokyo: McGraw-Hill.

Tak, N.; Kim, M; Lim, H.S.; Noh, J.M., (2011) ‘A Practical Method for Whole-Cor Thermal Analysis of a Prismatic Gas Cooled Reactor’, Nuclear Technology, 177, pp. 352-365.

World Nuclear Association (2020) ‘Generation IV Nuclear Reactors’, https://world-nuclear.org/information-library/nuclear-fuel-cycle/nuclear-power-reactors/generation-iv-nuclear-reactors.aspx

CHAPTER 5: CONCLUSIONS AND RECOMMENDATIONS

With the development of a full one-dimensional (1D) system network model of a 1/6th of a single channel fuel module (SCFM) and the development of a full 3D Star CCM+ model of the same 1/6th of an SCFM, the results obtained by the two models were compared with one another. The work performed was based on work done by Travis & El-Genk (2013b) and Nel & du Toit (2018). The study made use of a Uniform and a Cosine power profile for the heat input. Results from both the 1D & 3D simulation models were extracted, and it showed that the values predicted for the temperature distribution in the centre of the fuel compact and the wall of the fuel compact were in very good agreement with each other. As the comparison between the two simulation models is in good agreement it was concluded that Flownex is capable of predicting the temperature distribution in the fuel compact of an SCFM. The results obtained by the two constructed models only differ from 1% of each other.

The 1D system network model of the SCFM is the fundamental model on which the construction of the model of the full core of the PMR200 reactor can be based. As the different types of heat transfer mechanisms in a full core of a PMR200 reactor are very important for the optimal operation of the VHTR, different thermal characteristics must be evaluated to assure that the core can be utilised in a proper, safe and efficient manner. Several studies were done on the PMR200 reactor and on different sections of the reactor to assess the thermal characteristics. These studies amongst others considered the Single Channel Fuel Modules (Nel and du Toit, 2018), 1/12th of a fuel block (Ribeiro et al., 2013) and a 1/6th of the PMR200 reactor by Travis and El-Genk (2013). In this study, a full representative model of the PMR200 reactor was constructed which includes each section from the top head plenum down to the bottom support and from the inner reflector through the active core to the RPV of the reactor. Bypass gaps and cross flow gaps are also included in the model to get more representative results of the thermal characteristic. In the first part of the development of the reactor model (Chapter 3) the reactor cavity cooling system was not coupled to the model of the PMR200 reactor. Selected thermal characteristic results were extracted and discussed.

With the full representative, 1D system network model of the PMR200 reactor constructed Flownex obtained an outlet temperature of 949.8℃ at a pressure of 6.9923 MPa. The outlet temperature is within less than 1% of the prescribed nominal outlet temperature of 950℃. The maximum fuel temperature and maximum fluid temperatures were found to be 1134.66℃ and 1043.97℃ respectively. The maximum fuel temperature is below the design limit of 1250℃. The core is enclosed in a reactor pressure vessel (RPV) and between the core barrel and the RVP a vessel cooling system (VCS) is used to cool down the RPV. With the VCS cooling, the RPV maximum fluid temperature in the VCS was found to be 239.1℃ and the maximum temperature of the RPV was found to be 438.5℃ which is higher than the maximum allowable temperature of 371℃. For the RPV to remain under the allowable maximum temperature and without the RCCS the mass flow of the VCS needs to be larger than 5.4 kg/s.

An RCCS model was constructed and integrated with the PMR200 reactor model to evaluate how the RCCS enhances the removal of the heat released by the RPV. A 1D system network Air-cooled RCCS model was constructed in Flownex using the RCCS model developed by du Toit (2016) as a basis. Although the layout of the RCCS models is the same, there are dimensional differences. The adapted RCCS model with a uniform

temperature input of 250°C at the inner surface RPV extracted 792 kW worth of heat from the system. The adapted RCCS integrated with the PMR200 reactor removes heat released by the RPV that is generated by the active core. The RCCS model integrated with the PMR200 Flownex model removes 888 kW worth of heat, and the associated maximum temperature of the RPV was found to be 297.68°C which is below the maximum allowable temperature for the RPV.

Breaks were postulated to occur in the RCCS system between the OutHead and the InHead of the manifold. With breaks occurring in the manifold, the amount of heat that is extracted from the reactor was found to range from 887 kW to 842 kW for a break size ranging from 1% to 100%. In certain instances, it was found that is a flow reversal occurs in the system and that the heat removal capacity of the RCCS decreases between 3% and 4%.

With the construction of the 1D system network model of $1/6^{th}$ of an SCFM, the full representative PMR200 reactor model, the RCCS model and the integration of the RCCS and the full representative PMR200 reactor models, it can be concluded that Flownex can be employed to construct representative 1D networks models of a prismatic block reactor and the associated reactor cavity cooling system. The approach outlined to construct the model of the PMR200 prismatic block reactor and the RCCS can be implemented and adapted, as required, to construct a 1D model of a similar prismatic block reactor system.

It is recommended that the relevant PMR200 power profile is to be implemented and that the study should be extended to evaluate the performance of the reactor system during various prescribed transient accident conditions. Additional informational papers can be written to discuss more detailed information for specific sections of the constructed models described in the different papers above.

APPENDIX A: LAYOUT OF FLOWNEX PMR200 REACTOR MODEL

In Appendix A screen copies of the layout of the Flownex PMR200 reactor model is provided to assist the reader in the interpretation of the description that is given of the Flownex model that was constructed.

Fig. A-1 shows the layout of the complete Flownex PMR200 reactor model. The top part represents the Top Head Plenum and the Top Reflector which also contains the inlet plenum. The middle part represents the six Active Core layers and the Bottom Reflector. The bottom part represents the Outlet Plenum and the Bottom Support.

Fig. A-2 shows more detail of the Top Head Plenum and the Top Reflector including the inlet plenum.

Fig. A-3 shows more detail of the Inner Reflector and first Fuel Block ring in the top three layers of the Active Core.

Fig. A-4 shows more detail of the second and third Fuel Block rings in the top three layers of the Active Core.

Fig. A-5 shows more detail of the Outer Reflector, Permanent Reflector, Core Barrel, Vessel Cooling System and Reactor Pressure Vessel in the three layers of the Active Core.

Fig. A-6 shows more detail of part of the Bottom Reflector, the Outlet Plenum and the Bottom Support.

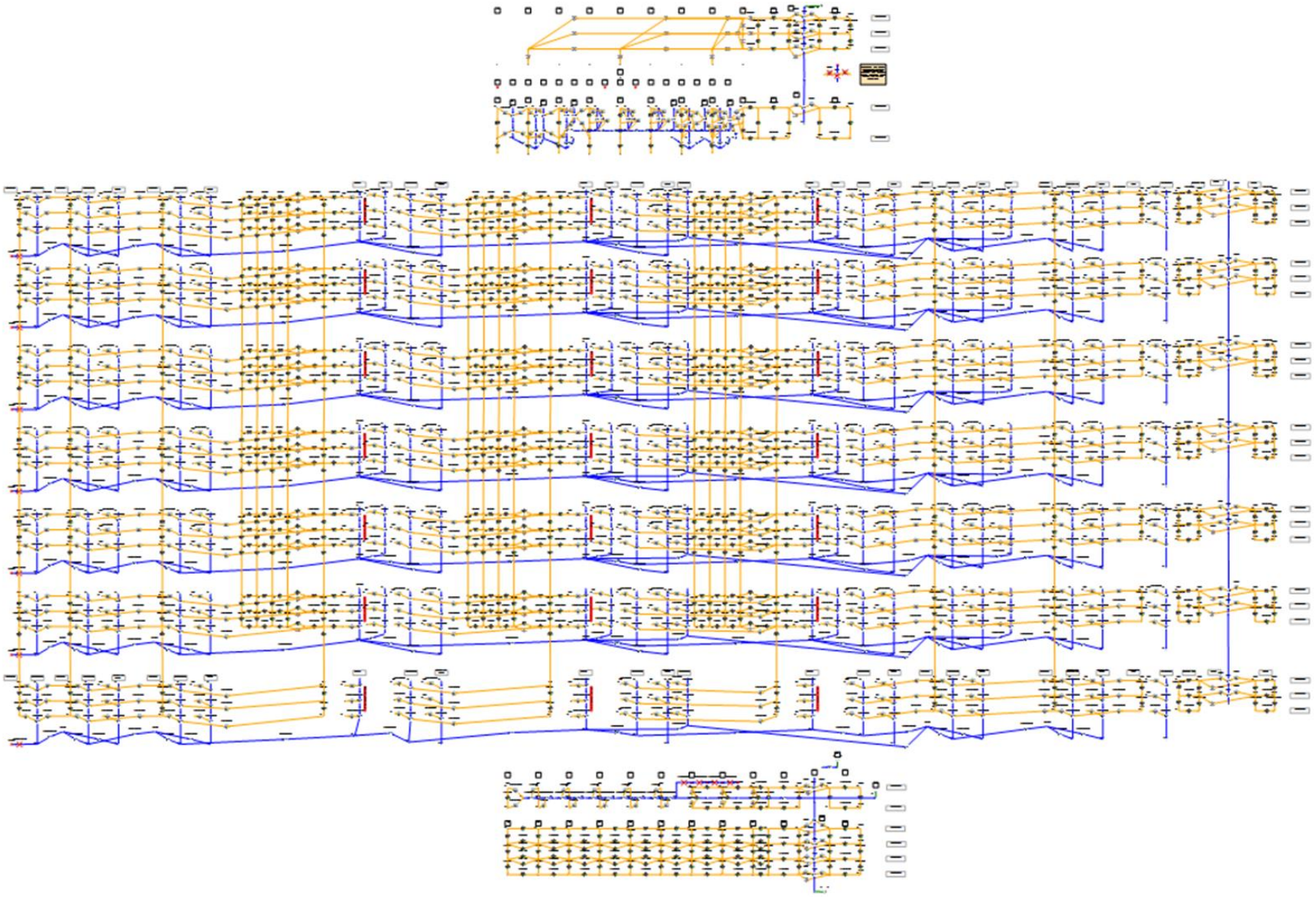

Fig. A-1: Layout of complete Flownex PMR200 reactor model.

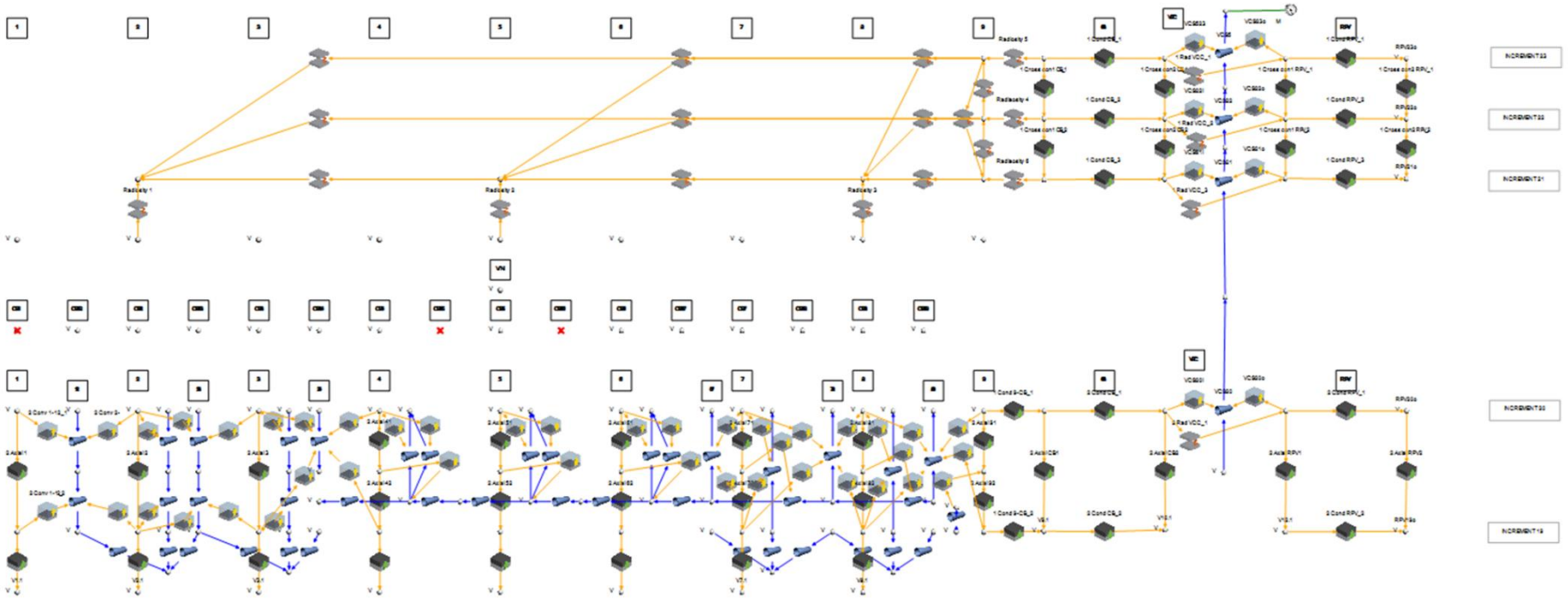

Fig. A-2: Layout of Top Head Plenum and op Reflector.

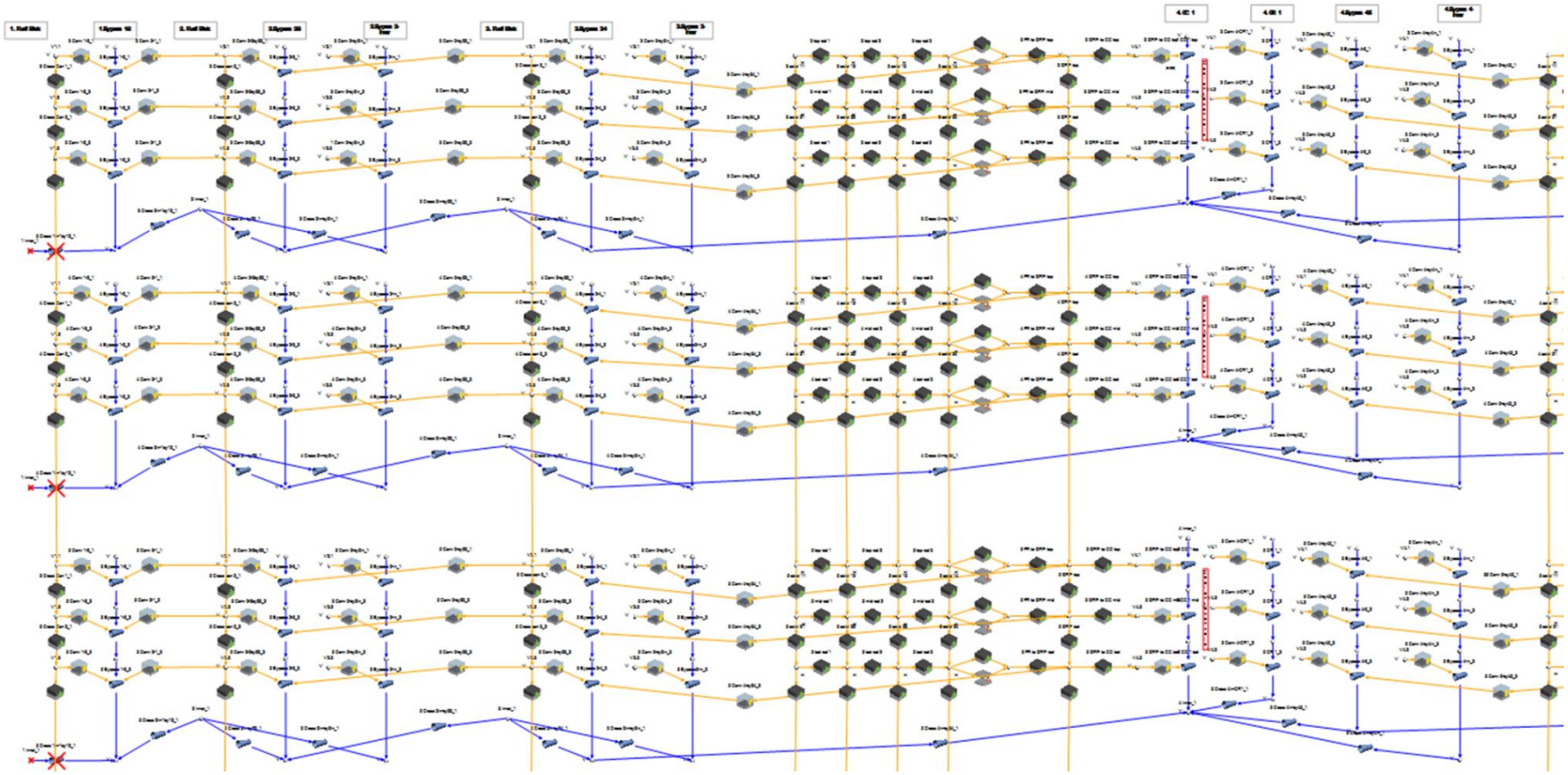

Fig. A-3: Layout of Inner Reflector and first Fuel Block ring of top three layers of the active core.

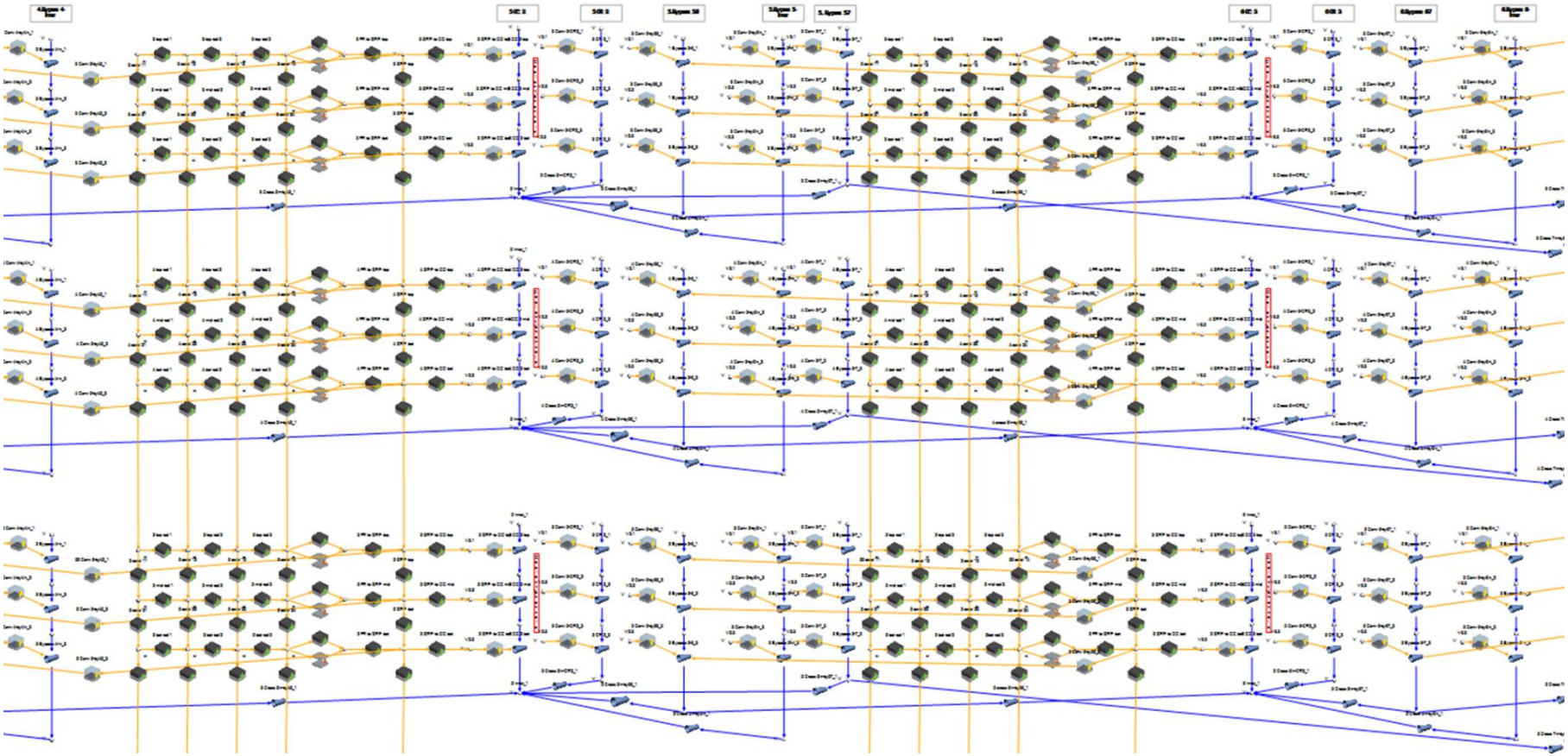

Fig. A-4: Layout of second and third Fuel Block rings of top three layers of the active core.

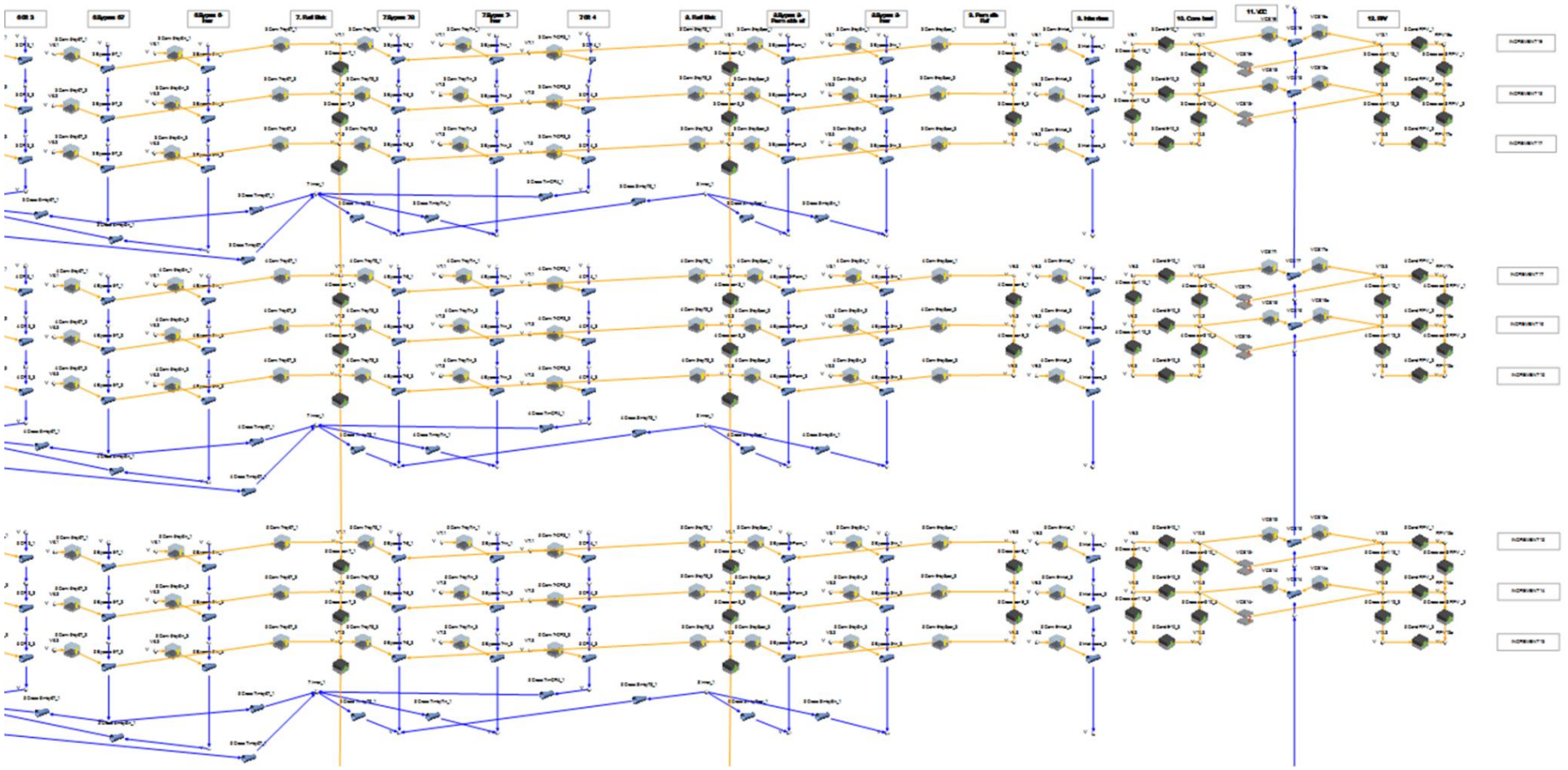

Fig. A-5: Layout of Outer Reflector, Permanent Reflector, Core Barrel, Vessel Cooling System and Reactor Pressure Vessel of top three layers of active core.

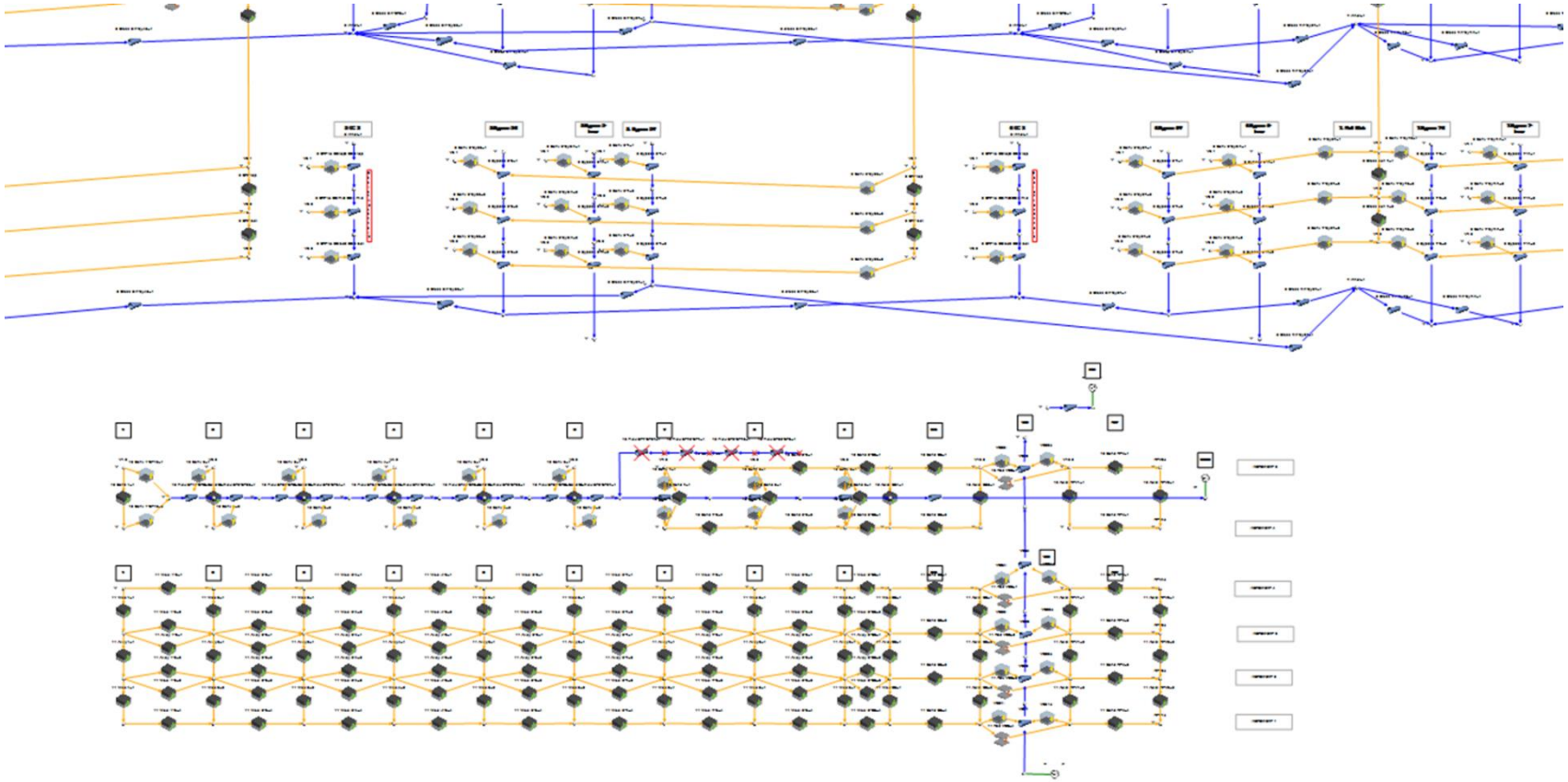

Fig. A-6: Layout of part of Bottom Reflector, the Outlet Plenum and the Bottom Support

.

APPENDIX B: COUPLED 3D AND 1D MODELS OF THE HEAT TRANSFER IN A PRISMATIC BLOCK OF A VHTR (CO-AUTHORED)

COUPLED 3D AND 1D MODELS OF THE HEAT TRANSFER IN A PRISMATIC BLOCK OF A VHTR

Koekemoer O.C.*, Nel G. J. and Du Toit C.G.
*Author for correspondence
Department of Mechanical and Nuclear Engineering,
North-West University,
Potchefstroom, 2527,
South Africa,
E-mail: ockie.koekemoer@gmail.com

ABSTRACT

Modelling prismatic block high temperature gas-cooled reactor units poses several challenges and typically requires significant computational resources and computational times. This is largely due to the complexity of prismatic block reactor models as these models must amongst others account for the fuel-compacts, graphite and coolant channels in fuel blocks, cross- and bypass gaps between blocks and the mixing in the lower plenum. This amount of detail however cannot be dealt with a single explicit three-dimensional model.

Motivated by recent advances in the field of Computational Fluid Dynamics (CFD) and recognizing the limitations on available computing power, this article is aimed at combining the desired features of a one-dimensional (1D) system code and three-dimensional (3D) CFD code. The goal is achieved by demonstrating the coupled 3D/1D CFD model that simulate the heat transfer and fluid flow in a single-channel fuel module of a prismatic block. The coupled 3D/1D model represents one sixth of a single-channel fuel model that accounts for conduction heat transfer in the solids (fuel compact and graphite moderator), convection heat transfer between the solids and the fluid (helium) and the fluid flow in the coolant channel. The validity of the coupled 3D/1D model is investigated by comparing the temperature distribution in the single-channel fuel model for a (i) uniform- and (ii) cosine power profile with the corresponding values obtained from published work as well as a full detailed 3D CFD analysis of the same specifications and setup. Since the 3D/1D models require significantly less resources than the detailed 3D CFD it can form the basis of an integrated model for the entire core.

INTRODUCTION

The Very High Temperature Reactor (VHTR) is a graphite-moderated helium-cooled reactor capable of delivering thermal power of up to 600MW_{th}. A potential benefit of the VHTR is that reactor outlet temperatures of as high as 1000 °C may be achieved for process heat and hydrogen production applications. However, the main focus at present is on the lower outlet temperatures as industrial processes and electricity production based on steam in the range of 700-850°C already have great potential and present significantly less technical risks [1]. The VHTR's inherent safety, high thermal efficiency and high temperature process heat led to the development and implementation of generation–IV, prismatic core, VHTRs. These reactors re-quire demonstrable and effective computational tools and methodologies for the design, operation and safety analyses [2].

NOMENCLATURE

Abbreviations

1D	One-dimensional
3D	Three dimensional
CFD	Computation Fluid Dynamics
NPPs	Nuclear Power Plants
SCFM	Single-Channel Fuel Module
TRISO	Tristructural-isotropic
VHTR	Very High Temperature Reactor
UDF	User Defined Function

Symbols

c_p	[J/kg.K]	Specific heat
D	[m]	Diameter
k	[W/m.K]	Thermal conductivity
μ	[Pa-s]	Dynamic viscosity
ρ	[kg/m^3]	Density
T	[K]	Temperature
z	[m]	Cartesian axis direction

In a prismatic VHTR, TRISO (Tristructural-isotropic) par-ticles are bonded together with a carbonaceous matrix into rod-shaped fuel compacts, which are stacked in the fuel holes of hexagonal graphite blocks. One of the challenging design issues in the development of the VHTR is an undesirably high temperature of the nuclear fuels in prismatic cores. Such a high fuel temperature affects the integrity of the TRISO

particles as well as the fission products released [3]. A high fuel temperature is therefore directly related to the increased core outlet temperature of the VHTR. To satisfy the widely accepted design limit (~1250 °C) [4-5] the maximum temperature difference between the fuel and the coolant should be less than ~250 °C. Considering the low heat transfer characteristics of the coolant (i.e. helium) and the non-uniform power distribution in the reactor core, the fuel temperature limit is a critical issue for the design of the VHTR. An understanding of the thermal behaviour of the prismatic fuels and the capability for an accurate pre-diction of the fuel- and coolant temperatures are therefore of considerable importance in the design of VHTRs. However, the complex geometry and nature of the numerical models hinders accurate evaluations of the fuel- and coolant temperatures without extensive numerical calculations.

Nuclear system codes such as RELAP5 [6], TRAC [7], CATHARE [8] and FLOWNEX [9] are widely used to investigate the thermal-hydraulic characteristics of the nuclear power plants (NPPs) either under normal steady-state conditions or during various accident scenarios. CFD codes such as STAR-CCM+ [10], CFX [11] and FLUENT [11] are also widely employed in nuclear reactor safety and design to analyse important and noticeable 3D effects. By combining 3D CFD codes and system codes, the advantageous coupled 3D/1D CFD approach can form the basis of an integrated model of the entire core. Explicit or semi-implicit coup-ling methodologies are available when coupling 3D CFD and systems CFD codes. Explicit methodology requires that the data are exchanged between the codes only once for each time-step. However, for the semi-implicit methodology, the data are exchanged several times for each time-step until convergence of the coupled parameters are reached. This paper demonstrates a 3D/1D approach that couples FLUENT and FLOWNEX in an explicit manner by simulating the heat transfer and fluid flow in a single-channel fuel module.

SINGLE-CHANNEL FUEL MODULE

The inner core section of a prismatic VHTR consists of columns of fuel assemblies with graphite reflector blocks at the top and bottom ends of the fuel assemblies. The graphite reflectors are added to reduce the amount of neutron leakage out of the system. A typical fuel block consists of 210 holes for the rod-shaped fuel compacts and 102 coolant holes. Ten fuel blocks, each with a height of 800mm, are stacked to form a fuel block assembly which has a total length of 8000mm [12].

A Single-Channel Fuel Module (SCFM) of a prismatic core block is shown in **Figure 1(a)** and **Figure 1(b)** where the red elements in **Figure 1(b)** represent the fuel compacts and the blue elements represent the coolant channels. A pattern of one single coolant channel surrounded by six fuel channels is repeated throughout the hexagonal blocks in the core. The SCFM is represented by the hexagonal cross section contained around the coolant channel in **Figure 1(a)** and the area outlined by the dashed hexagon in **Figure**

1(b). The fuel compacts have a diameter of 12.7mm whereas the diameter of the coolant chan-nels is 15.875mm. The fuel compact pitch is 37.6mm.

Based on the symmetry that can be observed in **Figure 1(b)** only a section of the SCFM needs to be modelled. **Figure 1(b)** illustrates three-unit cells, indicated by the dashed areas *a*, *b* and *c*. Unit cell *a* represents 1/12th of the SCFM, whilst unit cells *b* and *c* represent 1/6th of the SCFM. Unit cell *b* was selected for this study as Sambureni [13] had already characterized the con-duction shape factors for this unit cell.

As boundary conditions for the SCFM an inlet- temperature and pressure of 914K and 7.07Mpa respectively was assumed, with a mass flow rate 0.0306 kg/s for the coolant. A power of 55.4kW was applied to the SCFM, which corresponds to 600MW$_{th}$. Two power profiles were assumed, a (i) uniform- and (ii) cosine power distribution. In the case of the uniform distribution a power density of 27.406 MW$_{th}$/m^3 [12] was prescribed. For the cosine power profile the power density $PD(z)$ at a distance z from the entrance of the coolant channel is given as:

$$PD(z) = PD_{max}\cos(0.2566z - 0.8831)$$

With a maximum power density of $PD_{max} = 33.135$ MW$_{th}$/m^3.

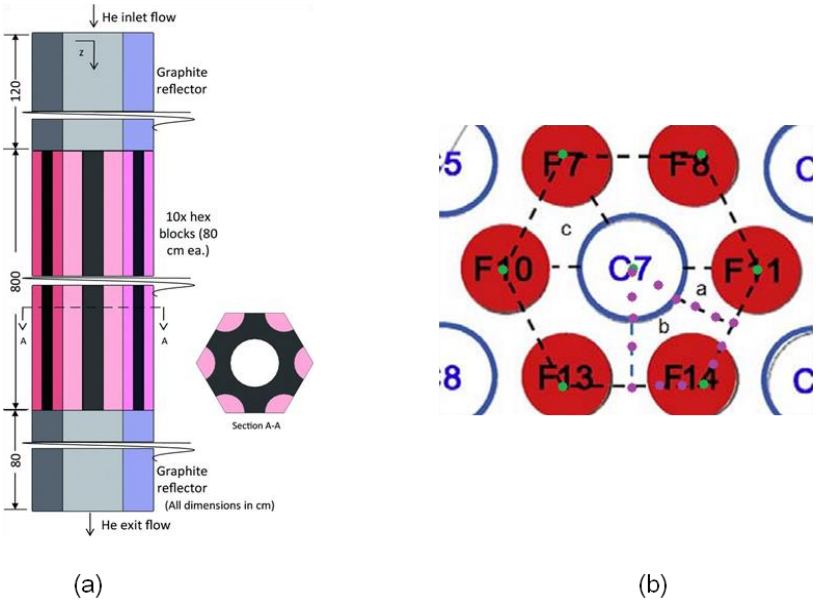

Figure 12: (a) Side and top view of the SCFM [12]; and (b) dashed hexagon outlining SCFM cross sectional area [13].

The properties of the different materials are summarized in **Table 1**.

Table 1: Material properties used in SCFM [12].

Property	Material	Correlation
Density, ρ (kg/m^3)	IG-110 graphite	1740
Specific heat, c_p (J/kg.K)		$6.05*10^{-7}T^3$ -0.00269T^2 +4.19T -294
Thermal conductivity, k (W/m.K)		-13.2 +$2.50*10^4/(T+268)^{0.78}$
Density, ρ (kg/m^3)	Composite Fuel	1650
Specific heat, c_p (J/kg.K)		$3.11*10^{-7}$ T^3 -0.00155 T^2 +2.73 T -82.4
Thermal conductivity, k (W/m.K)		8.5 +$7.68*10^4/(T+268)^{0.995}$

SINGLE-CHANNEL FUEL MODULE MODELLING

Coupling explicit 3D- and 1D models require that appropriate convection heat transfer correlations be used. Travis & El-Genk [12] performed an explicit 3D detailed simulation of a single-channel fuel module (SCFM) using the CFD code STAR-CCM+, to evaluate various convection heat transfer correlations. Based on the results obtained by Travis and El-Genk [14] it was found that the convection heat transfer regime can be considered as turbulent forced convection heat transfer. They then proposed an improved convection heat transfer correlation and implemented that in a coupled 3D/1D simulation of the SCFM. STAR-CCM+ was used to model the 3D heat transfer. However, no information is given on the 1D formulation that Travis & El-Genk employed. A 1D model of the fuel compact, graphite moderator and coolant channel using the systems code FLOWNEX was constructed by Nel & Du Toit [15]. They implemented the convection heat transfer coefficient correlation proposed by Travis & El-Genk [12] and found the coolant wall temperatures to be in good agreement with the corresponding temperatures obtained by Travis & El-Genk [14].

In this study models were considered that represent $1/6^{th}$ of the cross section of the SCFM considered by Travis and El-Genk [12]. The results obtained from the coupled 3D/1D method are compared to the values published by Travis & El-Genk [12] [14].

3D STAR-CCM+ MODEL

An explicit 3D model of the fuel compacts, graphite moderator and coolant channel of 1/6th of the SCFM was created using the CFD code STAR-CCM+. This model was constructed to recreate the results that were obtained by Travis & El-Genk [12] as well as aid in the investigation of the validity of the coupled 3D/1D model. The geometry of the entire SCFM model was constructed in SOLIDWORKS [16] and consisted of a 1200mm long section of the 1/6th SCFM. The assembly was imported into STAR-CCM+ and the associated physics continua associated with the fuel compact, graphite moderator and coolant channel was assigned. The material properties listed in **Table 1** were used in both the STAR-CCM+ and ANSYS FLUENT models. A single mesh continua was constructed for all the components in the STAR-CCM+ model to ensure that the cell faces on the interfaces between adjacent parts matched to form a conformal mesh. This ensured that no interpolation was necessary for the transfer of information across interfaces. It was found to play an important role in the stability of the solution. A basic base size of 6mm, based on the radius of the fuel compact, was chosen for the mesh. A total thickness for the five prism layers together was 0.4mm with a layer stretched factor of 1.2. This ensured that the temperature gradients at the interfaces were resolved sufficiently and assisted in the stability of the solution.

The prism layers, mesh, and conformal mapping across the interfaces of the generated mesh that was set up in STAR-CCM+ can be seen in **Figure 2**. The mesh for the 1200mm section of the SCFM was created. The mesh was then used as the basis for the extrusion meshing scheme used within the simulations. The total length of the 1/6th SCFM was assumed as 9200mm to account for the top reflector and the height of 8000mm of the heated section as shown in **Figure 1(a)**.

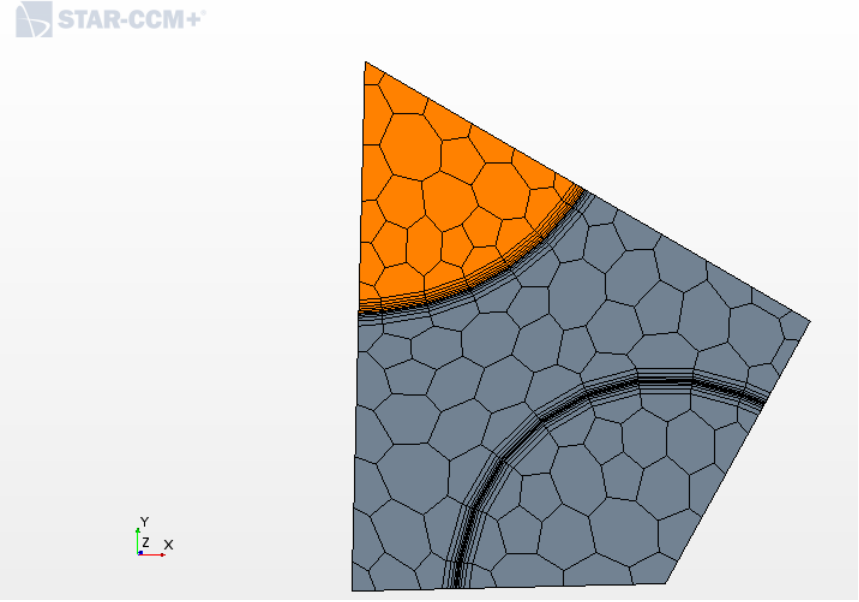

Figure 2: Cross section of STAR-CCM+ mesh.

Travis & El-Genk [12] commented that the 1200mm length of the reflector is 75 coolant channel diameters which is sufficient for fully developed turbulent flow to occur at the entrance to the heated section. The extrusion mesh consisted of 11500 layers that resulted in a layer having a thickness of 0.8mm, similar to that used by Travis & El-Genk [12]. New interfaces between the fuel compact and graphite moderator and between the graphite moderator and coolant channel had been created. This was done to ensure a uniform mesh distribution within the axial direction.

3D/1D COUPLING METHODOLOGY

Similar to Travis & El-Genk [12] the SCFM was also modelled using a 3D CFD approach to simulate the heat transfer in the fuel compact and the graphite moderator and the 1D approach to simulate the fluid flow in the coolant channel. The coolant channel was modelled in FLOWNEX while the fuel compact and the moderator were modelled in ANSYS FLUENT. During the simulation the two codes transfer the relevant data between each other in an explicit manner.

3D Simulation procedure

As FLOWNEX only accounts for the mass flow rate and the associated average velocity in the coolant channel, the coupled 3D/1D CFD model only considers the 8000mm heated section of the SCFM, and the reflector block is therefore not needed for the velocity profile to develop. Similar to the 3D STAR-CCM+ model, the 3D geometry of the SCFM consisting of the fuel compact and graphite moderator was assembled in SOLIDWORKS and imported into ANSYS FLUENT. This model was then divided into forty-nine axial increments corresponding to the axial increments of the FLOWNEX model described in the section below. The different increments of the fuel compact and the graphite moderator were categorized and assigned to reflect their nature, e.g. symmetry planes and walls. In the ANSYS FLUENT model, prism layers were only defined on the moderator side of the coolant channel wall. A sweep and assembly meshing scheme was adopted to ensure a conformal mesh throughout the entire model. The same meshing and solution strategies and material properties were applied as in the 3D STAR-CCM+ model. The conformal mapping across the inter-faces and prism layers of the generated mesh can be seen in **Figure 3** and as well as the mesh that was set up in ANSYS FLUENT for the graphite moderator and fuel compact.

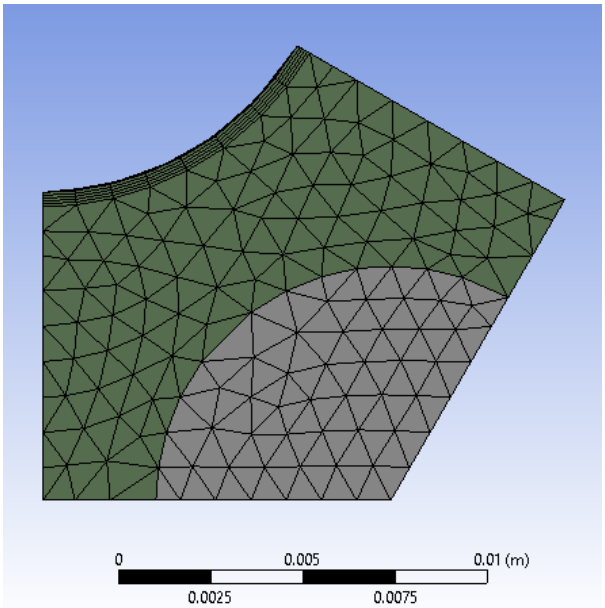

Figure 3: Cross section thought ANSYS Fluent mesh.

After the mesh was completed, the input and output parameters (to be transferred between FLOWNEX and ANSYS FLUENT) as well as the different boundary conditions were set up and assigned. The power profiles for (i) uniform- and (ii) cosine power distribution were applied as volumetric heat sources by using UDFs in ANSYS FLUENT.

1D Simulation procedure

The flow in the coolant channel was simulated in FLOWNEX. Similar to the 3D ANSYS FLUENT model, the 1D model is divided into forty-nine axial increments. The first 10 increments are each 40 mm in length followed by two 100mm increments and then thirty-seven increments each 200mm in length. This model uses only the convection and pipe elements and their corresponding nodal elements to represent the flow and convection heat transfer in the coolant channel. The properties of the pipe and convection components were similar to those used in full 1D FLOWNEX simulation by Nel & Du Toit [15].

The boundary conditions at the inlet and the outlet of the coolant channel were the same as the corresponding boundary conditions used by Nel & Du Toit [15] for the full 1D FLOW-NEX simulation. The inlet and first increment of the FLOW-NEX model are shown in **Figure 4.**

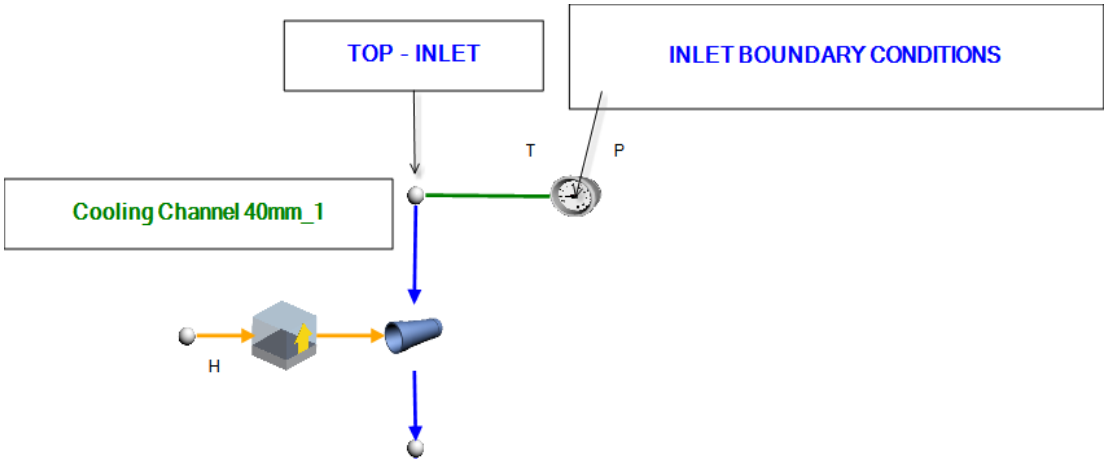

Figure 4: Inlet and first increment of the coupled FLOWNEX model.

3D/1D coupling procedure

After the 3D ANSYS FLUENT model and the 1D FLOWNEX model were constructed, the two codes had to be coupled to each other in order to define the data to be transferred between the two models. FLOWNEX was chosen as the man-aging code and to run ANSYS FLUENT in server mode. In FLOWNEX a Server Fluent Generic Interface component was inserted to control the transfer of data between FLOWNEX and ANSYS FLUENT. In the FLOWNEX model data transfer links that couple the FLOWNEX wall nodes to the relevant ANSYS FLUENT input / output parameters to account for the exchange of the coolant channel wall temperatures and the heat released by the coolant channel wall are defined. In **Figure 5** a representation can be seen of the main coupled model in FLOWNEX where the dashed lines signify the data transfer links to and from ANSYS FLUENT. Data transfer links must be defined for all the increments. Information transfer is initialized after steady-state solutions for both FLOWNEX and FLUENT are achieved. The coupled simulation could then be started. In FLOWNEX the wall temperature is transferred to ANSYS FLUENT to the corresponding increments. In ANSYS FLUENT a heat transfer report is used to transfer information for the heat generated to the corresponding elements in FLOWNEX. After the coupling of the two codes an iterative procedure was followed in which FLOWNEX completed a number of iterations and then transfers the necessary data to ANSYS FLUENT. ANSYS FLUENT then initialized with the inputs received and completed a number of iterations before the necessary information was sent back to FLOWNEX. This procedure was repeated until the specified convergence criteria were met.

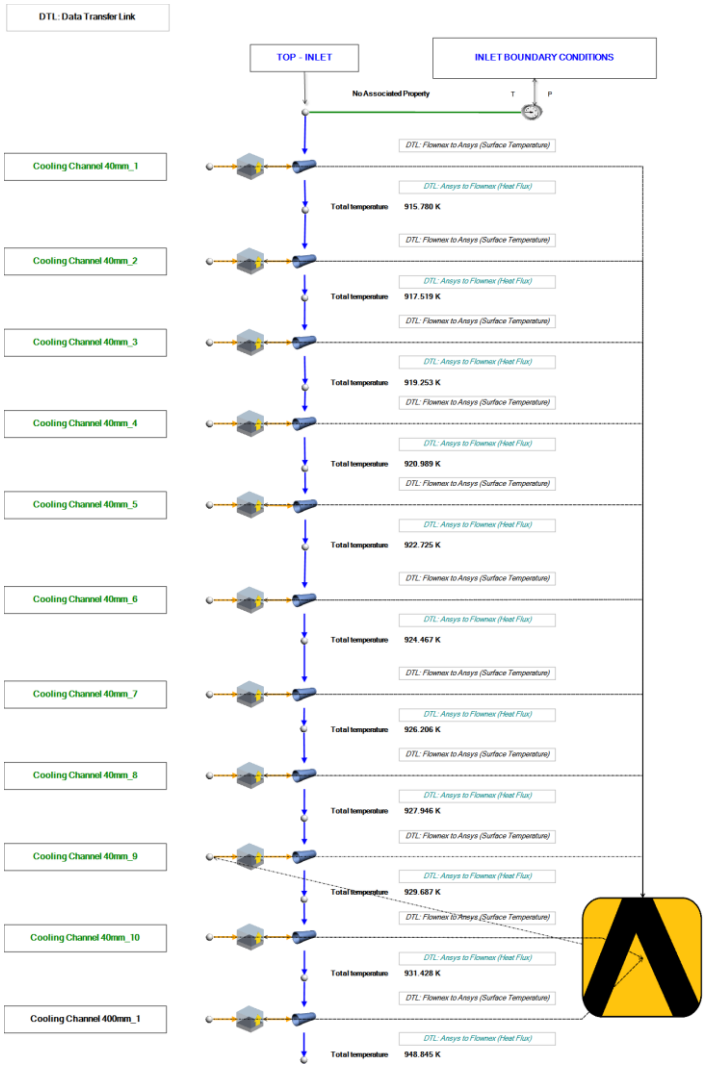

Figure 5: FLOWNEX/ANSYS FLUENT coupling.

NUMERICAL RESULTS AND DISCUSSIONS

The validity of the coupled 3D/1D model is investigated by comparing the temperature distribution in a single-channel fuel module for a (i) uniform- and (ii) cosine power profile with the corresponding values obtained from a full 3D CFD analysis of the same specification and setup. In **Figure 6** the axial variation in the temperature at the centre of the fuel compact for the uniform and cosine power profile as obtained in the 3D/1D model is compared with the corresponding results obtained in the full 3D STAR-CCM+ model. It can be seen that the agreement for both the uniform- and cosine power profiles is very good.

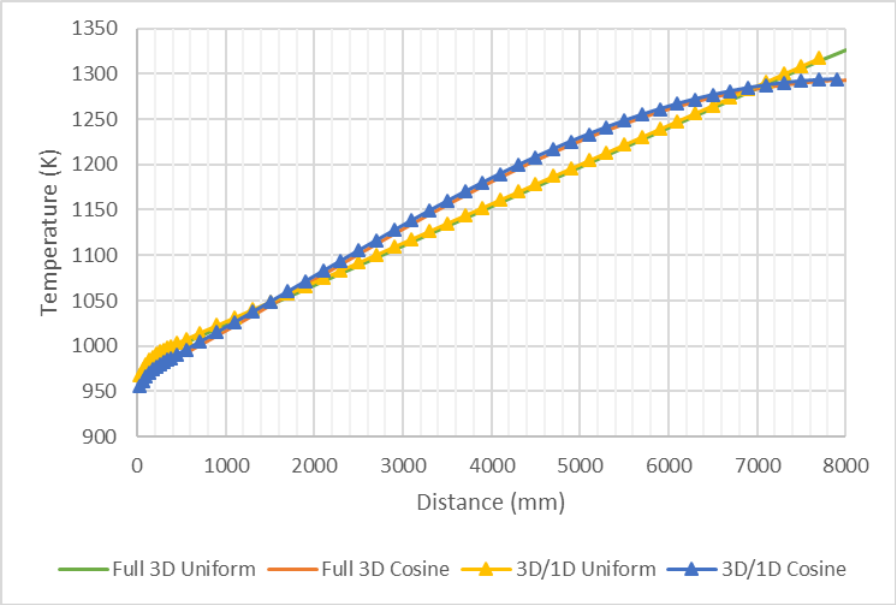

Figure 6: Fuel compact temperature as function of axial position for the uniform and cosine power profiles.

Figure 7 shows the comparison between the results obtained by the 3D model and the 3D/1D model for the variation in the axial direction of the coolant wall temperature for both the cosine- and uniform power profiles. It can again be seen that the agreement between the corresponding results is very good.

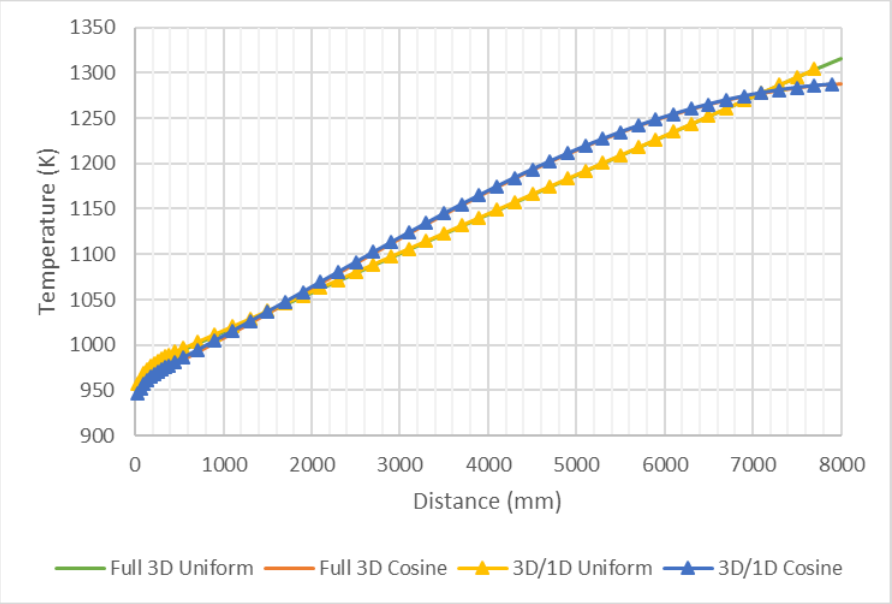

Figure 7: Coolant channel wall temperature as function of axial position for the uniform and cosine power profiles.

The coolant wall temperatures provided by each FLOWNEX increment in the coupled 3D/1D simulation to the corresponding ANSYS FLUENT coolant wall increments are received by ANSYS FLUENT as a constant value for each wall increment. This then results in a stepwise constant profile for the axial variation in the boundary values employed by ANSYS FLUENT for the coolant wall temperature. This is also reflected in the values obtained by the 3D/1D model for the variation in the temperatures along the centreline of the fuel compact. The temperature profiles shown in **Figure 7** are based on the temperatures that were extracted at the centre of each axial increment.

Figure 8 and **Figure 9** show the radial temperature distributions at three different axial locations within the SCFM obtained by the full 3D model and by the coupled 3D/1D model. The radial distributions are from the centre of the coolant channel to the centre of the fuel compact. **Figure 8** shows the results for the uniform power profile, whilst **Figure 9** illustrates the results for the cosine power profile.

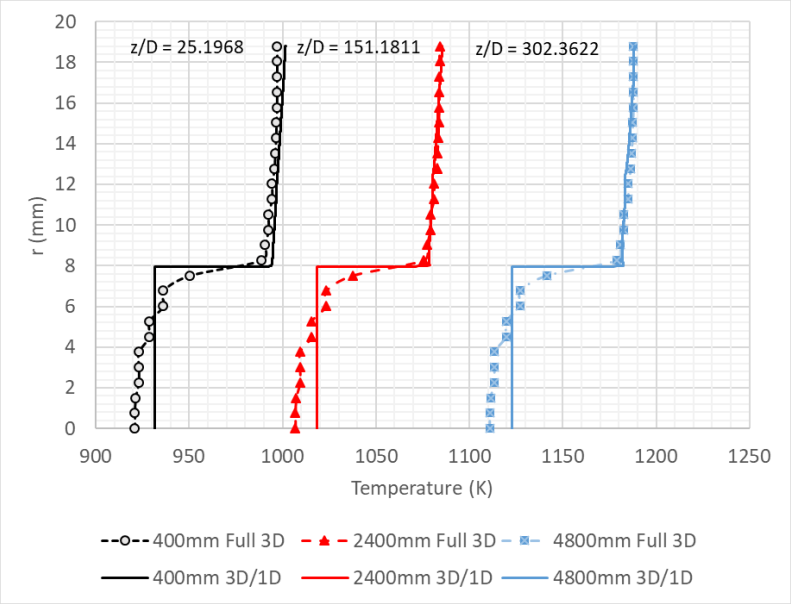

Figure 8: Radial temperature distribution at three axial locations for the 3D and 3D/1D uniform profile.

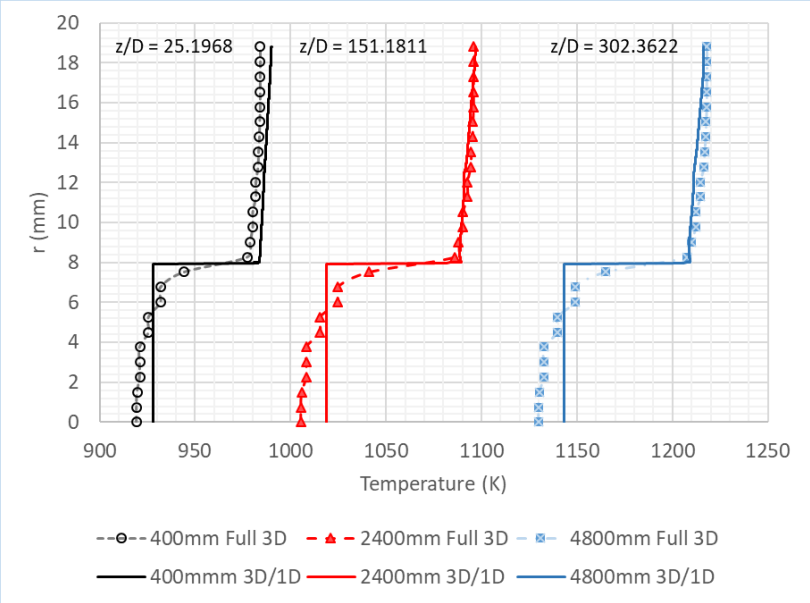

Figure 9: Radial temperature distribution at three axial locations for the 3D and 3D/1D cosine profile.

From **Figure 8** and **Figure 9**, it is evident that the coupled 3D/1D model can only predict the bulk fluid temperature. Although not shown in the figures, it was found that the bulk temperatures of the fluid predicted by the coupled 3D/1D models were in very good agreement when compared to the full 3D STAR-CCM+ models with a maximum of 3% deviation between the models. The temperature variations for the fuel compact and the graphite moderator predicted by the coupled 3D/1D model, and the full 3D model are also in very good agreement.

SUMMARY AND CONCLUSION

Understanding the thermal behaviour and predicting ac-curate fuel- and coolant temperatures is of considerable im-portance in the design of VHTRs. This paper discussed coupled 3D/1D CFD- and full 3D CFD models that simulate the heat transfer and fluid flow in a single-channel fuel module of a prismatic block. The study performed by Travis & El-Genk [12] on the numerically modelling of the heat transfer and flow in a SCFM was used as the basis for the current study.

The validity of the coupled 3D/1D model was investigated by comparing the temperature distribution in the single-channel fuel model for a (i) uniform- and (ii) cosine power profile with the corresponding values obtained from published work as well as a full detailed 3D CFD analysis of the same specifications and setup. The models developed in this study considered only $1/6^{th}$ of the cross section of the SCFM simulated by Travis and El-Genk [12] due to the symmetry in the geometry of the SCFM. An explicit 3D model of the fuel compact, graphite moderator and coolant channel of the $1/6^{th}$ of the SCFM was created using the CFD code STAR CCM+. The coupled 3D/1D model of the $1/6^{th}$ SCFM was generated using ANSYS FLUENT for the explicit 3D representation of the fuel compact and graphite moderator and the system CFD FLOWNEX for the 1D representation of the coolant channel. The Travis & El-Genk convection heat transfer correlation was employed to couple the heat transfer between the 3D and 1D formulations. The results for the coolant channel wall temperatures and fuel compact centre temperatures were found to be in very good agreement with corresponding values predicted by the full 3D explicit model.

It can therefore be concluded that the coupled 3D/1D simulation provide results for the coolant wall and fuel compact temperatures that are in very good agreement with the coolant wall and fuel compact temperatures obtained by the full 3D simulation. Due to the marked reduction in the grid requirements for the modelling of the flow in the coolant channel in the coupled 3D/1D model compared to the full 3D model, it also leads to reduction in the computational resources required. However, the coupling strategy used to transfer the relevant data between ANSYS FLUENT and FLOWNEX should be investigated to determine whether it might be possible to transfer a smoother profile for the coolant wall temperatures to be used as boundary conditions in ANSYS FLUENT.

ACKNOWLEDGEMENTS

This work is based on the research supported by the South African Research Chairs Initiative of the Department of Science and Technology and the National Research Foundation of South Africa (Grant No 61059).

Any opinion, findings and conclusion or recommendation expressed in this material is that of the authors and the NRF does not accept any liability in this regard.

REFERENCES

[1] GIF, 2014. *Technology Roadmap Update for Generation IV Nuclear Energy Systems*, s.l.: OECD Nuclear Energy Agency for the Generation IV International Forum. https://www.gen-4.org/gif/upload/docs/application/pdf/2014-03/gif-tru2014.pdf

[2] Schultz, RR. et al., 2004. *Next generation nuclear plant-design methods development and validation research and development program plan*, s.l.: Idaho National Engineering and Environmental Laboratory Technical Report. Rev 0

[3] Tak, NI, Kim, MH & Lee, WJ, 2008. Numerical investigation of a heat transfer within the prismatic fuel assembly of a very high temperature reactor. *Annals of Nuclear Energy*, Volume 35, p. 1892–1899.

[4] Gas Cooled Reactor Design and Safety, Technical Reports Series No. 312, Chapter 5.2, pp 91-116, IAEA, Vienna, 1990, ISSN 0074-1914.

[5] Next Generation Nuclear Plant Project Technology Development Roadmaps: The Technical Path Forward for 750 - 800°C Reactor Outlet Temperature, INL/EEXT-09-16598, Rev 0, August 2009.

[6] Idaho National Laboratory, Relap5-3D Version 4.4.2 http://relap53d.inl.gov/sitepages/home.aspx

[7] Jenkins, RP, Martinez, V., *TRAC (Transient Reactor Analysis Code) support software*, U.S. Department of Energy Office of Scientific and Technical Information, Technical Report, https://www.osti.gov/biblio/6941763-trac-transient-reactor-analysis-code-support-software.

[8] IRSN, ICARE-CATHARE, https://www.irsn.fr/EN/Research/Scientific-tools/Computer-codes/Pages/Computer-code-system-ICARE-CATHARE-2820.aspx

[9] M-Tech Industrial, Flownex SE Version 8.8.1.3243, http://www.flownex.com, 2017

[10] Siemens, STAR-CCM+, http://mdx.plm.automation.siemens.com/star-ccm-plus, 2018

[11] ANSYS Incorporated Version 18.2, https://www.ansys.com/products/fluids, 2018

[12] Travis, BW, El-Genk, MS (2013b). Numerical Simulation and Turbulent Convection Heat Transfer Correlation for Coolant Channels in a Very-High-Temperature Reactor. *Heat Transfer Engineering*, 34, no 1, pp. 1–14

[13] Sambureni, P (2015). *Thermal fluid network model for a prismatic block in a gas-cooled reactor using FLOWNEX*, Masters dissertation, North-West University.

[14] Travis, BW. & El-Genk, MS, (2013a). Thermal–hydraulics analyses for 1/6 prismatic VHTR core and fuel element with and without bypass flow. *Energy Conversion and Management*, Volume 67, p. 325–341.

[15] Nel GJ, du Toit CG., 2018. A System CFD model of a Single-Channel Fuel Module in a Prismatic Block VHTR. *Proceedings of the 11th SA Conference on Computational and Applied Mathematics*, SACAM 2018, held in Vanderbijlpark, South Africa.

[16] Dassault Systems, Solidworks
https://www.solidworks.com/category/3d-cad, 2017